



HHS Public Access

Author manuscript

J Med Chem. Author manuscript; available in PMC 2023 April 20.

Published in final edited form as:

J Med Chem. 2021 December 23; 64(24): 18025–18053. doi:10.1021/acs.jmedchem.1c01382.

Discovery of Novel Dual-Target Inhibitor of Bromodomain-Containing Protein 4/Casein Kinase 2 Inducing Apoptosis and Autophagy-Associated Cell Death for Triple-Negative Breast Cancer Therapy

Jifa Zhang^{||},

State Key Laboratory of Biotherapy and Cancer Center, Sichuan University-Oxford University Huaxi Gastrointestinal Cancer Centre, Innovation Center of Nursing Research, Nursing Key Laboratory of Sichuan Province, National Clinical Research Center for Geriatrics, West China Hospital of Sichuan University, Chengdu 610041 Sichuan, China

Pan Tang^{||},

State Key Laboratory of Biotherapy and Cancer Center, Sichuan University-Oxford University Huaxi Gastrointestinal Cancer Centre, Innovation Center of Nursing Research, Nursing Key Laboratory of Sichuan Province, National Clinical Research Center for Geriatrics, West China Hospital of Sichuan University, Chengdu 610041 Sichuan, China

Ling Zou^{||},

State Key Laboratory of Biotherapy and Cancer Center, Sichuan University-Oxford University Huaxi Gastrointestinal Cancer Centre, Innovation Center of Nursing Research, Nursing Key Laboratory of Sichuan Province, National Clinical Research Center for Geriatrics, West China Hospital of Sichuan University, Chengdu 610041 Sichuan, China

Jin Zhang,

State Key Laboratory of Biotherapy and Cancer Center, Sichuan University-Oxford University Huaxi Gastrointestinal Cancer Centre, Innovation Center of Nursing Research, Nursing Key Laboratory of Sichuan Province, National Clinical Research Center for Geriatrics, West China

Corresponding Authors Guan Wang – State Key Laboratory of Biotherapy and Cancer Center, Sichuan University-Oxford University Huaxi Gastrointestinal Cancer Centre, Innovation Center of Nursing Research, Nursing Key Laboratory of Sichuan Province, National Clinical Research Center for Geriatrics, West China Hospital of Sichuan University, Chengdu 610041 Sichuan, China; Phone: (+86) 28-85164063; guan8079@163.com; **Tinghong Ye** – State Key Laboratory of Biotherapy and Cancer Center, Sichuan University-Oxford University Huaxi Gastrointestinal Cancer Centre, Innovation Center of Nursing Research, Nursing Key Laboratory of Sichuan Province, National Clinical Research Center for Geriatrics, West China Hospital of Sichuan University, Chengdu 610041 Sichuan, China; Phone: (+86)28-85503817; yeth1309@scu.edu.cn; **Liang Ouyang** – State Key Laboratory of Biotherapy and Cancer Center, Sichuan University-Oxford University Huaxi Gastrointestinal Cancer Centre, Innovation Center of Nursing Research, Nursing Key Laboratory of Sichuan Province, National Clinical Research Center for Geriatrics, West China Hospital of Sichuan University, Chengdu 610041 Sichuan, China; Phone: (+86) 28-85503817; ouyangliang@scu.edu.cn.

^{||}Author Contributions

Jifa Zhang, Pan Tang, and Ling Zou contributed equally.

Supporting Information

The Supporting Information is available free of charge at <https://pubs.acs.org/doi/10.1021/acs.jmedchem.1c01382>.

Molecular formula strings and the associated biochemical and biological data (CSV)

Top 10 candidate dual-target inhibitors of BRD4 and CK2, BRD4 and CK2 inhibition rates of top 10 candidate compounds, toxicity of candidate compound **44e** to MCF-10A cells, representative images of main organ tissues after staining with hematoxylin–eosin (H&E) in MDA-MB-231 and MDA-MB-468 tumor xenograft models, molecular docking results, ATP competitive binding results, selectivity of **44e** against other kinases, and MS and NMR data (PDF)

The authors declare no competing financial interest.

Hospital of Sichuan University, Chengdu 610041 Sichuan, China; School of Pharmaceutical Sciences, Health Science Center, Shenzhen University, Shenzhen 518060, China

Juncheng Chen,

State Key Laboratory of Biotherapy and Cancer Center, Sichuan University-Oxford University Huaxi Gastrointestinal Cancer Centre, Innovation Center of Nursing Research, Nursing Key Laboratory of Sichuan Province, National Clinical Research Center for Geriatrics, West China Hospital of Sichuan University, Chengdu 610041 Sichuan, China

Chengcan Yang,

State Key Laboratory of Biotherapy and Cancer Center, Sichuan University-Oxford University Huaxi Gastrointestinal Cancer Centre, Innovation Center of Nursing Research, Nursing Key Laboratory of Sichuan Province, National Clinical Research Center for Geriatrics, West China Hospital of Sichuan University, Chengdu 610041 Sichuan, China

Gu He,

State Key Laboratory of Biotherapy and Cancer Center, Sichuan University-Oxford University Huaxi Gastrointestinal Cancer Centre, Innovation Center of Nursing Research, Nursing Key Laboratory of Sichuan Province, National Clinical Research Center for Geriatrics, West China Hospital of Sichuan University, Chengdu 610041 Sichuan, China

Bo Liu,

State Key Laboratory of Biotherapy and Cancer Center, Sichuan University-Oxford University Huaxi Gastrointestinal Cancer Centre, Innovation Center of Nursing Research, Nursing Key Laboratory of Sichuan Province, National Clinical Research Center for Geriatrics, West China Hospital of Sichuan University, Chengdu 610041 Sichuan, China

Jie Liu,

State Key Laboratory of Biotherapy and Cancer Center, Sichuan University-Oxford University Huaxi Gastrointestinal Cancer Centre, Innovation Center of Nursing Research, Nursing Key Laboratory of Sichuan Province, National Clinical Research Center for Geriatrics, West China Hospital of Sichuan University, Chengdu 610041 Sichuan, China

Cheng-Ming Chiang,

Simmons Comprehensive Cancer Center, Department of Pharmacology, and Department of Biochemistry, University of Texas Southwestern Medical Center, Dallas, Texas 75390, United States

Guan Wang,

State Key Laboratory of Biotherapy and Cancer Center, Sichuan University-Oxford University Huaxi Gastrointestinal Cancer Centre, Innovation Center of Nursing Research, Nursing Key Laboratory of Sichuan Province, National Clinical Research Center for Geriatrics, West China Hospital of Sichuan University, Chengdu 610041 Sichuan, China

Tinghong Ye,

State Key Laboratory of Biotherapy and Cancer Center, Sichuan University-Oxford University Huaxi Gastrointestinal Cancer Centre, Innovation Center of Nursing Research, Nursing Key Laboratory of Sichuan Province, National Clinical Research Center for Geriatrics, West China Hospital of Sichuan University, Chengdu 610041 Sichuan, China

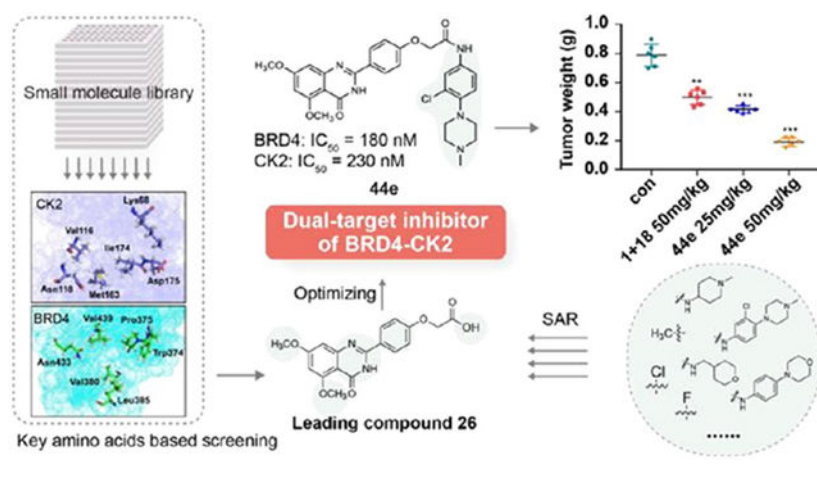
Liang Ouyang

State Key Laboratory of Biotherapy and Cancer Center, Sichuan University-Oxford University Huaxi Gastrointestinal Cancer Centre, Innovation Center of Nursing Research, Nursing Key Laboratory of Sichuan Province, National Clinical Research Center for Geriatrics, West China Hospital of Sichuan University, Chengdu 610041 Sichuan, China

Abstract

Bromodomain-containing protein 4 (BRD4) is an attractive epigenetic target in human cancers. Inhibiting the phosphorylation of BRD4 by casein kinase 2 (CK2) is a potential strategy to overcome drug resistance in cancer therapy. The present study describes the synthesis of multiple BRD4–CK2 dual inhibitors based on rational drug design, structure–activity relationship, and *in vitro* and *in vivo* evaluations, and **44e** was identified to possess potent and balanced activities against BRD4 ($IC_{50} = 180$ nM) and CK2 ($IC_{50} = 230$ nM). *In vitro* experiments show that **44e** could inhibit the proliferation and induce apoptosis and autophagy-associated cell death of MDA-MB-231 and MDA-MB-468 cells. In two *in vivo* xenograft mouse models, **44e** displays potent anticancer activity without obvious toxicities. Taken together, we successfully synthesized the first highly effective BRD4–CK2 dual inhibitor, which is expected to be an attractive therapeutic strategy for triple-negative breast cancer (TNBC).

Graphical Abstract



INTRODUCTION

Breast cancer (BC) is the most common female malignant tumor in the world, and more than 42 170 women died of BC in 2020.^{1,2} Triple-negative breast cancer (TNBC), which does not express estrogen receptor (ER), progesterone receptor (PR), or HER2/neu, significantly overlaps with the molecular subtype of basal-like breast cancer (BLBC).³ TNBC/BLBC cases account for 15% of all BC and mainly affect young women, people of African or Spanish origin, and those with BRCA1 mutations. It is highly aggressive and features high recurrence, metastasis, and heterogeneity. At present, surgery and conventional systemic cytotoxic chemotherapy are commonly used for TNBC treatment. However, its prognosis is far from satisfactory compared with advanced BC cases of other subtypes.⁴⁻⁶ Fortunately,

targeted therapy drugs have improved cancer treatment for many people in a certain period of time.

So far, the main targets and pathways of TNBC, including the bromodomain-containing protein 4 (BRD4),⁷ epidermal growth factor receptor (EGFR),⁸ mitogen-activated protein kinase (MAPK)–extracellular regulated protein kinases (ERK),⁹ phosphatidylinositol 3 kinase (PI3K)–protein kinase B (AKT),¹⁰ polyADP–ribose polymerase (PARP),¹¹ vascular endothelial growth factor receptor 2 (VEGFR2),¹² and human epidermal growth factor receptor 2 (HER2),^{12,13} have been well studied. However, drug resistance has become challenging with increased application of small molecule targeted drugs.^{14–16} How to prevent and reverse drug resistance in cancer patients has been a major concern. BRD4 is a member of the BET family, which serves as a vital transcriptional and epigenetic regulatory factor in cell cycle progression. It is also involved in cancer progression by promoting oncogene transcription through RNA polymerase II (Pol II) or regulating oncogene networks by inducing signal transduction after recognizing acetylated histones.^{17–19} BRD4 is of great significance in many hematopoietic and solid tumors expressing *Myc* and other oncogenes.^{20,21} It has been reported that dysregulated BRD4 was detected in breast cancer, colon cancer, and prostate cancer.²² The large-scale genome analysis of TNBC demonstrated that BRD4 is essential for the survival of TNBC cell populations.²³ Knockdown of BRD4 in TNBC cells significantly inhibits the activity of Notch1, thus suppressing metastasis and invasion.^{24,25} Dysfunctional BRD4 is closely linked to the occurrence, development, invasion, metastasis, and prognosis of TNBC. Furthermore, inhibition of BRD4 could induce autophagy in breast cancer cells. BRD4 inhibitors are capable of inhibiting the transcription of oncogenes in TNBC, serving as promising therapeutic agents.^{26,27} BRD4 inhibitors have drawn significant attention in recent years. Multiple BET inhibitors have been reported, including JQ1 (**1**), I-BET726 (**2**), RVX-208 (**3**), mivebresib (**4**), ZL0516 (**5**), ZL0454 (**6**), GSK046 (**7**), SJ018 (**8**), GSK789 (**9**), and LT052 (**10**) (Figure 1A), and clinical trials with some BRD4 inhibitors evaluating the therapeutic efficacy against cancers are in progress.^{5,28,29} A growing number of BRD4 inhibitors have been discovered and applied to the treatment of TNBC, but the emergence of drug resistance was one of the reasons that greatly limited the clinical application.^{30,31} The latest study in 2021 suggested that the drug resistance mechanism of BET inhibitors varies with the cancer type, and inhibiting the phosphorylation of BRD4 by casein kinase 2 (CK2) is a potential strategy to overcome drug resistance in cancer patients.³²

CK2 is upregulated in various types of cancers, presenting a vital function in essential biological processes. It is considered as a potential therapeutic target for cancers.³³ CK2 is composed of catalytic α/α' and regulatory β subunits. During the past four decades, multiple CK2 inhibitors have been developed for human disease treatment, including quercetin (**11**), DRB (**12**), DMAT (**13**), TBB (**14**), coumestrol (**15**), CX-5011 (**16**), emodin (**17**), CX-4945 (**18**), HY1-Pt (**19**), and SGC-CK2-1 (**20**) (Figure 1B).^{34,35} Among them, **18** is the only small molecule CK2 inhibitor explored in phase I/II clinical trials. In addition, **18** effectively induces autophagy and apoptosis in pancreatic cancer cells. Studies have shown that CK2 could regulate autophagy through downstream targets of phosphorylation.³⁶ CK2 has been validated as one of the proteins with the most genetic

diversity in eukaryotic systems. It contains more than 300 phosphorylated substrates and is involved in various cellular processes, including the AKT/PI3K pathway, DNA damage repair, cell cycle progress, and cell growth. Among them, CK2-induced phosphorylation is essential for BRD4 binding to acetylated chromatin and occurs at the N-terminal cluster of phosphorylation sites (NPS), situated downstream of the second bromodomain (BD2), and the C-terminal cluster of phosphorylation sites (CPS), located downstream of the extraterminal (ET) domain, of BRD4.³⁷ Both NPS and CPS are also found in other bromodomain and ET (BET) family proteins, including BRD2, BRD3, and BRDT.³⁷ Shu et al.³⁸ explored the inhibitory effect of BET in human breast cancer. It was found that MED1, a widely existing protein for Pol II-dependent transcription, binds to BRD4 in drug-resistant cells more tightly than in drug-sensitive cells, which results from BRD4-independent transcriptional activation of *Myc* gene caused by an increase of BRD4 phosphorylation due to decreased protein phosphatase 2A (PP2A) activity. In addition, CK2 inhibition leads to increased uptake of known drugs in multidrug-resistant cells.³⁹⁻⁴¹ Currently, development of multitarget approaches targeting different proteins, especially dual target inhibitors with synergistic effects, has received increasing attention in anticancer drug development. Many dual BET/kinase inhibitors have been described.⁵ They can simultaneously regulate multiple targets in the disease network and have synergistic antitumor effects, providing a rationale for the development of dual inhibitors of BRD4. Therefore, we speculate that inhibition of BRD4 and CK2 could both solve the problem of resistance of BRD4 inhibitors caused by phosphorylation and could further inhibit the proliferation and induce apoptosis and autophagy-associated cell death in TNBC. In conclusion, the design and synthesis of BRD4–CK2 dual inhibitors may provide a new therapeutic option for TNBC.

To achieve this goal, we first identified that BRD4 and CK2 could influence the progression and prognosis of TNBC through apoptosis and autophagy-associated cell death by networks and systems biology. A series of small molecule BRD4–CK2 dual inhibitors were then synthesized via virtual screening and rational drug design and assessed for their *in vivo* and *in vitro* biological activities. The obtained candidate compound **44e** was found to inhibit colony formation of MDA-MB-231 and MDA-MB-468 TNBC cells, and dose-dependently induced cell apoptosis and autophagy-associated cell death. *In vivo* experiments further validated an acceptable anticancer effect of **44e** in mice. Our findings demonstrated the therapeutic efficacy of **44e** on TNBC through dual-inhibition of BRD4 and CK2, which is expected to be a promising candidate drug for TNBC.

RESULTS AND DISCUSSION

Bioinformatics Analysis.

Bioinformatic analysis was performed to investigate the potential functions of BRD4 and CK2 in the development of breast cancer susceptibility genes (Figure 2A). First, the interacting proteins of BRD4 and CK2 were searched using the PrePPI database.^{42,43} It is shown that there are 359 and 4241 proteins interacting with BRD4 and CK2, respectively, with a regulatory relationship. These interacting proteins were subsequently annotated and clustered using the Gene Ontology (GO) and DAVID databases.^{44,45} Among them, 453 and 131 proteins were enriched in the apoptosis and autophagy pathways, respectively (Figure

2B,C). Finally, the GEPIA tool was used to analyze the breast cancer transcriptome data of BRD4 and CK2 obtained from the TCGA database; as shown in Figure 2D, a significantly positive correlation was identified between BRD4 and CK2 ($R = 0.5$, $p = 7.1 \times 10^{-76}$).⁴⁶ This bioinformatic analysis correlates interaction between BRD4 and CK2 and underlines the progression and prognosis of TNBC through apoptosis and autophagy-associated cell death.

Design of Novel BRD4–CK2 Dual Inhibitors.

BET inhibitors are mainly categorized as pan-BET inhibitors, selective BRD4 inhibitors, and BET-BD1 or BET-BD2 inhibitors.⁵ BRD4 contains two conserved N-terminal bromodomains (BD1 and BD2) with high sequence similarity.¹⁸ There are many studies describing the unique functions of BD1 and BD2. However, in cancer research, the functional differences between BD1 and BD2 are not very clear.¹⁴ Currently, BRD4 inhibitors based on BD1 or BD2 selectivity have been reported.⁵

To design BRD4–CK2 dual inhibitors, we first analyzed the crystal structures of BRD4 (BD2) and CK2 for key inhibitor contact amino acid sites via molecular docking. BRD4 and CK2 small-molecule inhibitor complexes were downloaded from the Crystallography Open Database. Based on the reported interaction between BRD4 (BD2) or CK2 and small molecule inhibitors, key amino acid residues in different spatial positions in the active pocket were summarized. As shown in Figure 3, Trp374, Pro375, Val380, Leu385, Asn433, and Val439 were identified as key amino acid residues in BRD4-BD2 for interaction with small molecule inhibitors, while Lys68, Val116, Asn118, Met163, Ile174, and Asp175 were key amino acid residues for CK2 interaction with small molecule inhibitors. Subsequently, we screened BRD4–CK2 dual inhibitors through the multiple-docking strategy. A total of 217 836 compounds in the SPECS library of Topscience, ACDB, and MCDB were initially screened based on the Lipinski's rule, and finally, 198 445 small molecules were obtained as a compound library for further analyses.^{2,47} Rapid molecular docking of compounds with BRD4 (BD2) (PDB ID 5UOO) and CK2 (PDB ID 6RFE) in the generated library was conducted using the LibDock module of Discovery Studio software (version 3.5), and the top 1000 matches that could bind to BRD4 and CK2 were selected. Molecular docking of the 1000 matches with BRD4 and CK2 was performed using the CDOCKER module. The obtained 80 matched compounds that could bind to BRD4 and CK2 were further analyzed for the docking mode, structural diversity, and conformational stability with key amino acids as important references, and finally, 10 compounds were obtained (Figure S1). Through assessing their kinase activity *in vitro*, we found that compound **26** at 10 μM presented an inhibitory effect on BRD4 and CK2 with an inhibitory ratio of 63% and 45%, respectively (Figure S2). Thus, **26** was selected as the lead compound for further design and structural optimization of BRD4–CK2 dual inhibitors.

Synthetic Routes of BRD4–CK2 Dual Inhibitors.

The synthetic routes of all target compounds are shown in Schemes 1-3. Target compounds **33a–d** and **34a–c** were initially synthesized as shown in Scheme 1. Briefly, hydroxyacetophenone derivatives dissolved in pyridine were induced with benzoyl chloride derivatives under alkaline conditions for 1.5 h, thus obtaining the intermediates **31a–d**. The

intermediates were then dissolved in pyridine, heated at 50 °C for 1 h, and induced with KOH at 80 °C for 1 h. The obtained intermediates **32a–d** resolved in HOAc were treated at 90 °C for 1 h, followed by cooling, vacuum distillation, and incubation with H₂SO₄ 1% (v/v) in HOAc solution for 1 h, thus obtaining compounds **33a–d**. They were then dissolved in toluene and subjected to heating reflux using the Lawesson's reagent for 4 h. Finally, target compounds **34a–c** were obtained.

Target compounds **38a–s** and the lead compound **26** were obtained as shown in Scheme 2. First, 3,5-dimethoxyaniline was converted into hydrochloride salt, which was then reacted with (COCl)₂ at high temperature to obtain 4,6-dimethoxyindolinedione (**35a**). Compound **35a** was subjected to 0.5 h heating reflux under alkaline conditions by adding the oxidant H₂O₂, and the intermediate 2-amino-4,6-dimethoxybenzamide (**36a**) was obtained after suction filtration. Compound **36a** was induced with the carboxylic acid activator HOBt, the coupling agent EDCI, and *N*-methylmorpholine in THF solution. After condensation using ammonium hydroxide, an amide product, 2-amino-4,6-dimethoxybenzamide (**37a**), was obtained. The synthetic routes of intermediates **37b,c** were similar to that of **37a**. Finally, **37a–c** were reacted with various aldehydes using PTSA as the catalyst and NaHSO₃ as the additive, heated to reflux for 4–8 h, and purified by column chromatography, thus obtaining target compounds **38a–s** and the lead compound **26**.

Target compounds **42a–j**, **43a–q**, and **44a–n** were synthesized according to the preparation pathways depicted in Scheme 3. Under alkaline conditions, *tert*-butyl bromoacetate and *p*-hydroxybenzaldehyde derivatives in DMF developed substitution reaction, thus obtaining intermediates **39a–c**. Later, intermediates **40a–c** were obtained by hydrolysis of *tert*-butyl ester. Anthranilamide derivatives and **40a–c** were dissolved in DMAc and reacted with NaHSO₃ and the catalyst PTSA at high temperature for 4–8 h. The obtained intermediates **41a–h** were incubated with amino substitution derivatives in DMF solution containing HOBt and EDCI. After 24 h stirring at room temperature, target compounds **42a–j**, **43a–q**, and **44a–n** were separated by column chromatography.

Structural Optimization of the BRD4–CK2 Dual Inhibitors.

To optimize the structure of the lead compound, we analyzed the binding mode of compound **26** and the target proteins. Molecular docking analysis showed that the binding mode of compound **26** within BRD4 was similar to that of BRD4 inhibitor **3** (Figure 4A). As the binding mode of compound **26** within CK2 showed, the quinazolinone core scaffold was inserted deeply into the hydrophobic pocket, in which the O atom and the *para*-position N atom of amide groups formed two key hydrogen bonds with Lys158 and Asp175, respectively. Furthermore, the conjugation of the benzene ring of the quinazolinone core scaffold and Asp175 maintained the stable binding of the quinazolinone core scaffold and CK2, while the benzene ring on the other side formed hydrophobic interactions with Val53 and Ile174. However, the tail group of the compounds did not occupy the channel surrounding the hinge region. In addition, **26** did not have interactions with key amino acids like Asn118 and Met163 in the core group, which may be vital factors for influencing the binding stability and affinity with CK2 (Figure 4B).

In the first round of modification, we verified the importance of the quinazolinone core scaffold in the lead compound with dual inhibition of BRD4 and CK2. The key N atom of quinazolinone was first replaced to synthesize compounds **33a–d**. Their inhibitory rates against BRD4 and CK2 were determined at a concentration of 1 μM (Table 1), which, as expected, were lower than 15%. Compounds lost almost all inhibitory activity against TNBC cells. The inhibitory effects of **33a–d** on target proteins were significantly reduced. Subsequently, compounds **34a–c** were synthesized through introducing a S atom to replace the oxygen carbonyl, which barely had activity. Therefore, it is suggested that the quinazolinone core scaffold was the vital fragment for maintaining the compounds' activities.

In the second round of optimization, we retained the quinazolinone core scaffold and further optimized the tail group of **26**. Target compounds **38a–s** were synthesized by introducing various substituents (R_1 , R_2) on the benzene ring. We speculated that these structures were able to form various interactions with channels surrounding the hinge region of CK2. Our findings showed that **38d**, in which a 3,5-dimethyl-4-hydroxyphenyl group served as the R_2 group, inhibited BRD4 by 21.25%. Compound **38p** was synthesized by introducing an electron-withdrawing group, $-\text{COOH}$, and **38i** introduced an electron-donating group, $-\text{OCH}_3$. Compared with **26**, **38p** (16.81%) and **38i** (16.83%) still presented a low inhibitory rate against CK2, and their inhibitory rate against BRD4 was not elevated (17.46% and 11.74%). In addition, compounds synthesized by substituting R_1 as the H atom (**38j–l**) or a single methoxy (**38m–o**) presented a low inhibitory rate against BRD4, with no antiproliferative activity on MDA-MB-231 cells ($\text{IC}_{50} > 50 \mu\text{M}$). The dimethoxyphenyl group was found to be the key group responsible for inhibiting BRD4, which was similar to that of **3**. Interestingly, inhibition was elevated to varying degrees in **38a**, **38d**, and **38f** by substituting R_1 with the dimethoxy group (Table 2).

Further, **38q** and **38r** were synthesized by moving the *para*-substituted acetic acid group on the benzene ring to the *meta*-position or *ortho*-position. Their inhibitory rate against CK2 was slightly reduced, but that against BRD4 was significantly reduced. Compounds **38q** and **38r** exhibited lower efficiency on TNBC cells compared with **26**. Collectively, through altering the acetic acid chain at the end of the benzene group, the BRD4 and CK2 inhibition rates and *in vitro* antiproliferative activities of synthesized compounds were not elevated, suggesting that the terminal acetic acid group is an important group to maintain the inhibitory activity of the target compound.

According to the interaction between the lead compound **26** and CK2, we considered that extending the tail group of the molecule to strengthen the interactions, such as hydrophobic interactions, hydrogen bond interactions, and π - π stacking, in the hydrophobic channel surrounding the hinge region of CK2 could be a feasible approach. The quinazolinone core scaffold of **26** and the *para*-carboxyl substitution of the benzene ring are important structures for maintaining activity (Figure 4B). Therefore, the important pharmacophore was retained in the third round of modification, only optimizing the tail group.

Through analyzing the structures of other BRD4 and CK2 inhibitors, it was found that the amide bond is responsible for the interaction formed in the hydrophobic channel.

Therefore, it could be used to extend the molecular structure. Here, the amide bond was introduced to further boost the interaction to amino acid residues surrounding the hinge region of CK2. Later, compounds **42a–j** were synthesized, retaining the dimethoxyphenyl group (Table 3) and the quinazolinone core scaffold. Through introduction of the morpholine derivatives (**42a,b**), tetrahydropyran derivatives (**42c,d**), *N*-methylpiperidine derivatives (**42e,f**), 1-methylpiperazine derivative (**42g**), and substituted benzene (**42h,i**), the extended length of substituents further strengthened the interaction between small molecules and the hinge region of CK2. BRD4 and CK2 activities of these compounds were elevated to a certain extent. Notably, the inhibitory rates of **42g** against BRD4 and CK2 were 55.71% and 53.64% at the concentration of 1 μM . Meanwhile, **42g** also showed acceptable cellular potency in MDA-MB-231 and MDA-MB-468 cells ($\text{IC}_{50} = 12.82$ and $13.65 \mu\text{M}$, respectively). The introduction of the 1-methylpiperazine group was also conducive to the antiproliferative ability in TNBC cells.

The docking mode of **42g** with BRD4 and CK2 revealed a similar key interaction site between the core scaffold structure of **42g** and BRD4 to that of lead compounds (Figure 4). In particular, the introduction of the amide bond induced the formation of a hydrogen bond with Leu45 of CK2 and an intermolecular hydrogen bond between the 1-methylpiperazine group and Asn118. Since the hinge region of CK2 is relatively large, the length of the molecule was speculated to be prolonged here. We then introduced a phenyl group between the amide bond and the 1-methylpiperazine group, hoping to improve the interaction between this part and the hinge region of CK2, thus stabilizing the conformation of the 1-methylpiperazine group.

Subsequently, we further increased the length of the terminal substituents, while retaining the amide bond. As a result, the inhibitory activity of the newly synthesized compounds **43a,b** against CK2 was not significantly improved. Considering the lack of correlation between the compounds and the wider hinge region of CK2, we introduced 1-methylpiperazine derivatives, morpholine derivatives, and five- and six-membered heterocyclic derivatives linking benzene rings to synthesize compounds **43c–q**. Their inhibitory activities against BRD4 and CK2 have been greatly improved. Particularly, **43f**, modified by introducing the 1-methylpiperazine group in the *para*-position of the benzene ring, presented pronounced inhibitory activity against BRD4 and CK2 with inhibitory rates of 82.30% and 80.02%, respectively, at a concentration of 1 μM , and its antiproliferative rate in TNBC cells was also improved ($\text{IC}_{50} = 6.46$ and $8.80 \mu\text{M}$ in individual MDA-MB-231 and MDA-MB-468 cells). Moving the 1-methylpiperazine group from the *para*-position of the benzene ring to the *meta*- (**43g**) and *ortho*-positions (**43h**) resulted in reduced inhibition against BRD4 and CK2. Later, we analyzed the structure–activity relationship (SAR) on the phenyl group, which directly bonded to the amide bond, and synthesized **44a–i**. Compound **44e**, modified by introducing a Cl atom at the *meta*-position, presented the optimal inhibitory activity against BRD4 (92.28%) and CK2 (90.65%), as well as the highest antiproliferative rates in MDA-MB-231 and MDA-MB-468 cells ($\text{IC}_{50} = 2.66$ and $3.52 \mu\text{M}$, respectively), which was slightly better than that of **44c** with substitution of the F atom at the *meta*-position. The introduction of the Cl atom at the *meta*-position of the benzene ring and of the 1-methylpiperazine group at the *para*-position were optimal

groups for BRD4 and CK2. Next, the inhibitory activity of **44j–n** with the Cl atom and the 1-methylpiperazine group against BRD4 was significantly reduced, further validating the importance of the dimethoxyphenyl group. However, in MDA-MB-231 and MDA-MB-468 cells, the antiproliferative effect of **44m** was more pronounced than others, which may be explained by an off-target effect. The docking mode analysis revealed that the introduction of phenyl induced interaction between the benzene ring and Met163. The Cl atom on the benzene ring was of great significance in maintaining the conformation of the 1-methylpiperazine group and promoting the formation of intermolecular hydrogen bonds between H atoms of the 1-methylpiperazine group and Asn118 and Asp120 of CK2, thus triggering the stable combination with CK2.

Based on the above analysis, the dimethoxyphenyl group was of great significance to the inhibitory activity against BRD4. After being replaced with single methoxy or halogens (F, Cl) at different positions or H, the inhibitory activity against BRD4 was significantly affected (Figure 5). The quinazolinone core scaffold is a critical group leading to compounds' activities. The inhibitory activity of target compounds with H substitution on the benzene ring connected to the quinazolinone core scaffold was superior to that of the compounds with methyl and Br substitutions. The introduction of the benzene ring linking the Cl atom at the *meta*-position and methylpiperazine at the *para*-position through an amide bond resulted in the best BRD4–CK2 dual inhibitory activity, as well as the antiproliferative ability of TNBC cells. During the process of evaluating the activity, **1** and **18** were used as positive control drugs (Table 3). In MDA-MB-231 and MDA-MB-468 cells, **1** and **18** might show a certain synergistic effect; the combination index (CI) calculated by the Chou–Talalay method was 0.78 and 0.61.⁴⁸ In addition, we tested inhibitory activities of **44e** against BET BDs and CK1 and CK2 because of the pronounced enzymatic activity and antiproliferative activity *in vitro* (Table 4). It is shown that **44e** presented the most significant inhibitory activity against BRD4 (IC₅₀ = 180 nM) compared with the other isoforms of BRD proteins. Moreover, compared with BRD4-BD1 (IC₅₀ = 193 nM), **44e** showed weak selectivity for BRD4-BD2 (IC₅₀ = 98 nM). Compared with that of CK1, **44e** presented higher selectivity to inhibition against CK2 (IC₅₀ = 230 nM). Hence, **44e** is an effective BRD4–CK2 dual inhibitor.

Molecular docking analysis revealed the binding modes of **44e** in the active pocket of BRD4(BD2) and CK2. The core scaffold of **44e** was located inside the active pocket, forming intermolecular hydrogen bonds with amino acid residues Pro375 and Asn433 of BRD2 (BD2) and hydrophobic interactions with Pro375, Leu385, Leu387, and Val439, showing a similar molecular binding mode to that of **3**. Compared to the lead compound **26**, the hydrophobic interaction formed by the hydrogen on the side-chain benzene ring and Pro434 and intermolecular hydrogen bonds formed by the 1-methylpiperazine group and Tyr432 further promoted the binding of **44e** and BRD4 (BD2). The core part of **44e** was deeply inserted into the hydrophobic pocket of CK2, forming intermolecular hydrogen bonds with amino acid residues Lys77, Lys158, Asn161 of CK2 and a conjugation force with Asp175. An intermolecular hydrogen bond formed between the carbonyl group of the amide bond and the amino acid residue Leu45 was responsible for fixing the position and conformation of the compound in CK2. Compared with compound **42g**, a conjugation

force formed by the increased side-chain benzene ring and Met163, and intermolecular hydrogen bonds formed by the 1-methylpiperazine group and Asn118 and Asp120 in the hinge region enhanced the binding stability with CK2 as well (Figure 4B). Collectively, **44e** is a novel chemical type for BRD4-CK2 dual inhibition, which might be helpful for subsequent exploration of novel BRD4-CK2 inhibitors.

Compound **44e** Induces TNBC Cell Death by Targeting BRD4 and CK2.

A combination administration of **1** and **18** (at a mole ratio of 1:1) in MDA-MB-231 and MDA-MB-468 cells resulted in a synergistic effect, while administration of the candidate compound **44e** presented the most effective kinase inhibition and antiproliferation (Figure 6A and Table 3). Notably, it did not have obvious toxicity to the normal breast cell line MCF-10A (Figure S3). Considering the common concern of drug resistance with BRD4 inhibitors, we first assessed the anticancer activity of **44e** against BRD4 inhibitor-resistant breast cancer cells. Briefly, compound **1**-resistant MDA-MB-231 cell line (MDA-MB-231R) was generated by low-dose **1** selection at different time points. MDA-MB-231R cells and their parental cells were treated with different doses of **1**, aiming to generate MDA-MB-231R.⁴⁹ Later, MDA-MB-231R cells and their parental cells were treated with different doses of **1** or **44e**. It was shown that **44e** was able to alleviate drug resistance of **1** in MDA-MB-231R cells ($p < 0.01$), suggesting that **44e** still presented an acceptable anticancer effect on **1**-resistant breast cancers (Figure 6B).

To further verify the BRD4 and CK2 inhibition efficacy of **44e** treatment in TNBC cells, we silenced the expression of BRD4, CK2, and BRD4/CK2 in MDA-MB-231 cell lines with the BRD4 shRNA, CK2 shRNA, and BRD4/CK2 shRNA, respectively (Figure 7A). The expression of BRD4 and CK2 was significantly downregulated in MDA-MB-231 cells. Following a 24 h exposure to **44e**, the results showed that the inhibitory effect of **44e** was reduced to a certain extent after knockdown. This finding also verified the inhibition of BRD4 and CK2 by **44e** in TNBC cell lines (Figure 7B). Next, to investigate whether **44e** could bind to BRD4 and CK2 α in cells, we performed CETSA assay in MDA-MB-231 cells. The results demonstrated that **44e** improved the thermal stability of BRD4 and CK2 α , indicating that **44e** could directly combine with BRD4 and CK2 α (Figure 8A). Subsequently, we determined whether **44e** affects the key downstream proteins of BRD4 and CK2 α . MDA-MB-231 and MDA-MB-468 cells were treated with 0, 2.5, 5, and 10 μM of **44e** for 24 h, followed by detection of protein levels of BRD4, c-Myc, CK2 α , and p-AKT^{S129} by Western blotting. Previously, the Chiang lab reported that the NPS in BRD4 is enriched in acidic residues, containing seven CK2 phosphorylation sites (S484, S488, S492, S494, S498, S499, S503).³⁷ We verified that **44e** dose-dependently downregulated the level of p-BRD4^{S492} (Figure 8B,C). Taken together, **44e** could bind to BRD4 and CK2 in cells and inhibit the proliferation pathway regulated by BRD4 and CK2 but had no significant effect on the protein levels of BRD4 and CK2.

Compound **44e** Inhibits Colony Formation and Promotes Apoptosis in TNBC Cells.

To further investigate the effect of **44e** on TNBC cells, we first performed the colony formation assay to detect the long-term proliferation ability of TNBC cells after **44e** treatment. The results showed that **44e** dose-dependently suppressed growth and reduced the

number of colonies in MDA-MB-231 and MDA-MB-468 cells (Figure 9A,B). In addition, MDA-MB-231 and MDA-MB-468 cells were treated with different doses of **44e** for 24 h, followed by Hoechst 33258 staining to determine whether apoptosis was induced after **44e** treatment. The results showed that the number of dead cells was dose-dependently elevated (Figure 9C,D). Collectively, these results revealed that apoptosis might be involved in **44e**-induced cell death.

In order to confirm that **44e** could induce apoptosis, flow cytometry was performed to measure cell apoptosis. Interestingly, **44e** dose-dependently induced apoptosis of MDA-MB-231 and MDA-MB-468 cells (Figure 10A,B). As expected, **44e** dose-dependently downregulated Bcl-2 but upregulated Bax and cleaved caspase-3 (Figure 10C,D). Taken together, **44e** induces apoptosis in MDA-MB-231 and MDA-MB-468 cells.

Compound **44e** Induces Autophagy in TNBC Cells.

In our previous work, we found that BRD4 inhibition could induce autophagy in breast cancer cells.⁵⁰ So we next checked whether **44e** could induce autophagy in TNBC cells. MDA-MB-231 and MDA-MB-468 cells were transfected with the autophagy biosensor GFP-mRFP-LC3. With an inverted microscope, it was shown that **44e**-induced autophagy flux was significantly increased (Figure 11A). Protein levels of autophagy markers were further detected by Western blotting. As expected, **44e** significantly down-regulated the autophagy substrate p62 and up-regulated beclin-1 and LC3II (Figure 11B,C). Taken together, **44e** significantly induced autophagy in MDA-MB-231 and MDA-MB-468 cells.

To investigate the role of autophagy in **44e**-induced cell death, we employed the autophagy inhibitor 3-methyladenine (3-MA), which is commonly used to inhibit the autophagic process by blocking autophagosome formation.⁵¹ And according to previous findings, 3-MA was applied to show the relationship between cell death and autophagy.⁵² Upon the addition of 3-MA, the effect of **44e** on cell death was significantly reduced, suggesting that autophagy plays a role in promoting TNBC cell death (Figure 12A,B). Similar results were also obtained from colony formation assay (Figure 12D,E), indicating that **44e** induces autophagy-associated cell death in TNBC cells. In addition, a significantly lower apoptotic rate was detected in MDA-MB-231 and MDA-MB-468 cells treated with both **44e** and 3-MA for 24 h compared to that of cells treated with **44e** only (Figure 12C), suggesting that application of 3-MA was able to partially reverse **44e**-induced apoptosis in TNBC cells. These data indicate that **44e**-induced autophagy inhibited cell proliferation and promoted cell apoptosis.

Preliminary Assessment of Pharmacokinetics (PK) profile of **44e**.

Based on the most potent BRD4–CK2 inhibitory activity of compound **44e** and its antiproliferation and ability to induce apoptosis and autophagy-associated cell death in TNBC cells, we further studied the pharmacokinetic properties. As shown in Table 5, compound **44e** was administered as a single dose at 1 mg/kg and 10 mg/kg by intravenous and oral routes, respectively. The results indicated that **44e** could be absorbed rapidly from the intestine with the highest concentration observed at 5.14 ± 0.71 h and a maximum plasma concentration (C_{\max}) value of 206 ± 6 ng/mL. Furthermore, **44e** had a reasonable

area under the curve ($AUC_{0-\infty}$) value of 2079 ± 130 ng·h/mL and an acceptable oral bioavailability of 32.5%. Thus, it is of great significance to further conduct *in vivo* tests of **44e** on antitumor activity.

Compound **44e** Inhibits Tumor Growth in TNBC Xenograft Models.

To further investigate the *in vivo* inhibitory effect of **44e** on BRD4 and CK2, we generated MDA-MB-468 and MDA-MB-231 xenograft tumor models in mice. In each model, a total of 24 mice were randomly assigned into a control group (normal saline, $n = 6$), a combination group (**1** and **18** combined at a mole ratio of 1:1, $n = 6$), a **44e** 25 mg/kg group ($n = 6$), and a **44e** 50 mg/kg group ($n = 6$). Intragastric administration of normal saline, **1** and **18**, and **44e** was given for consecutive 19 days. Compared with the control group, mice in the latter three groups all presented a dose-dependent tumor growth inhibition (TGI). In particular, 50 mg/kg intervention with **44e** had the most pronounced TGI (63.8%) in the MDA-MB-231 xenograft tumor model (Figure 13A). No significant changes in mouse body weight and death were observed in both xenograft models treated with **44e**. However, **1** + **18** demonstrated weak toxicity measured by body weight loss in treated mice (Figure 13A,B), which may be attributed to side effects of drug combinations.⁵ As expected, there was a significant difference between the **44e** groups and the combination group. Compound **44e** was more effective in these *in vivo* studies. Its safety was slightly better than that of the **1** + **18** combination. In addition, **44e**'s skeleton is worthy of further study and may have a positive effect on the development of BRD4–CK2 inhibitors. Moreover, the discovery of a potent inhibitor of BRD4–CK2 might provide chemical tools to help further research the physiological function of the two targets. Taken together, **44e** is a promising potent anticancer candidate against TNBC without significant toxicities.

Next, the mouse heart, liver, spleen, lung, and kidney tissues were collected for HE staining. No significant morphologic or structural changes were observed (Figures S4 and S5). In addition, the immunohistochemical staining of Ki-67 in tumor tissue also indicated that **44e** could significantly inhibit the proliferation of MDA-MB-231 xenograft tumor model (Figure 14A). To further clarify the therapeutic index of **44e** *in vivo*, we detected positive expression of BRD4, CK2 (Figure 14A), and their downstream proteins c-Myc and p-AKT^{S129} (Figure 14B,C) in MDA-MB-231 xenograft tumor tissues by immunohistochemistry. Compared with those in the control group, the expression of c-Myc and p-AKT^{S129} was significantly reduced in **44e** treated groups. Increased expression of LC3II in TNBC tissues of the **44e** 25 mg/kg group and the **44e** 50 mg/kg group further highlighted the occurrence of autophagy. Consistently, Western blot analysis showed similar results of c-Myc and p-AKT^{S129} protein levels in xenograft tissues of TNBC (Figure 14D). Altogether, **44e** is a promising BRD4–CK2 dual inhibitor that exerts acceptable anticancer effect on TNBC.

CONCLUSION

In summary, this study aimed to identify small molecule BRD4–CK2 dual inhibitors that can be used as potential therapeutic for TNBC. An important interaction between BRD4 and CK2 in TNBC was validated through network analysis and systems biology. With available BRD4 (BD2) inhibitor and CK2 inhibitor cocrystal structures, key amino acids

were first discovered. Following the virtual screening workflow, the lead compound **26** was first obtained. Then, a series of quinazolinone core scaffold derivatives was synthesized through rational drug design, synthesis, and *in vivo* and *in vitro* biological evaluations. We for the first time synthesized a selective inhibitor, **44e**, that could target both BRD4 and CK2. Moreover, **44e** was able to inhibit the proliferation of MDA-MB-231 and MDA-MB-468 cells and dose-dependently induce apoptotic and autophagy-associated cell death. Its dose-dependent TGI effect was also illustrated in mouse xenograft models of TNBC. Interestingly, **44e** showed better anticancer activity, not only expanding the therapeutic index of BRD4 inhibitors but also reducing or preventing acquired resistance. Another advantage of **44e** may be the reduction of toxicity against normal breast cell lines and tissues. In addition, **44e** shows acceptable pharmacokinetic properties. Collectively, our findings support that the BRD4–CK2 dual inhibitor **44e** used in the treatment of TNBC is worthy of further development and analysis.

EXPERIMENTAL SECTION

Chemistry Methods.

All chemicals including reagents and solvents were purchased as analytically pure forms from commercial sources and used without further purification. HRESIMS data were obtained on a Q-TOF micro-mass spectrometer (Waters, USA). The ^1H and ^{13}C nuclear magnetic resonance (NMR) spectra were recorded on a Bruker AV 400 spectrometer (Bruker Co. Ltd., Germany). Chemical shifts are given in parts per million (ppm), and TMS was used as an internal standard. High-performance liquid chromatography (HPLC) was performed on a Shimadzu LC-20 instrument (Kyoto, Japan) with Agilent ZORBAX Eclipse Plus C18 Column (3.5 μm , 150 mm \times 4.6 mm) using MeOH/H₂O as the mobile phase at a flow rate of 1.0 mL/min. The purity of the synthesized compounds was over 95% by HPLC. The HPLC trace of each compound is provided in the Supporting Information (SI). Melting points of the compounds were obtained on a Melting Point M-565 (Buchi, Switzerland).

Preparation of intermediate 31a.—1-(2-Hydroxy-4,6-dimethoxyphenyl)ethan-1-one (2.5 g, 12.7 mmol) dissolved in 20 mL of pyridine was incubated in 5 mL of the alkaline reagent DBU for 0.5 h. Then, 3,5-dimethylbenzoyl chloride (3.5 g, 20.8 mmol) was slowly dropped into the mixture, and the mixture was heated at 80 °C for 1 h. After cooling to room temperature, the pH of the mixture was adjusted to 5.0 by adding HCl. Then the mixture was extracted three times using ethyl acetate (EA), and the organic layers were combined. The extraction was dried using anhydrous Na₂SO₄, followed by vacuum distillation, and purified by column chromatography (PE/EA = 30:1–5:1), and finally the intermediate **31a** (4 g, 95% yield) was obtained. ^1H NMR (400 MHz, DMSO-*d*₆), δ (ppm): 7.83 (2H, s), 7.58 (1H, s), 7.20 (1H, s), 6.56 (1H, s), 3.88 (3H, s), 3.82 (3H, s), 2.47 (3H, s), 2.33 (6H, s). HRMS (ESI)⁺ Calculated for C₁₉H₂₁O₅ [M + H]⁺ *m/z* 329.1389, found 329.1387.

Preparation of Intermediate 32a.—The intermediate **31a** (1 g, 3 mmol) was dissolved in 5 mL of pyridine at 50 °C for 1 h, and then KOH powder (0.4 g, 7 mmol) was added, and the mixture was heated at 80 °C for 1 h. After cooling to room temperature, the pH of the mixture was adjusted to 5.0 by adding HCl. Then the mixture was extracted three times

using EA, and the organic layers were combined. The extraction was dried using anhydrous Na_2SO_4 , followed by vacuum distillation, and intermediate **32a** (0.5 g, 50% yield) was obtained. It was not necessary to purify **32a**.

Preparation of 33a.—Intermediate **32a** (200 mg, 0.6 mmol) was dissolved in 4 mL of HOAc at 90 °C for 1 h. After vacuum concentration, 5 mL of 1% H_2SO_4 –HOAc (v/v) was added for reaction at 110 °C at 1 h. The reaction mixture was cooled in an ice–water mixture, and then the precipitant was filtered for purification by column chromatography ($\text{CH}_2\text{O}_2/\text{CH}_3\text{OH} = 80:1-1:1$). Finally, the target compound **33a** (120 mg, 76% yield) was obtained.

Synthesis routes of **33b–d** were similar to that of **33a**.

Preparation of 34a.—Compound **33a** (100 mg, 0.3 mmol) dissolved in 4 mL of methylbenzene was incubated with Lawesson's reagent (0.2 mmol) at 110 °C for 4 h. After concentration under vacuum conditions and purification by column chromatography ($\text{CH}_2\text{Cl}_2/\text{CH}_3\text{OH} = 100:1-1:1$), the target compound **34a** (55 mg, 56% yield) was obtained.

Synthesis routes of **34b,c** were similar to that of **34a**.

Preparation of 35a.—3,5-Dimethoxyaniline (8 g, 52 mmol) was dissolved in 100 mL of Et_2O and stirred at 0 °C. After addition of 25 mL of saturated HCl– Et_2O solution and reaction for 0.5 h, the mixture was then reacted at room temperature for 12 h. A total of 7 g of the hydrochloride was filtered and collected. Later, the hydrochloride (4 g, 21 mmol) was dissolved in 6 mL of $(\text{COCl})_2$ and refluxed at 160 °C for 2.5 h. After vacuum concentration, 20 mL of MeOH was added at 0 °C, followed by heating for 1 h, filtration, and washing. At last, intermediate **35a** (5 g, 65% yield) was obtained. ^1H NMR (400 MHz, CDCl_3), δ (ppm): 11.06 (1H, s), 6.41 (2H, s), 5.81 (2H, s), 3.94 (3H, s), 3.76 (3H, s). HRMS (ESI)⁺ Calculated for $\text{C}_{10}\text{H}_{10}\text{NO}_4$ [M + H]⁺ m/z 208.0611, found 208.0610.

Preparation of 36a.—Intermediate **35a** was dissolved in 20 mL of 33% NaOH aqueous solution and reacted with 5 mL of 30% H_2O_2 aqueous solution. After refluxing at 80 °C for 1 h, the solution was cooled and then incubated in 20 mL of $\text{Na}_2\text{S}_2\text{O}_3$ solution. The pH of the mixture was adjusted to 8.0 by addition of concentrated HCl, and then it was adjusted to 5.0 by addition of HOAc. The precipitant was washed using water and dried, and thus the intermediate **36a** (1.3 g, 34% yield) was obtained. ^1H NMR (400 MHz, CDCl_3), δ (ppm): 11.06 (1H, s), 6.42 (2H, s), 5.81 (2H, s), 3.94 (3H, s), 3.76 (3H, s). HRMS (ESI)⁺ Calculated for $\text{C}_9\text{H}_{12}\text{NO}_4$ [M + H]⁺ m/z 198.0766, found 198.0760.

Preparation of 37a.—EDCI (0.75 g, 3.8 mmol), HOBt (0.50 g, 3.8 mmol), and NMM (0.38 g, 3.8 mmol) were added in 2-amino-4,6-dimethoxybenzoic acid (0.60 g, 3.0 mmol) dissolved in 20 mL of THF and reacted at room temperature for 15 min. Later, ammonium hydroxide 50% (v/v) aqueous solution was added and reacted for 12 h. After dilution by addition of 8 mL of H_2O and extraction using CH_2Cl_2 (30 mL \times 3), the extract was subjected to vacuum distillation and purified by column chromatography (DCM/MeOH = 100:1–60:1), and finally the intermediate **37a** (0.46 g, 85% yield) was obtained. ^1H NMR

(400 MHz, DMSO- d_6), δ (ppm): 7.46 (1H, s), 7.01 (1H, s), 6.88 (2H, s), 5.89 (1H, d, J = 2.4 Hz), 5.75 (1H, d, J = 2.4 Hz), 3.75 (3H, s), 3.69 (3H, s). HRMS (ESI)⁺ Calculated for C₉H₁₃N₂O₃ [M + H]⁺ m/z 197.0926, found 197.0924.

Compound **37c** was synthesized based on a similar route, and **37b** was commercially purchased.

General Procedures for Synthesizing 38a–s and the Lead Compound 26.—

Intermediates **37a–c** (0.9 mmol, 1 equiv) and benzaldehyde derivatives (0.9 mmol, 1 equiv) were dissolved in 15 mL of DMAc, in which NaHSO₄ (1.05 mmol, 1.2 equiv) and PTSA (0.22 mmol, 0.24 equiv) were added. The reaction solution was stirred and refluxed at 120 °C for 4–8 h. Later, 100 mL of \hat{O} was added, and the precipitant was filtered. The solid was purified by flash chromatography on silica gel (CH₂O₂/CH₃OH = 80:1–10:1), and finally **38a–s** and the lead compound **26** (41–65% synthetic yield) were obtained.

Preparation of Intermediate 39a.—*tert*-Butyl bromoacetate (3.0 mL, 1.2 equiv) and *p*-hydroxybenzaldehyde (2.5 g, 1 equiv) were dissolved in 10 mL of DMF, in which 5.2 g of K₂O₃ was added for 3 h reaction at 80 °C. Later, 80 mL of H₂O was added, and the precipitant was filtered and dried. The solid was purified by flash chromatography on silica gel (CH₂Cl₂/CH₃OH = 80:1–5:1), and finally intermediate **39a** (2.6 g, 57% yield) was obtained. It was not necessary to purify **39a**. ¹H NMR (400 MHz, CD₃OD), δ (ppm): 9.84 (1H, s), 7.86 (2H, d, J = 8.8 Hz), 7.06 (2H, d, J = 8.8 Hz), 4.71 (2H, s), 1.48 (9H, s). HRMS (ESI)⁺ Calculated for C₁₃H₁₇O₃ [M + H]⁺ m/z 221.1178, found 221.1170.

Synthesis routes of **39b,c** were similar to that of **39a**.

Preparation of Intermediate 40a.—The intermediate **39a** (2 g, 9 mmol) was dissolved in 5 mL of CH₂Cl₂ and reacted with 1.5 mL of TFA at room temperature for 2 h. The reaction solution was subjected to vacuum concentration, and the white solid **40a** (1.2 g, 74% of synthesis yield) was obtained. It was not necessary to purify **40a**. ¹H NMR (400 MHz, CD₃OD), δ (ppm): 12.28 (1H, s), 9.82 (1H, s), 7.84 (2H, d, J = 8.8 Hz), 7.04 (2H, d, J = 8.8 Hz), 3.68 (2H, s). HRMS (ESI)⁺ Calculated for C₉H₉O₄ [M + H]⁺ m/z 181.0501, found 181.0507.

Synthesis routes of **40b,c** were similar to that of **40a**.

Preparation of 42a–j, 43a–q, and 44a–n.—Intermediates **40a–c** (0.9 mmol, 1 equiv) and benzaldehyde derivatives (0.9 mmol, 1 equiv) were dissolved in 15 mL of DMAc, in which NaHSO₄ (1.05 mmol, 1.2 equiv) and PTSA (0.22 mmol, 0.24 equiv) were added. The reaction solution was stirred and refluxed at 120 °C for 4–8 h. Later, 100 mL of H₂O was added, and the precipitant was filtered. The solid was purified by flash chromatography on silica gel (CH₂Cl₂/CH₃OH = 30:1–1:1), and finally **41a–h** (42–66% synthetic yield) were obtained. Intermediates **41a–h** (0.42 mmol, 1.2 equiv) were dissolved in 3 mL of DMF, in which HOBt (0.54 mmol, 1.3 equiv) was added and stirred at 0 °C for 10 min. Subsequently, EDCI (0.54 mmol, 1.3 equiv), reactants containing amino substitutions, and TEA (1.5 mmol, 3.5 equiv) were added and reacted at 0 °C for 1 h. The reaction mixture was further reacted

at room temperature for 24 h. Later, 80 mL of H₂O was added, and the precipitant was filtered. The solid was purified by flash chromatography on silica gel (CH₂Cl₂/CH₃OH = 30:1–1:1), and finally end products **42a–j**, **43a–q**, and **44a–n** (43–66% synthetic yield) were obtained.

2-(3,5-Dimethylphenyl)-5,7-dimethoxy-4H-chromen-4-one (33a).—White powder, mp 214–216 °C, yield 50.1%. ¹H NMR (400 MHz, DMSO-*d*₆), δ (ppm): 7.65 (2H, s), 7.19 (1H, s), 6.87 (1H, d, *J* = 2.4 Hz), 6.70 (1H, s), 6.49 (1H, d, *J* = 2.4 Hz), 3.90 (3H, s), 3.82 (3H, s), 2.35 (6H, s). ¹³C NMR (100 MHz, CF₃COOD), δ (ppm): 178.6, 175.7, 173.3, 163.3, 162.1, 143.2(2), 140.1, 130.7, 127.8(2), 104.6, 103.4, 102.5, 96.8, 59.9, 58.8, 22.1(2). HRMS (ESI)⁺ Calculated for C₁₉H₁₉O₄ [M + H]⁺ *m/z* 311.1283, found 311.1288.

2-(3,5-Dimethylphenyl)-6-methoxy-4H-chromen-4-one (33b).—White powder, mp 210–212 °C, yield 55.7%. ¹H NMR (400 MHz, CDCl₃), δ (ppm): 7.58 (1H, d, *J* = 2.4 Hz), 7.50–7.52 (3H, m), 7.28 (1H, dd, *J* = 8.0, 2.4 Hz), 7.16 (1H, s), 6.78 (1H, s), 3.90 (3H, s), 2.40 (6H, s). ¹³C NMR (100 MHz, CDCl₃), δ (ppm): 178.5, 163.8, 157.1, 151.3, 138.8(2), 133.4, 131.9, 124.7, 124.2(2), 123.8, 119.6, 106.9, 56.1, 21.5(2). HRMS (ESI)⁺ Calculated for C₁₈H₁₇O₃ [M + H]⁺ *m/z* 281.1178, found 281.1184.

6-Methoxy-2-(2-methoxyphenyl)-4H-chromen-4-one (33c).—White powder, mp 180–183 °C, yield 58.4%. ¹H NMR (400 MHz, DMSO-*d*₆), δ (ppm): 7.90 (1H, dd, *J* = 8.4, 2.0 Hz), 7.68 (1H, dd, *J* = 8.4, 2.0 Hz), 7.56 (1H, td, *J* = 8.0, 2.4 Hz), 7.39–7.42 (1H, m), 7.25 (1H, d, *J* = 8.4 Hz), 7.15 (1H, td, *J* = 8.0, 2.4 Hz), 6.91 (1H, s), 3.92 (3H, s), 3.86 (3H, s). ¹³C NMR (100 MHz, CDCl₃), δ (ppm): 178.9, 160.8, 158.1, 156.9, 151.5, 132.5, 129.4, 124.5, 123.8, 121.1, 120.9, 119.6, 112.0, 111.9, 104.8, 56.1, 55.8. HRMS (ESI)⁺ Calculated for C₁₇H₁₅O₄ [M + H]⁺ *m/z* 283.0970, found 283.0963.

6-Methoxy-2-(2-methoxyphenyl)-4H-chromen-4-one (33d).—White powder, mp 192–195 °C, yield 51.2%. ¹H NMR (400 MHz, CDCl₃), δ (ppm): 8.36 (1H, d, *J* = 2.4 Hz), 7.91 (2H, dd, *J* = 8.4, 2.4 Hz), 7.78 (1H, dd, *J* = 8.4, 2.4 Hz), 7.51–7.56 (3H, m), 7.47 (1H, d, *J* = 8.4 Hz), 6.83 (1H, s). ¹³C NMR (100 MHz, CDCl₃), δ (ppm): 177.2, 163.9, 155.2, 136.9, 132.0, 131.5, 129.3(2), 128.5, 126.5, 125.4(2), 120.2, 118.8, 107.7, 104.8, 56.1, 55.8. HRMS (ESI)⁺ Calculated for C₁₅H₁₀BrO₂ [M + H]⁺ *m/z* 300.9864, found 300.9866.

6-Methoxy-2-(2-methoxyphenyl)-4H-chromen-4-one (34a).—White powder, mp 211–213 °C, yield 53.4%. ¹H NMR (400 MHz, CDCl₃), δ (ppm): 7.54 (1H, s), 7.51 (2H, s), 7.13 (1H, s), 6.58 (1H, d, *J* = 2.4 Hz), 6.40 (1H, d, *J* = 2.4 Hz), 3.93 (3H, s), 3.91 (3H, s), 2.38 (6H, s). ¹³C NMR (100 MHz, CDCl₃), δ (ppm): 200.3, 164.0, 161.6, 155.9, 150.3, 138.8(2), 133.2, 130.8, 124.1(2), 122.5, 117.9, 97.0, 92.9, 56.0(2), 21.5(2). HRMS (ESI)⁺ Calculated for C₁₉H₁₉O₃S [M + H]⁺ *m/z* 327.1055, found 327.1049.

6-Methoxy-2-(2-methoxyphenyl)-4H-chromen-4-one (34b).—White powder, mp 223–225 °C, yield 48.4%. ¹H NMR (400 MHz, CDCl₃), δ (ppm): 7.95–7.99 (3H, m), 7.81 (1H, s), 7.49–7.55 (4H, m), 7.32 (1H, dd, *J* = 8.4, 2.4 Hz), 3.93 (1H, s). ¹³C NMR (100 MHz, CDCl₃), δ (ppm): 200.9, 158.0, 154.2, 146.5, 131.8, 131.3, 130.7, 129.3(2), 126.6(2),

124.6, 120.0, 119.9, 107.9, 56.1. HRMS (ESI)⁺ Calculated for C₁₆H₁₃O₂S [M + H]⁺ *m/z* 269.0636, found 269.0628.

6-Methoxy-2-(2-methoxyphenyl)-4H-chromen-4-one (34c).—Light yellow solid, mp 193–195 °C, yield 55.1%. ¹H NMR (400 MHz, CDCl₃), δ (ppm): 8.15 (1H, s), 8.01 (1H, d, *J* = 3.2 Hz), 7.92 (1H, dd, *J* = 8.0, 2.4 Hz), 7.46–7.51 (2H, m), 7.30 (1H, dd, *J* = 8.0, 2.4 Hz), 7.10 (1H, td, *J* = 3.2 Hz), 7.03 (1H, d, *J* = 8.4 Hz), 3.95 (3H, s), 3.93 (3H, s). ¹³C NMR (100 MHz, CDCl₃), δ (ppm): 201.0, 158.2, 157.9, 152.4, 146.8, 132.8, 130.6, 129.7, 124.9, 124.5, 121.1, 120.3, 119.9, 112.0, 107.9, 56.0, 55.9. HRMS (ESI)⁺ Calculated for C₁₇H₁₅O₃S [M + H]⁺ *m/z* 299.0742, found 299.0750.

5,7-Dimethoxy-2-(p-tolyl)quinazolin-4(3H)-one (38a).—White powder, mp 254–256 °C, yield 56.1%. ¹H NMR (400 MHz, DMSO-*d*₆), δ (ppm): 11.95 (1H, s), 8.07 (2H, d, *J* = 8.0 Hz), 7.32 (2H, d, *J* = 8.0 Hz), 6.73 (1H, d, *J* = 2.0 Hz), 6.52 (1H, d, *J* = 2.0 Hz), 3.88 (3H, s), 3.84 (3H, s), 2.37 (3H, s). ¹³C NMR (100 MHz, DMSO-*d*₆), δ (ppm): 164.2, 160.9, 159.8, 153.0, 152.8, 141.4, 129.5, 129.1(2), 127.5(2), 104.7, 101.2, 97.6, 55.9, 55.6, 21.0. HRMS (ESI)⁺ Calculated for C₁₇H₁₇N₂O₃ [M + H]⁺ *m/z* 297.1239, found 297.1242.

2-(4-Bromo-3,5-dimethylphenyl)-5,7-dimethoxyquinazolin-4(3H)-one (38b).—White powder, mp 261–263 °C, yield 49.5%. ¹H NMR (400 MHz, DMSO-*d*₆), δ (ppm): 11.95 (1H, s), 7.99 (2H, s), 6.76 (1H, s), 6.54 (1H, s), 3.89 (3H, s), 3.85 (3H, s), 2.45 (6H, s). ¹³C NMR (100 MHz, CDCl₃), δ (ppm): 164.8, 161.5, 160.1, 153.1, 152.7, 138.6(2), 131.2, 130.8, 127.9(2), 105.2, 101.6, 98.4, 56.5, 56.2, 23.9(2). HRMS (ESI)⁺ Calculated for C₁₈H₁₈BrN₂O₃ [M + H]⁺ *m/z* 391.0480, found 391.0472.

2-(4-Aminophenyl)-5,7-dimethoxyquinazolin-4(3H)-one (38c).—White powder, mp 244–246 °C, yield 55.2%. ¹H NMR (400 MHz, DMSO-*d*₆), δ (ppm): 7.94 (1H, s), 7.91 (1H, s), 6.66 (1H, d, *J* = 4.8 Hz), 6.63 (2H, d, *J* = 2.0 Hz), 6.45 (1H, d, *J* = 4.0 Hz), 3.88 (3H, s), 3.83 (3H, s). ¹³C NMR (100 MHz, DMSO-*d*₆), δ (ppm): 164.2, 161.0(2), 159.6, 153.3, 152.4, 129.3(2), 117.3, 113.0(2), 103.9, 99.9, 96.8, 55.9, 55.6. HRMS (ESI)⁺ Calculated for C₁₆H₁₆N₃O₃ [M + H]⁺ *m/z* 298.1192, found 298.1184.

2-(4-Hydroxy-3,5-dimethylphenyl)-5,7-dimethoxyquinazolin-4(3H)-one (38d).—Light yellow solid, mp 232–234 °C, yield 42.9%. ¹H NMR (400 MHz, DMSO-*d*₆), δ (ppm): 7.81 (2H, s), 6.75 (1H, d, *J* = 2.0 Hz), 6.54 (1H, d, *J* = 2.0 Hz), 3.89 (3H, s), 3.85 (3H, s), 2.24 (6H, s). ¹³C NMR (100 MHz, DMSO-*d*₆), δ (ppm): 164.3, 161.0, 159.6, 156.9, 153.2, 152.1, 128.2(2), 124.2(2), 121.9, 104.0, 100.3, 97.3, 56.0, 55.7, 16.7(2). HRMS (ESI)⁺ Calculated for C₁₈H₁₉N₂O₄ [M + H]⁺ *m/z* 327.1345, found 327.1350.

2-(3-Bromo-4-hydroxyphenyl)-5,7-dimethoxyquinazolin-4(3H)-one (38e).—White powder, mp 246–249 °C, yield 56.0%. ¹H NMR (400 MHz, DMSO-*d*₆), δ (ppm): 11.1 (1H, s), 8.37 (1H, d, *J* = 2.4 Hz), 8.04 (1H, dd, *J* = 8.8, 2.4 Hz), 6.73 (1H, d, *J* = 2.4 Hz), 6.52 (1H, d, *J* = 2.4 Hz), 3.89 (3H, s), 3.84 (3H, s), 2.24 (6H, s). ¹³C NMR (100 MHz, DMSO-*d*₆), δ (ppm): 164.4, 161.0, 159.5, 157.4, 153.9, 151.9, 132.7, 128.6, 123.6, 116.0, 109.5, 104.3, 100.5, 97.6, 56.0, 55.7. HRMS (ESI)⁺ Calculated for C₁₆H₁₄BrN₂O₄ [M + H]⁺ *m/z* 379.0116, found 379.0102.

N-(4-(5,7-Dimethoxy-4-oxo-1,4-dihydroquinazolin-2-yl)phenyl)acetamide (38f).

—White powder, mp 245–247 °C, yield 64.3%. ¹H NMR (400 MHz, DMSO-*d*₆), δ (ppm): 11.91 (1H, s), 10.23 (1H, s), 8.12 (2H, d, *J* = 8.8 Hz), 7.71 (1H, d, *J* = 8.8 Hz), 6.71 (1H, d, *J* = 2.4 Hz), 6.51 (1H, d, *J* = 2.4 Hz), 3.88 (3H, s), 3.84 (3H, s), 2.08 (3H, s). ¹³C NMR (100 MHz, DMSO-*d*₆), δ (ppm): 168.8, 164.2, 161.0, 159.8, 153.1, 152.4, 142.2, 128.4(2), 126.4, 118.3(2), 104.6, 101.1, 97.5, 55.9, 55.6. HRMS (ESI)⁺ Calculated for C₁₈H₁₈N₃O₄ [M + H]⁺ *m/z* 340.1297, found 340.1292.

5,7-Dimethoxy-2-(*m*-tolyl)quinazolin-4(3H)-one (38g).

—White powder, mp 237–239 °C, yield 52.9%. ¹H NMR (400 MHz, DMSO-*d*₆), δ (ppm): 11.94 (1H, s), 8.01 (1H, s), 7.93–7.95 (1H, m), 7.39–7.41 (2H, m), 6.76 (1H, d, *J* = 2.4 Hz), 6.53 (1H, d, *J* = 2.4 Hz), 3.89 (3H, s), 3.85 (3H, s), 2.39 (3H, s). ¹³C NMR (100 MHz, DMSO-*d*₆ + CF₃COOD), δ (ppm): 166.0, 162.1, 157.4(2), 143.8, 138.9, 135.0, 130.0, 129.2, 126.9, 126.7, 103.4, 99.0, 96.1, 56.7, 56.3, 20.9. HRMS (ESI)⁺ Calculated for C₁₇H₁₇N₂O₃ [M + H]⁺ *m/z* 297.1239, found 297.1237.

5,7-Dimethoxy-2-(2-methoxyphenyl)quinazolin-4(3H)-one (38h).

—White powder, mp 257–260 °C, yield 48.2%. ¹H NMR (400 MHz, DMSO-*d*₆), δ (ppm): 11.51 (1H, s), 7.74 (1H, dd, *J* = 11.6, 2.4 Hz), 7.52 (1H, td, *J* = 11.6, 2.4 Hz), 7.18 (1H, d, *J* = 11.6 Hz), 7.08 (1H, t, *J* = 11.6 Hz), 6.71 (1H, d, *J* = 2.4 Hz), 6.54 (1H, d, *J* = 2.4 Hz), 3.87 (3H, s), 3.86 (3H, s), 3.84 (3H, s). ¹³C NMR (100 MHz, DMSO-*d*₆), δ (ppm): 164.1, 160.9, 158.8, 157.2, 153.3, 152.9, 132.3, 130.3, 122.1, 120.4, 111.9, 104.9, 101.2, 97.7, 56.0, 55.8, 55.6. HRMS (ESI)⁺ Calculated for C₁₇H₁₇N₂O₄ [M + H]⁺ *m/z* 313.1188, found 313.1186.

5,7-Dimethoxy-2-(3-methoxyphenyl)quinazolin-4(3H)-one (38i).

—Light yellow solid, mp 225–227 °C, yield 41.0%. ¹H NMR (400 MHz, DMSO-*d*₆), δ (ppm): 12.03 (1H, s), 7.77 (1H, d, *J* = 8.0 Hz), 7.73 (1H, s), 7.43 (1H, t, *J* = 8.0 Hz), 7.12 (1H, dd, *J* = 8.0, 2.4 Hz), 6.76 (1H, d, *J* = 2.4 Hz), 6.56 (1H, d, *J* = 2.4 Hz), 3.89 (3H, s), 3.85 (6H, s). ¹³C NMR (100 MHz, DMSO-*d*₆ + CF₃COOD), δ (ppm): 166.0, 162.1, 159.6, 157.5, 157.0, 144.0, 130.2, 128.1, 121.8, 120.4, 114.6, 103.5, 99.1, 96.3, 56.8, 56.3, 55.8. HRMS (ESI)⁺ Calculated for C₁₇H₁₆NaN₂O₄ [M + Na]⁺ *m/z* 335.1008, found 335.0999.

2-(*p*-Tolyl)quinazolin-4(3H)-one (38j).

—White powder, mp 244–246 °C, yield 51.7%. ¹H NMR (400 MHz, DMSO-*d*₆), δ (ppm): 12.44 (1H, s), 8.14 (1H, dd, *J* = 8.0, 2.0 Hz), 8.10 (2H, d, *J* = 8.0 Hz), 7.82 (1H, td, *J* = 8.0, 2.0 Hz), 7.12 (1H, dd, *J* = 8.0, 2.0 Hz), 7.50 (1H, t, *J* = 8.0 Hz), 7.35 (1H, d, *J* = 8.0 Hz), 2.39 (3H, s). ¹³C NMR (100 MHz, DMSO-*d*₆), δ (ppm): 162.2, 152.2, 148.8, 141.4, 134.5, 129.7, 129.2(2), 127.7(2), 127.4, 126.4, 125.8, 120.9, 21.0. HRMS (ESI)⁺ Calculated for C₁₃H₁₃N₂O [M + H]⁺ *m/z* 237.1028, found 237.1029.

N-(4-(4-Oxo-1,4-dihydroquinazolin-2-yl)phenyl)acetamide (38k).

—White powder, mp 231–234 °C, yield 47.0%. ¹H NMR (400 MHz, DMSO-*d*₆), δ (ppm): 12.39 (1H, s), 10.22 (1H, s), 8.12–8.16 (3H, m), 7.81 (1H, t, *J* = 8.0 Hz), 7.82 (1H, td, *J* = 8.0, 2.4 Hz), 7.69–7.75 (3H, m), 7.49 (1H, td, *J* = 8.0, 2.4 Hz), 2.09 (3H, s). ¹³C NMR (100 MHz, DMSO-*d*₆), δ (ppm): 168.8, 162.2, 158.8, 148.9, 142.2, 134.5, 128.5(2), 127.3, 126.8, 126.2,

125.8, 120.8, 118.4(2), 24.2. HRMS (ESI)⁺ Calculated for C₁₆H₁₄N₃O₂ [M + H]⁺ *m/z* 280.1086, found 280.1090.

2-(4-Hydroxy-3,5-dimethoxyphenyl)quinazolin-4(3H)-one (38l).—White powder, mp 246–248 °C, yield 60.2%. ¹H NMR (400 MHz, DMSO-*d*₆), δ (ppm): 12.37 (1H, s), 9.11 (1H, s), 8.12 (1H, dd, *J* = 8.0, Hz), 7.81 (1H, td, *J* = 8.0, 2.4 Hz), 7.71 (1H, d, *J* = 8.0 Hz), 7.57 (2H, s), 7.47 (1H, td, *J* = 8.0, 2.4 Hz), 3.88 (6H, s). ¹³C NMR (100 MHz, DMSO-*d*₆), δ (ppm): 162.4, 152.0, 148.9, 147.8(2), 139.1, 134.5, 127.3, 126.0, 125.8, 122.1, 120.0, 105.3(2), 56.2(2). HRMS (ESI)⁺ Calculated for C₁₆H₁₅N₂O₄ [M + H]⁺ *m/z* 299.1032, found 299.1031.

N-(4-(6-Methoxy-4-oxo-1,4-dihydroquinazolin-2-yl)phenyl)-acetamide (38m).—White powder, mp 252–255 °C, yield 62.1%. ¹H NMR (400 MHz, DMSO-*d*₆), δ (ppm): 12.36 (1H, s), 10.20 (1H, s), 8.12 (2H, d, *J* = 8.4 Hz), 7.72 (2H, d, *J* = 8.4 Hz), 7.65 (1H, d, *J* = 8.4 Hz), 7.52 (1H, d, *J* = 2.4 Hz), 7.51 (1H, dd, *J* = 8.8, 2.4 Hz), 3.88 (3H, s), 2.09 (3H, s). ¹³C NMR (100 MHz, DMSO-*d*₆), δ (ppm): 168.6, 161.9, 157.4, 149.5, 143.2, 141.7, 128.9, 128.1(2), 126.8, 123.9, 121.4, 118.3(2), 105.7, 55.5, 24.0. HRMS (ESI)⁺ Calculated for C₁₇H₁₆N₃O₃ [M + H]⁺ *m/z* 310.1192, found 310.1193.

2-(4-Hydroxy-3,5-dimethoxyphenyl)-6-methoxyquinazolin-4(3H)-one (38n).—Light yellow solid, mp 261–263 °C, yield 65.0%. ¹H NMR (400 MHz, DMSO-*d*₆), δ (ppm): 7.68 (1H, d, *J* = 8.8 Hz), 7.53 (3H, s), 7.42 (1H, dd, *J* = 8.8, 2.8 Hz), 3.89 (9H, s). ¹³C NMR (100 MHz, DMSO-*d*₆), δ (ppm): 162.0, 157.5, 150.3(2), 147.9, 142.5, 139.0, 128.4, 124.2, 121.7, 121.3, 106.0, 105.2(2), 56.2, 55.7, 55.6. HRMS (ESI)⁺ Calculated for C₁₇H₁₇N₂O₅ [M + H]⁺ *m/z* 329.1137, found 329.1135.

6-Methoxy-2-(*p*-tolyl)quinazolin-4(3H)-one (38o).—White powder, mp 249–251 °C, yield 64.8%. ¹H NMR (400 MHz, DMSO-*d*₆), δ (ppm): 8.07 (2H, d, *J* = 8.0 Hz), 7.68 (1H, d, *J* = 8.0 Hz), 7.54 (1H, d, *J* = 2.4 Hz), 7.43 (1H, dd, *J* = 8.8, 2.4 Hz), 7.34 (1H, d, *J* = 8.0 Hz), 3.89 (3H, s), 2.39 (3H, s). ¹³C NMR (100 MHz, DMSO-*d*₆), δ (ppm): 162.0, 157.7, 150.3, 142.8, 141.2, 129.7, 129.2(2), 128.8, 127.5(2), 124.1, 121.6, 105.9, 55.6, 21.0. HRMS (ESI)⁺ Calculated for C₁₆H₁₅N₂O₂ [m + h]⁺ *m/z* 267.1134, found 267.1137.

4-(5,7-Dimethoxy-4-oxo-1,4-dihydroquinazolin-2-yl)benzoic Acid (38p).—White powder, mp 217–219 °C, yield 58.9%. ¹H NMR (400 MHz, DMSO-*d*₆), δ (ppm): 13.19 (1H, s), 12.17 (1H, s), 8.26 (2H, d, *J* = 8.8 Hz), 8.05 (2H, d, *J* = 8.8 Hz), 6.78 (1H, d, *J* = 2.4 Hz), 6.56 (1H, d, *J* = 2.4 Hz), 3.89 (3H, s), 3.86 (3H, s), 3.36 (4H, t, *J* = 6.4 Hz), 1.96–1.99 (4H, m). ¹³C NMR (100 MHz, DMSO-*d*₆), δ (ppm): 166.8, 164.3, 161.0, 159.7, 152.8, 152.2, 136.2, 133.0, 129.4(2), 127.9(2), 104.9, 101.5, 98.1, 56.0, 55.7. HRMS (ESI)⁺ Calculated for C₁₇H₁₅N₂O₅ [M + Na]⁺ *m/z* 349.0800, found 349.0782.

2-(3-(5,7-Dimethoxy-4-oxo-1,4-dihydroquinazolin-2-yl)-phenoxy)acetic Acid (38q).—White powder, mp 209–211 °C, yield 45.2%. ¹H NMR (400 MHz, DMSO-*d*₆), δ (ppm): 12.04 (1H, s), 7.79 (1H, d, *J* = 8.0 Hz), 7.71 (1H, s), 7.11 (1H, dd, *J* = 8.0, 2.4 Hz), 6.75 (1H, d, *J* = 2.4 Hz), 6.54 (1H, d, *J* = 2.4 Hz), 4.77 (2H, s), 3.89 (3H, s), 3.84 (3H, s). ¹³C NMR (100 MHz, DMSO-*d*₆), δ (ppm): 164.7, 161.4, 160.2, 158.4, 153.2, 152.9,

149.3, 133.9, 130.1, 120.8, 118.7, 113.3, 105.2, 101.8, 98.3, 60.3, 56.4, 56.1. HRMS (ESI)⁺ Calculated for C₁₈H₁₇N₂O₆ [M + H]⁺ *m/z* 357.1087, found 357.1077.

2-(2-(5,7-Dimethoxy-4-oxo-1,4-dihydroquinazolin-2-yl)-phenoxy)acetic Acid (38r).—Light yellow solid, mp 235–237 °C, yield 47.1%. ¹H NMR (400 MHz, DMSO-*d*₆), δ (ppm): 7.88 (1H, dd, *J* = 8.0, 2.4 Hz), 7.77 (1H, dt, *J* = 8.0, 2.4 Hz), 7.30–7.36 (2H, m), 6.89 (1H, d, *J* = 2.0 Hz), 6.76 (1H, d, *J* = 2.0 Hz), 4.96 (2H, s), 3.99 (3H, s), 3.97 (3H, s). ¹³C NMR (100 MHz, DMSO-*d*₆ + CF₃COOD), δ (ppm): 160.0, 163.2, 158.4, 155.0, 154.8, 152.3, 151.9, 138.2, 132.2, 126.8, 118.4, 109.8, 98.7, 95.1, 90.7, 61.8, 51.8, 51.551.8, 51.5. HRMS (ESI)⁺ Calculated for C₁₈H₁₆N_aN₂O₆ [M + Na]⁺ *m/z* 379.0906, found 379.0897.

Methyl 2-(4-(5,7-Dimethoxy-4-oxo-1,4-dihydroquinazolin-2-yl)-phenoxy)acetate (38s).—White powder, mp 224–227 °C, yield 60.3%. ¹H NMR (400 MHz, DMSO-*d*₆), δ (ppm): 8.13 (2H, d, *J* = 8.8 Hz), 7.08 (2H, d, *J* = 8.8 Hz), 6.72 (1H, d, *J* = 2.0 Hz), 6.52 (1H, d, *J* = 2.0 Hz), 4.92 (2H, s), 3.89 (3H, s), 3.85 (3H, s), 3.71 (3H, s). ¹³C NMR (100 MHz, DMSO-*d*₆), δ (ppm): 168.9, 164.4, 161.1, 160.4, 159.6, 152.9, 129.6(2), 124.4, 114.6(2), 104.4, 100.4, 97.6, 64.6, 56.1, 55.7, 51.9. HRMS (ESI)⁺ Calculated for C₁₉H₁₈N_aN₂O₆ [M + Na]⁺ *m/z* 393.1063, found 393.1058.

2-(4-(5,7-Dimethoxy-4-oxo-1,4-dihydroquinazolin-2-yl)-phenoxy)acetic Acid (26).—White powder, mp 251–253 °C, yield 44.2%. ¹H NMR (400 MHz, DMSO-*d*₆), δ (ppm): 11.97 (1H, s), 8.13 (2H, d, *J* = 8.8 Hz), 7.04 (2H, d, *J* = 8.8 Hz), 6.72 (1H, d, *J* = 2.0 Hz), 6.51 (1H, d, *J* = 2.0 Hz), 4.79 (2H, s), 3.88 (3H, s), 3.84 (3H, s). ¹³C NMR (100 MHz, DMSO-*d*₆), δ (ppm): 169.9, 168.6, 164.3, 161.0, 160.4, 159.8, 152.6, 129.4(2), 124.7, 114.5(2), 104.5, 100.9, 97.5, 64.5, 56.0, 55.6. HRMS (ESI)⁺ Calculated for C₁₈H₁₆N_aN₂O₆ [M + Na]⁺ *m/z* 379.0906, found 379.0910.

2-(4-(5,7-Dimethoxy-4-oxo-1,4-dihydroquinazolin-2-yl)-phenoxy)-N-morpholinoacetamide (42a).—Light yellow solid, mp 262–264 °C, yield 54.4%. ¹H NMR (400 MHz, DMSO-*d*₆), δ (ppm): 9.29 (1H, s), 8.90 (1H, s), 8.09–8.15 (2H, m), 7.08 (1H, d, *J* = 8.8 Hz), 7.02 (1H, d, *J* = 8.8 Hz), 6.71–6.73 (1H, m), 6.53 (1H, d, *J* = 2.4 Hz), 5.0 (1H, s), 4.56 (2H, s), 3.89 (3H, s), 3.85 (3H, s), 3.62 (4H, t, *J* = 4.4 Hz), 2.79 (4H, t, *J* = 4.4 Hz). ¹³C NMR (100 MHz, DMSO-*d*₆ + CF₃COOD), δ (ppm): 170.0, 167.2, 166.5, 164.1, 163.1, 157.8, 143.1, 133.0, 132.8, 118.9, 116.4, 116.3, 103.7, 99.8, 95.8, 67.2, 67.1, 65.6, 57.2, 57.0, 56.8, 56.0. HRMS (ESI)⁺ Calculated for C₂₂H₂₄N_aN₄O₆ [M + Na]⁺ *m/z* 463.1594, found 463.1601.

2-(4-(5,7-Dimethoxy-4-oxo-1,4-dihydroquinazolin-2-yl)-2,6-dimethylphenoxy)-N-morpholinoacetamide (42b)—White powder, mp 265–267 °C, yield 48.1%. ¹H NMR (400 MHz, DMSO-*d*₆), δ (ppm): 9.39 (1H, s), 8.81 (1H, s), 7.92 (2H, s), 6.69 (1H, s), 6.45 (1H, s), 4.60 (1H, s), 4.25 (2H, s), 3.87 (3H, s), 3.63 (3H, s), 3.64 (4H, t, *J* = 4.4 Hz), 2.82 (4H, t, *J* = 4.4 Hz), 2.30 (6H, s). ¹³C NMR (100 MHz, DMSO-*d*₆), δ (ppm): 169.3, 164.8, 163.6, 160.7, 158.1, 157.4, 153.7, 130.4(2), 128.3(2), 128.2, 105.0, 100.7, 97.0, 70.5, 65.9(2), 55.8, 55.5, 54.5(2), 16.1(2). HRMS (ESI)⁺ Calculated for C₂₄H₂₉N₄O₆ [M + H]⁺ *m/z* 469.2087, found 469.2103.

2-(4-(5,7-Dimethoxy-4-oxo-1,4-dihydroquinazolin-2-yl)-phenoxy)-N-((tetrahydro-2H-pyran-4-yl)methyl)acetamide (42c).—White powder, mp 253–255 °C, yield 60.3%. ¹H NMR (400 MHz, DMSO-*d*₆), δ (ppm): 11.93 (1H, s), 8.16 (3H, d, *J* = 8.8 Hz), 7.07 (2H, d, *J* = 8.8 Hz), 6.71 (1H, d, *J* = 2.4 Hz), 6.52 (1H, d, *J* = 2.4 Hz), 4.59 (2H, s), 3.89 (3H, s), 3.84 (3H, s), 3.79–3.81 (2H, m), 3.23 (2H, t, *J* = 8.8 Hz), 3.03 (2H, t, *J* = 8.8 Hz), 1.49–1.52 (2H, m). ¹³C NMR (100 MHz, DMSO-*d*₆ + CF₃COOD), δ (ppm): 167.9, 166.8, 164.0, 162.8, 157.8, 157.6, 142.9, 132.6(2), 118.4, 116.1(2), 103.4, 99.5, 95.6, 67.8, 67.6(2), 57.1, 55.6, 44.9, 35.8, 31.2(2). HRMS (ESI)⁺ Calculated for C₂₄H₂₈N₃O₆ [M + H]⁺ *m/z* 454.1978, found 454.1978.

2-(4-(5,7-Dimethoxy-4-oxo-1,4-dihydroquinazolin-2-yl)-2,6-dimethylphenoxy)-N-((tetrahydro-2H-pyran-4-yl)methyl)acetamide (42d).—Light yellow solid, mp 224–226 °C, yield 47.2%. ¹H NMR (400 MHz, DMSO-*d*₆), δ (ppm): 11.78 (1H, s), 8.24 (1H, t, *J* = 6.0 Hz), 7.90 (2H, s), 6.73 (1H, d, *J* = 2.4 Hz), 6.51 (1H, d, *J* = 2.4 Hz), 4.28 (2H, s), 3.88 (3H, s), 3.84 (3H, s), 3.26 (2H, t, *J* = 11.6 Hz), 3.09 (2H, t, *J* = 7.6 Hz), 2.31 (6H, s), 1.55 (2H, d, *J* = 8.8 Hz), 1.16–1.19 (2H, m). ¹³C NMR (100 MHz, DMSO-*d*₆ + CF₃COOD), δ (ppm): 168.1, 166.5, 162.5, 160.8, 157.4, 157.3, 143.0, 132.5(2), 131.0(2), 125.0, 103.4, 99.4, 95.7, 71.3, 67.4(2), 57.0, 56.5, 44.6, 35.5, 31.1(2), 16.5(2). HRMS (ESI)⁺ Calculated for C₂₆H₃₁N₃O₆ [M + Na]⁺ *m/z* 504.2111, found 504.2106.

2-(2,6-Dibromo-4-(5,7-dimethoxy-4-oxo-1,4-dihydroquinazolin-2-yl)phenoxy)-N-(1-methylpiperidin-4-yl)acetamide (42e).—White powder, mp 267–269 °C, yield 45.5%. ¹H NMR (400 MHz, DMSO-*d*₆), δ (ppm): 9.50 (1H, s), 8.50 (2H, s), 6.80 (1H, s), 6.57 (1H, s), 4.48 (2H, s), 3.90 (3H, s), 3.86 (3H, s), 3.45–3.47 (2H, m), 3.07–3.08 (2H, m), 2.75–2.77 (2H, m), 2.97–2.99 (2H, m). ¹³C NMR (100 MHz, DMSO-*d*₆), δ (ppm): 166.0, 164.4, 160.9, 159.5, 154.1, 152.4, 149.7, 132.0(2), 131.2, 117.6(2), 104.8, 101.5, 98.2, 71.0, 56.0, 55.7, 52.7(2), 43.5, 42.6, 28.8(2). HRMS (ESI)⁺ Calculated for C₂₄H₂₇Br₂N₂O₅ [M + H]⁺ *m/z* 611.0328, found 611.0320.

2-(4-(5,7-Dimethoxy-4-oxo-1,4-dihydroquinazolin-2-yl)-2,6-dimethylphenoxy)-N-(1-methylpiperidin-4-yl)acetamide (42f).—White powder, mp 270–272 °C, yield 43.0%. ¹H NMR (400 MHz, CDCl₃), δ (ppm): 7.78 (1H, t, *J* = 6.0 Hz), 6.78 (1H, s), 6.41 (1H, s), 4.27 (2H, s), 3.91 (6H, s), 2.80 (2H, d, *J* = 4.8 Hz), 2.29 (6H, s), 2.14 (2H, t, *J* = 8.8 Hz), 2.01–2.03 (2H, m), 1.57–1.60 (2H, m). ¹³C NMR (100 MHz, CDCl₃), δ (ppm): 167.0(2), 165.0, 164.8, 161.0, 157.2, 154.1, 131.1, 128.5(2), 125.1, 123.0, 105.0, 101.2, 98.2, 70.6, 56.2, 55.7, 54.5(2), 46.3, 45.8, 32.3(2), 16.5(2). HRMS (ESI)⁺ Calculated for C₂₆H₃₃N₄O₅ [M + H]⁺ *m/z* 481.2451, found 481.2443.

2-(4-(5,7-Dimethoxy-4-oxo-1,4-dihydroquinazolin-2-yl)-phenoxy)-N-(4-methylpiperazin-1-yl)acetamide (42g).—Light yellow solid, mp 256–258 °C, yield 62.5%. ¹H NMR (400 MHz, CDCl₃ + CD₃OD), δ (ppm): 8.25 (2H, d, *J* = 2.4 Hz), 7.35 (2H, d, *J* = 2.4 Hz), (1H, s), 6.72 (1H, s), 4.82 (2H, s), 4.16 (3H, s), 4.15 (3H, s), 3.09–3.12 (4H, m), 2.85–2.87 (4H, m), 2.57 (3H, s). ¹³C NMR (100 MHz, CDCl₃ + CD₃OD), δ (ppm): 166.0, 165.9, 165.2, 161.1, 159.9,

152.7, 129.2(2), 126.0, 114.8(2), 104.5, 100.8, 97.9, 66.7, 55.8, 55.5, 53.9(2), 49.2(2), 45.2.
HRMS (ESI)⁺ Calculated for C₂₃H₂₇N_aN₅O₅ [M + Na]⁺ *m/z* 476.1910, found 476.1904.

2-(4-(5,7-Dimethoxy-4-oxo-1,4-dihydroquinazolin-2-yl)-phenoxy)-N-(3,4,5-trimethoxyphenyl)acetamide (42h).—White powder, mp 269–271 °C,

yield 63.7%. ¹H NMR (400 MHz, DMSO-*d*₆), δ (ppm): 10.07 (1H, s), 8.15 (2H, d, *J* = 8.8 Hz), 7.13 (2H, d, *J* = 8.8 Hz), 7.06 (2H, s), 6.74 (1H, d, *J* = 2.4 Hz), 6.53 (1H, d, *J* = 2.4 Hz), 4.80 (2H, s), 3.89 (3H, s), 3.85 (3H, s), 3.74 (6H, s), 3.62 (3H, s). ¹³C NMR (100 MHz, DMSO-*d*₆), δ (ppm): 166.0, 164.4, 161.0, 160.7, 159.5, 153.0, 152.7(2), 151.7, 134.5, 133.7, 129.7(2), 124.2, 114.7(2), 104.3, 100.2, 97.6, 97.4(2), 67.1, 60.1(2), 56.0, 55.7(2).
HRMS (ESI)⁺ Calculated for C₂₇H₂₇N_aN₃O₈ [M + N_a]⁺ *m/z* 544.1696, found 544.1694.

2-(4-(5,7-Dimethoxy-4-oxo-1,4-dihydroquinazolin-2-yl)-2,6-dimethylphenoxy)-N-(3,4,5-trimethoxyphenyl)acetamide (42i).—Off-white solid, mp 240–242 °C,

yield 54.9%. ¹H NMR (400 MHz, DMSO-*d*₆), δ (ppm): 9.98 (1H, s), 7.92 (2H, s), 7.18 (2H, s), 6.76 (1H, d, *J* = 2.4 Hz), 6.54 (1H, d, *J* = 2.4 Hz), 4.48 (2H, s), 3.89 (3H, s), 3.85 (3H, s), 3.75 (6H, s), 3.63 (3H, s), 2.36 (6H, s). ¹³C NMR (100 MHz, DMSO-*d*₆), δ (ppm): 166.3, 164.4, 161.0, 159.5, 157.8, 152.8, 152.7(2), 152.0, 134.5, 133.8, 130.9(2), 128.6(2), 127.3, 104.5, 100.6, 97.7, 97.6(2), 71.0, 60.1, 56.0, 55.8(2), 55.7, 16.2(2).
HRMS (ESI)⁺ Calculated for C₂₉H₃₁N_aN₃O₈ [M + N_a]⁺ *m/z* 572.2009, found 572.2007.

N-(1H-Benzo[d]imidazol-2-yl)-2-(4-(5,7-dimethoxy-4-oxo-1,4-dihydroquinazolin-2-yl)-2,6-dimethylphenoxy)acetamide (42j).—White

powder, mp 257–260 °C, yield 57.2%. ¹H NMR (400 MHz, DMSO-*d*₆), δ (ppm): 7.93 (2H, s), 7.45–7.47 (2H, m), 7.10–7.11 (1H, m), 6.74 (1H, d, *J* = 2.4 Hz), 6.50 (1H, d, *J* = 2.4 Hz), 4.67 (2H, s), 3.89 (3H, s), 3.84 (3H, s), 2.37 (6H, s). ¹³C NMR (100 MHz, DMSO-*d*₆), δ (ppm): 168.3, 164.2, 160.9, 160.1, 159.7, 159.1, 158.0, 153.1, 152.7, 146.6, 130.6(2), 130.4, 128.7, 128.4(2), 128.0, 121.2(2), 104.7, 101.1, 97.5, 70.9, 55.9, 55.6, 16.3(2).
HRMS (ESI)⁺ Calculated for C₂₇H₂₆N₅O₅ [M + Na]⁺ *m/z* 522.1753, found 522.1752.

tert-Butyl-(2-(4-(5,7-dimethoxy-4-oxo-1,4-dihydroquinazolin-2-yl)phenoxy)acetamido)piperidine-1-carboxylate (43a).—White powder, mp 244–

246 °C, yield 64.4%. ¹H NMR (400 MHz, CDCl₃), δ (ppm): 8.26 (2H, d, *J* = 8.4 Hz), 7.06 (2H, d, *J* = 8.4 Hz), 6.46 (1H, d, *J* = 2.4 Hz), 6.42 (1H, d, *J* = 8.4 Hz), 4.56 (2H, s), 3.98 (3H, s), 3.93 (3H, s), 4.03–4.06 (4H, m), 2.87 (2H, t, *J* = 12.4 Hz), 1.94 (2H, t, *J* = 12.4 Hz), 1.45 (9H, s). ¹³C NMR (100 MHz, CDCl₃), δ (ppm): 166.9, 161.9, 161.5, 159.9, 154.7, 152.2, 129.8(2), 115.0(2), 104.9, 98.5, 79.9, 67.5, 56.6, 55.9, 46.7, 42.8, 42.5, 32.1(2), 28.6(5).
HRMS (ESI)⁺ Calculated for C₂₈H₃₅N₄O₇ [M + H]⁺ *m/z* 539.2506, found 539.2514.

tert-Butyl-(2-(4-(5,7-dimethoxy-4-oxo-1,4-dihydroquinazolin-2-yl)-2,6-dimethylphenoxy)acetamido)piperidine-1-carboxylate (43b).—White powder,

mp 236–239 °C, yield 63.8%. ¹H NMR (400 MHz, DMSO-*d*₆), δ (ppm): 8.13 (1H, d, *J* = 8.4 Hz), 7.90 (2H, s), 6.72 (1H, d, *J* = 2.4 Hz), 6.48 (1H, d, *J* = 2.4 Hz), 4.26 (2H, s), 3.91–3.93 (2H, m), 3.89 (3H, s), 3.83 (3H, s), 3.31–3.33 (2H, m), 2.80–2.82 (2H, m), 2.29 (6H, s), 1.70–1.72 (2H, m), 1.39 (9H, s). ¹³C NMR (100 MHz, DMSO-*d*₆), δ (ppm): 166.8, 164.0, 161.9, 160.9, 160.5, 153.2, 152.9, 130.6(2), 128.3(2),

104.8, 100.9, 97.4, 78.6, 70.8, 55.9, 55.5, 45.7, 42.7, 42.2, 31.2(2), 28.1(3), 16.1(2).
HRMS (ESI)⁺ Calculated for C₃₀H₃₉N₄O₄ [M + Na]⁺ *m/z* 589.2638, found 589.2635.

2-(4-(5,7-Dimethoxy-4-oxo-1,4-dihydroquinazolin-2-yl)-2,6-dimethylphenoxy)-N-(4-(4-methylpiperazin-1-yl)phenyl)acetamide (43c).—Off-white solid, mp 240–243 °C, yield 60.3%. ¹H NMR (400 MHz, DMSO-*d*₆), δ (ppm): 11.86 (1H, s), 9.86 (1H, s), 7.92 (2H, s), 7.55 (2H, d, *J* = 8.8 Hz), 6.90 (2H, d, *J* = 8.8 Hz), 6.74 (1H, d, *J* = 2.0 Hz), 6.51 (1H, d, *J* = 2.0 Hz), 4.47 (2H, s), 3.88 (3H, s), 3.84 (3H, s), (4H, t, *J* = 4.8 Hz), 2.44 (4H, t, *J* = 4.8 Hz), 2.35 (6H, s), 2.21 (3H, s). ¹³C NMR (100 MHz, DMSO-*d*₆), δ (ppm): 165.9, 164.3, 161.0, 159.8, 157.8, 153.1, 152.4, 147.6, 130.8(2), 130.2, 128.4(2), 127.9, 121.1(2), 115.6(2), 104.7, 101.2, 97.6, 71.2, 56.0, 55.7, 54.6(2), 48.5(2), 45.8, 16.8(2).
HRMS (ESI)⁺ Calculated for C₃₁H₃₆N₅O₅ [M + H]⁺ *m/z* 558.2716, found 558.2719.

2-(4-(5,7-Dimethoxy-4-oxo-1,4-dihydroquinazolin-2-yl)-2,6-dimethylphenoxy)-N-(3-(4-methylpiperazin-1-yl)phenyl)acetamide (43d).—White powder, mp 237–240 °C, yield 57.2%. ¹H NMR (400 MHz, DMSO-*d*₆), δ (ppm): 11.88 (1H, s), 10.01 (1H, s), 7.93 (2H, s), 7.42 (1H, s), 7.28 (1H, t, *J* = 8.0 Hz), 7.23 (1H, t, *J* = 8.0 Hz), 6.77 (1H, d, *J* = 2.4 Hz), 6.73 (1H, s), 6.51 (1H, d, *J* = 2.4 Hz), 4.49 (2H, s), 3.88 (3H, s), 3.84 (3H, s), 3.35–3.37 (4H, m), 3.17 (4H, s), 2.86 (3H, s), 2.36 (6H, s). ¹³C NMR (100 MHz, DMSO-*d*₆), δ (ppm): 166.4, 165.6, 160.9, 159.7, 157.6, 153.0, 152.4, 149.9, 139.2, 130.7(2), 129.3, 128.3(2), 127.9, 111.7, 107.5, 104.6, 101.1, 97.6, 71.0, 57.8, 55.9, 55.6, 52.2(2), 45.7(2), 16.2(2).
HRMS (ESI)⁺ Calculated for C₃₁H₃₅NaN₅O₅ [M + Na]⁺ *m/z* 580.2536, found 580.2534.

2-(2,6-Dibromo-4-(5,7-dimethoxy-4-oxo-1,4-dihydroquinazolin-2-yl)phenoxy)-N-(4-(4-methylpiperazin-1-yl)phenyl)acetamide (43e).—Off-white solid, mp 270–272 °C, yield 55.7%. ¹H NMR (400 MHz, acetic acid-*d*₄), δ (ppm): 8.58 (2H, s), 7.58 (2H, d, *J* = 8.8 Hz), 7.22 (2H, d, *J* = 8.8 Hz), 7.05 (1H, d, *J* = 2.0 Hz), 6.71 (1H, d, *J* = 2.0 Hz), 5.01 (2H, s), 4.10 (3H, s), 4.11 (3H, s), 3.92 (4H, t, *J* = 4.8 Hz), 3.41 (4H, t, *J* = 4.8 Hz), 3.12 (3H, s). ¹³C NMR (100 MHz, acetic acid-*d*₄), δ (ppm): 168.7, 167.8, 164.9, 163.1, 156.1, 154.8, 151.0, 148.8, 133.9(2), 132.9, 132.4, 123.9(2), 119.7(2), 119.2(2), 105.7, 103.0, 72.6, 57.2, 57.1, 54.7(2), 48.7(2), 44.3.
HRMS (ESI)⁺ Calculated for C₂₉H₃₀Br₂N₅O₅ [M + H]⁺ *m/z* 688.0593, found 688.0596.

2-(4-(5,7-Dimethoxy-4-oxo-1,4-dihydroquinazolin-2-yl)-2,6-dimethylphenoxy)-N-(4-(4-methylpiperazin-1-yl)phenyl)acetamide (43f).—White powder, mp 267–269 °C, yield 58.2%. ¹H NMR (400 MHz, acetic acid-*d*₄), δ (ppm): 8.31 (2H, d, *J* = 8.0 Hz), 7.82 (2H, d, *J* = 8.0 Hz), 7.39 (2H, d, *J* = 8.0 Hz), 7.23 (2H, d, *J* = 8.0 Hz), 7.12 (1H, s), (1H, s), 5.00 (2H, s), 4.12 (3H, s), 4.09 (3H, s), 3.94 (4H, brs), 2.44 (4H, brs), 3.16 (3H, s). ¹³C NMR (100 MHz, acetic acid-*d*₄), δ (ppm): 169.6, 167.9, 165.0, 163.2, 162.2, 154.9, 154.4, 148.8, 132.5, 131.6(2), 126.8, 124.2(2), 119.2(2), 116.8(2), 105.4, 102.3, 100.0, 68.8, 57.2, 57.1, 54.6(2), 48.7(2), 44.4. HRMS (ESI)⁺ Calculated for C₂₉H₃₂N₅O₅ [M + H]⁺ *m/z* 530.2403, found 530.2401.

2-(4-(5,7-Dimethoxy-4-oxo-1,4-dihydroquinazolin-2-yl)-phenoxy)-N-(3-(4-methylpiperazin-1-yl)phenyl)acetamide (43g).—White powder, mp 256–

258 °C, yield 66.0%. ¹H NMR (400 MHz, DMSO-*d*₆), δ (ppm): 11.95 (1H, s), 10.12 (1H, s), 8.17 (2H, d, *J* = 8.4 Hz), 7.38 (1H, s), 7.21 (1H, t, *J* = 8.0 Hz), 7.11–7.15 (2H, m), 6.77 (1H, dd, *J* = 8.0, 2.4 Hz), 6.72 (1H, d, *J* = 2.4 Hz), 6.52 (1H, d, *J* = 2.0 Hz), 4.82 (2H, s), 3.85 (3H, s), 3.82 (3H, s), 3.74–3.76 (2H, m), 3.51–3.53 (2H, m), 3.16 (2H, s), 2.96–2.98 (2H, m), 2.86 (3H, s). ¹³C NMR (100 MHz, DMSO-*d*₆), δ (ppm): 166.8, 166.6, 164.7, 161.5, 160.9, 153.5, 152.9, 150.5, 139.8, 129.9(2), 125.5, 115.1(2), 112.3, 112.0, 107.8, 105.0, 101.5, 97.9, 89.7, 67.5, 56.0, 55.7, 52.7(2), 46.2(2), 42.5. HRMS (ESI)⁺ Calculated for C₂₉H₃₁NaN₅O₅ [M + Na]⁺ *m/z* 552.2223, found 552.2222.

2-(4-(5,7-Dimethoxy-4-oxo-1,4-dihydroquinazolin-2-yl)-phenoxy)-N-(2-(4-methylpiperazin-1-yl)phenyl)acetamide (43h).—Off-white solid, mp 252–255 °C, yield 58.6%. ¹H NMR (400 MHz, DMSO-*d*₆), δ (ppm): 9.96 (1H, s), 8.23 (2H, d, *J* = 2.4 Hz), 8.15 (1H, d, *J* = 8.4 Hz), 7.14–7.28 (4H, m), 6.71 (1H, d, *J* = 2.0 Hz), 6.52 (1H, d, *J* = 2.0 Hz), 4.90 (2H, s), 3.89 (3H, s), 3.85 (3H, s), 3.51–3.53 (4H, m), 2.98–3.03 (4H, m), 2.87 (3H, s). ¹³C NMR (100 MHz, DMSO-*d*₆), δ (ppm): 166.0, 164.3, 161.1, 160.0, 159.9, 158.7, 152.8, 152.5, 141.0, 132.0, 129.8(2), 125.5, 125.3, 124.8, 120.8, 114.8(2), 104.6, 100.9, 97.5, 67.4, 56.0, 55.6, 53.3(2), 48.5(2), 42.4. HRMS (ESI)⁺ Calculated for C₂₉H₃₁NaN₅O₅ [M + Na]⁺ *m/z* 552.2223, found 552.2215.

2-(4-(5,7-Dimethoxy-4-oxo-1,4-dihydroquinazolin-2-yl)-phenoxy)-N-(4-morpholinophenyl)acetamide (43i).—White powder, mp 273–275 °C, yield 61.8%. ¹H NMR (400 MHz, DMSO-*d*₆), δ (ppm): 11.87 (1H, s), 9.89 (1H, s), 7.92 (2H, s), 7.57 (2H, d, *J* = 8.4 Hz), 6.92 (2H, d, *J* = 8.4 Hz), 6.74 (1H, d, *J* = 2.0 Hz), 6.52 (1H, d, *J* = 2.0 Hz), 4.45 (2H, s), 3.89 (3H, s), 3.84 (3H, s), 3.73 (4H, t, *J* = 4.8 Hz), 3.05 (4H, t, *J* = 4.8 Hz). ¹³C NMR (100 MHz, DMSO-*d*₆ + CF₃COOD), δ (ppm): 166.4, 165.3, 161.6, 159.5, 157.8, 155.4, 145.9, 142.0, 131.5(2), 129.9(2), 123.4(2), 121.1, 121.0(2), 119.5, 103.5, 98.5, 97.1, 71.2, 65.0(2), 56.4, 56.1, 52.0(2), 16.3(2). HRMS (ESI)⁺ Calculated for C₃₀H₃₃N₄O₄ [M + H]⁺ *m/z* 545.2400, found 545.2400.

2-(4-(5,7-Dimethoxy-4-oxo-1,4-dihydroquinazolin-2-yl)-2,6-dimethylphenoxy)-N-(3-morpholinophenyl)acetamide (43j).—White powder, mp 264–267 °C, yield 48.3%. ¹H NMR (400 MHz, DMSO-*d*₆), δ (ppm): 11.87 (1H, s), 9.91 (1H, s), 7.92 (2H, s), 7.34 (1H, s), 7.15–7.23 (2H, m), 6.74 (1H, d, *J* = 2.4 Hz), 6.69 (1H, dd, *J* = 8.4, 2.4 Hz), 6.51 (1H, d, *J* = 2.8 Hz), 4.47 (2H, s), 3.88 (3H, s), 3.84 (3H, s), (4H, t, *J* = 4.8 Hz), 3.08 (4H, t, *J* = 4.8 Hz), 2.35 (6H, s). ¹³C NMR (100 MHz, DMSO-*d*₆), δ (ppm): 167.7, 166.4, 164.3, 162.5, 161.0, 157.7, 152.4, 151.5, 139.1, 130.8(2), 129.1, 128.4(2), 127.9, 110.9(2), 106., 104.6, 101.2, 97.6, 71.0, 66.1(2), 56.0, 55.7, 48.5(2), 16.2(2). HRMS (ESI)⁺ Calculated for C₃₀H₃₂N₄N_aO₆ [M + N_a]⁺ *m/z* 567.2220, found 567.2211.

2-(2,6-Dibromo-4-(5,7-dimethoxy-4-oxo-1,4-dihydroquinazolin-2-yl)phenoxy)-N-(4-morpholinophenyl)acetamide (43k).—White powder, mp 242–244 °C, yield 49.7%. ¹H NMR (400 MHz, DMSO-*d*₆ + CF₃COOD), δ (ppm): 10.34 (1H, s), 8.39 (2H, s), 7.87 (2H, d, *J* = 8.4 Hz), 7.62 (2H, d, *J* = 8.4 Hz), 6.80 (1H, d, *J* = 2.0 Hz), 6.62 (1H, d, *J* = 2.0 Hz), 4.74 (2H, s), 3.95 (4H, t, *J* = 4.8 Hz), 3.86 (6H, s), 3.58 (4H, t, *J* = 4.8 Hz). ¹³C NMR (100 MHz, DMSO-*d*₆ + CF₃COOD),

δ (ppm): 166.6, 166.4, 162.6, 156.9, 156.8, 153.8, 139.9, 138.6, 134.6(2), 122.5(2), 122.2(2), 118.6(2), 116.8, 115.0, 104.5, 99.8, 98.4, 72.4, 65.0(2), 57.0, 56.6, 55.4(2). HRMS (ESI)⁺ Calculated for C₂₈H₂₇Br₂N₄O₆ [M + H]⁺ m/z 675.0277, found 675.0275.

2-(4-(5,7-Dimethoxy-4-oxo-1,4-dihydroquinazolin-2-yl)-2,6-dimethylphenoxy)-N-(4-morpholinophenyl)acetamide (43l).—Off-white solid, mp 276–278 °C, yield 60.7%. ¹H NMR (400 MHz, DMSO-*d*₆), δ (ppm): 11.92 (1H, s), 9.93 (1H, s), 7.50 (2H, d, J = 8.8 Hz), 7.12 (2H, d, J = 8.8 Hz), 6.91 (2H, d, J = 8.8 Hz), 6.71 (1H, d, J = 2.4 Hz), 6.50 (1H, d, J = 2.4 Hz), 4.76 (2H, s), 3.88 (3H, s), 3.84 (3H, s), 3.72 (4H, t, J = 4.8 Hz), 3.05 (4H, t, J = 4.8 Hz). ¹³C NMR (100 MHz, CDCl₃ + CF₃COOD), δ (ppm): 169.0, 163.2, 162.0, 160.0, 156.4, 137.5, 131.3, 131.0, 123.4, 123.3, 121.8, 121.5, 119.0, 117.0, 116.9, 116.1, 116.0, 113.3, 101.0, 98.5, 94.8, 67.0, 64.5, 64.2, 56.9, 56.3, 56.1(2). HRMS (ESI)⁺ Calculated for C₂₈H₂₉N₄O₄ [M + H]⁺ m/z 517.2087, found 517.2086.

2-(4-(5,7-Dimethoxy-4-oxo-1,4-dihydroquinazolin-2-yl)-phenoxy)-N-(3-morpholinophenyl)acetamide (43m).—White powder, mp 272–274 °C, yield 51.0%. ¹H NMR (400 MHz, DMSO-*d*₆), δ (ppm): 10.02 (1H, s), 8.16 (2H, d, J = 8.4 Hz), 7.28 (1H, t, J = 2.4 Hz), 7.09–7.16 (4H, m), 6.72 (1H, d, J = 2.4 Hz), 6.68 (1H, dd, J = 8.4, 2.4 Hz), 6.51 (1H, d, J = 2.4 Hz), 4.79 (2H, s), 3.88 (3H, s), 3.84 (3H, s), 3.72 (4H, t, J = 4.8 Hz), 3.06 (4H, t, J = 4.8 Hz). ¹³C NMR (100 MHz, DMSO-*d*₆), δ (ppm): 166.1(2), 164.3, 161.0, 160.5, 152.9, 152.5, 151.5, 139.2, 129.4(2), 129.2, 125.0, 114.6(2), 110.9, 110.7, 106.4, 104.5, 100.9, 97.5, 67.1, 66.1(2), 56.0, 55.6, 48.5(2). HRMS (ESI)⁺ Calculated for C₂₈H₂₉N₄O₆ [M + H]⁺ m/z 517.2087, found 517.2053.

2-(4-(5,7-Dimethoxy-4-oxo-1,4-dihydroquinazolin-2-yl)-2,6-dimethylphenoxy)-N-(4-(piperidin-1-yl)phenyl)acetamide (43n).—Off-white solid, mp 265–267 °C, yield 56.1%. ¹H NMR (400 MHz, DMSO-*d*₆), δ (ppm): 11.87 (1H, s), 9.58 (1H, s), 7.92 (2H, s), 7.53 (2H, d, J = 8.8 Hz), 6.89 (2H, d, J = 8.8 Hz), 6.74 (1H, s), 6.52 (1H, s), 4.45 (2H, s), 3.89 (3H, s), 3.84 (3H, s), 3.06–3.08 (4H, m), 2.35 (6H, s), 1.58–1.63 (4H, m), 1.51–1.52 (2H, m). ¹³C NMR (100 MHz, DMSO-*d*₆), δ (ppm): 165.8, 164.2, 160.9, 157.8, 153.1, 152.4, 148.4, 130.8(2), 129.9, 128.7(2), 127.9, 121.1(2), 116.1(2), 104.7, 101.2, 97.6, 71.1, 56.0, 55.6, 50.0(2), 35.8, 25.3(2), 23.9, 16.2(2). HRMS (ESI)⁺ Calculated for C₃₁H₃₅N₄O₅ [M + H]⁺ m/z 543.2607, found 535.2607.

2-(2,6-Dibromo-4-(5,7-dimethoxy-4-oxo-1,4-dihydroquinazolin-2-yl)phenoxy)-N-(4-(piperidin-1-yl)phenyl)acetamide (43o).—White powder, mp 271–273 °C, yield 62.0%. ¹H NMR (400 MHz, DMSO-*d*₆ + CF₃COOD), δ (ppm): 10.48 (1H, s), 8.52 (2H, s), 7.94 (2H, d, J = 8.8 Hz), 7.73 (2H, d, J = 8.8 Hz), 6.85 (1H, d, J = 2.4 Hz), 6.65 (1H, d, J = 2.4 Hz), 4.78 (2H, s), 3.93 (3H, s), 3.91 (3H, s), 3.58–3.61 (4H, m), 1.94–1.97 (4H, m), 1.70 (2H, s). ¹³C NMR (100 MHz, DMSO-*d*₆ + CF₃COOD), δ (ppm): 166.0, 165.4, 165.3, 161.7, 155.2, 151.8, 142.1, 139.8, 138.2, 133.2(2), 122.4(2), 121.5, 121.4(2), 118.0(2), 104.6, 99.8, 98.9, 71.7, 56.8(2), 56.5, 56.1, 23.8(2), 21.0. HRMS (ESI)⁺ Calculated for C₂₉H₂₉Br₂N₄O₅ [M + H]⁺ m/z 673.0484, found 673.0490.

2-(4-(5,7-Dimethoxy-4-oxo-1,4-dihydroquinazolin-2-yl)-phenoxy)-N-(4-(piperidin-1-yl)phenyl)acetamide (43p).—White powder, mp 253–

256 °C, yield 63.4%. ¹H NMR (400 MHz, DMSO-*d*₆), δ (ppm): 11.93 (1H, s), 9.89 (1H, s), 8.17 (2H, d, *J* = 8.8 Hz), 7.45 (1H, d, *J* = 8.8 Hz), 7.12 (2H, d, *J* = 8.8 Hz), 6.88 (1H, d, *J* = 8.8 Hz), 6.71 (1H, d, *J* = 2.4 Hz), 6.51 (1H, d, *J* = 2.4 Hz), 4.75 (2H, s), 3.88 (3H, s), (3H, s), 3.04–3.07 (4H, m), 1.57–1.62 (4H, m), 1.50–1.51 (2H, m). ¹³C NMR (100 MHz, DMSO-*d*₆ + CF₃COOD), δ (ppm): 166.6, 165.8, 162.8, 161.9, 157.6, 156.4, 144.2, 139.7, 137.9, 131.7(2), 122.3(2), 120.9, 120.8(2), 119.2, 115.3(2), 103.1, 98.7, 96.1, 67.2, 56.5(2), 56.2, 23.6(2), 20.8. HRMS (ESI)⁺ Calculated for C₂₉H₃₁N₄O₅ [M + H]⁺ *m/z* 515.2294, found 515.2300.

2-(4-(5,7-Dimethoxy-4-oxo-1,4-dihydroquinazolin-2-yl)-phenoxy)-N-(4-(pyrrolidin-1-yl)phenyl)acetamide (43q).—Off-white solid, mp

243–245 °C, yield 50.7%. ¹H NMR (400 MHz, DMSO-*d*₆), δ (ppm): 9.80 (1H, s), 8.16 (2H, d, *J* = 9.2 Hz), 7.42 (2H, d, *J* = 9.2 Hz), 7.14 (2H, d, *J* = 8.8 Hz), 6.72 (1H, d, *J* = 2.4 Hz), 6.50–6.53 (2H, m), 4.74 (2H, s), 3.89 (3H, s), 3.85 (3H, s), 3.17–3.19 (4H, m), 1.92–1.95 (4H, m). ¹³C NMR (100 MHz, DMSO-*d*₆ + CF₃COOD), δ (ppm): 166.2, 163.2, 162.1(2), 157.3, 156.9, 143.3, 141.4, 132.0(2), 121.1(2), 119.9, 119.8(2), 118.6, 115.5(2), 103.0, 98.9, 95.6, 67.4, 56.8, 56.3, 55.3(2), 23.9(2). HRMS (ESI)⁺ Calculated for C₂₈H₂₉N₄O₅ [M + H]⁺ *m/z* 501.2138, found 501.2133.

2-(4-(5,7-Dimethoxy-4-oxo-1,4-dihydroquinazolin-2-yl)-2,6-dimethylphenoxy)-N-(3-fluoro-4-morpholinophenyl)acetamide (44a).—White powder, mp 258–260

°C, yield 55.9%. ¹H NMR (400 MHz, DMSO-*d*₆ + CF₃COOD), δ (ppm): 7.80 (1H, dd, *J* = 14.0, 2.4 Hz), 7.68 (2H, s), 7.47 (1H, dd, *J* = 9.2, 2.4 Hz), 7.36 (1H, t, *J* = 9.2 Hz), 6.83 (1H, d, *J* = 2.0 Hz), 6.55 (1H, d, *J* = 2.0 Hz), 4.46 (2H, s), 3.82–3.85, (4H, m), 3.81 (3H, s), 3.78 (3H, s), 3.34–3.36 (4H, m), 2.30 (6H, s). ¹³C NMR (100 MHz, DMSO-*d*₆ + CF₃COOD), δ (ppm): 169.2, 168.8, 164.3, 162.6, 159.3, 158.9, 155.8(250.2 Hz), 143.9, 134.7(2), 130.6(2), 132.6(2), 126.4, 126.2, 124.6, 122.9, 104.8, 101.2, 97.0, 72.7, 65.9, 65.5, 58.0, 57.7, 56.2(2), 17.7(2). HRMS (ESI)⁺ Calculated for C₃₀H₃₂FN₄O₆ [M + Na]⁺ *m/z* 585.2125, found 585.2122.

2-(4-(5,7-Dimethoxy-4-oxo-1,4-dihydroquinazolin-2-yl)-phenoxy)-N-(3-fluoro-4-morpholinophenyl)acetamide (44b).—White powder, mp 236–238 °C, yield 58.0%.

¹H NMR (400 MHz, DMSO-*d*₆), δ (ppm): 10.1 (1H, s), 8.15 (2H, d, *J* = 8.8 Hz), 7.56 (1H, dd, *J* = 14.8, 2.4 Hz), 7.32 (1H, dd, *J* = 14.8, 2.4 Hz), 7.14 (2H, d, *J* = 14.8 Hz), 7.02, (1H, t, *J* = 9.6 Hz), 6.73 (1H, d, *J* = 2.4 Hz), 6.53 (1H, d, *J* = 2.4 Hz), 4.80 (2H, s), 3.89 (3H, s), 3.85 (3H, s), 3.71–3.74 (4H, m), 2.94–2.96, (4H, m). ¹³C NMR (100 MHz, DMSO-*d*₆), δ (ppm): 166.1, 164.5, 161.1, 160.7, 159.6, 155.6, 153.2, 153.0, 151.8, 135.7(40.6 Hz), 133.5(36.0 Hz), 129.7(2), 124.3, 119.2, 115.8, 114.7, 108.2(100.8 Hz), 104.4, 100.3, 97.6, 67.1, 66.2(2), 56.1, 55.7, 50.8(2). HRMS (ESI)⁺ Calculated for C₂₈H₂₈FN₄O₆ [M + H]⁺ *m/z* 535.1993, found 535.1992.

2-(4-(5,7-Dimethoxy-4-oxo-1,4-dihydroquinazolin-2-yl)-phenoxy)-N-(3-fluoro-4-(4-methylpiperazin-1-yl)phenyl)acetamide (44c).—Off-white solid,

mp 245–247 °C, yield 59.9%. ¹H NMR (400 MHz, DMSO-*d*₆), δ (ppm): 11.94 (1H, s), 10.16 (1H, s),

8.17 (2H, d, $J = 8.8$ Hz), 7.55 (1H, dd, $J = 14.8, 2.4$ Hz), 7.30 (2H, dd, $J = 8.8, 2.4$ Hz), 7.13 (1H, d, $J = 2.4$ Hz), 7.00 (1H, t, $J = 8.8$ Hz), 6.71 (1H, d, $J = 2.4$ Hz), 6.51 (1H, d, $J = 2.4$ Hz), 4.79 (2H, s), 3.88 (3H, s), 3.84 (3H, s), 2.96, (4H, t, $J = 4.8$ Hz), 2.46 (4H, brs), 2.22 (3H, s). ^{13}C NMR (100 MHz, DMSO- d_6 + CF₃COOD), δ (ppm): 166.2, 166.1, 163.3, 162.8, 162.2, 157.4, 157.0, 156.2, 153.7, 143.2, 134.7(42.8 Hz), 134.5(36.8 Hz), 120.2, 118.6, 116.0, 115.5(2), 108.5(100.8 Hz), 103.1, 98.9, 95.5, 67.4, 56.8, 56.7, 56.4, 56.3, 53.1(2), 47.9. HRMS (ESI)⁺ Calculated for C₂₉H₃₁FN₅O₅ [M + H]⁺ m/z 548.2309, found 548.2311.

2-(4-(5,7-Dimethoxy-4-oxo-1,4-dihydroquinazolin-2-yl)-2,6-dimethylphenoxy)-N-(3-fluoro-4-(4-methylpiperazin-1-yl)phenyl)-acetamide (44d).—White powder, mp 253–256 °C, yield 61.4%. ^1H NMR (400 MHz, CDCl₃), δ (ppm): 8.60 (1H, s), 7.85 (2H, s), 7.58 (1H, dd, $J = 14.0, 2.4$ Hz), 7.26–7.27 (1H, m), 6.94 (1H, d, $J = 8.8$ Hz), 6.81 (1H, s), 6.44 (1H, s), 4.40 (2H, s), 3.92 (6H, s), 3.10 (4H, t, $J = 4.4$ Hz), 2.61 (4H, t, $J = 4.4$ Hz), 2.36 (9H, s). ^{13}C NMR (100 MHz, CDCl₃), δ (ppm): 166.1, 165.2, 161.4, 157.0, 156.7, 154.2, 153.9, 152.3, 137.3(36.4 Hz), 131.9(36.8 Hz), 131.3(2), 129.1, 128.5(2), 119.1, 115.9, 109.2(56.4 Hz), 105.0, 101.4, 98.4, 70.5, 56.3, 55.8, 55.2(2), 50.7(2), 46.2, 16.5(2). HRMS (ESI)⁺ Calculated for C₃₁H₃₅FN₅O₅ [M + H]⁺ m/z 576.2622, found 576.2624.

N-(3-Chloro-4-(4-methylpiperazin-1-yl)phenyl)-2-(4-(5,7-dimethoxy-4-oxo-1,4-dihydroquinazolin-2-yl)phenoxy)acetamide (44e).—White powder, mp 273–276 °C, yield 62.9%. ^1H NMR (400 MHz, DMSO- d_6), δ (ppm): 10.29 (1H, s), 8.17 (2H, d, $J = 8.4$ Hz), 7.85 (1H, s), 7.55 (1H, d, $J = 8.8$ Hz), 7.21 (1H, d, $J = 8.8$ Hz), 7.12 (2H, d, $J = 8.8$ Hz), 6.71 (1H, s), 6.50 (1H, s), 4.81 (2H, s), 3.88 (3H, s), 3.84 (3H, s), 3.30–3.37 (8H, m), 2.86 (3H, s). ^{13}C NMR (100 MHz, DMSO- d_6), δ (ppm): 166.3, 164.2, 160.9, 160.3, 159.8, 153.1, 152.3, 143.1, 135.1, 129.3(2), 127.5, 125.1, 121.3(2), 119.3, 114.6(2), 104.5, 101.1, 97.4, 67.0, 55.9, 55.6, 52.9(2), 48.1(2), 42.2. HRMS (ESI)⁺ Calculated for C₂₉H₃₁ClN₅O₅ [M + H]⁺ m/z 564.2014, found 564.2011.

N-(3-Chloro-4-(4-methylpiperazin-1-yl)phenyl)-2-(4-(5,7-dimethoxy-4-oxo-1,4-dihydroquinazolin-2-yl)-2,6-dimethylphenoxy)-acetamide (44f).—White powder, mp 260–263 °C, yield 45.8%. ^1H NMR (400 MHz, DMSO- d_6), δ (ppm): 10.22 (1H, s), 7.93 (2H, s), 7.91 (1H, d, $J = 2.4$ Hz), 7.61 (1H, dd, $J = 8.8, 2.4$ Hz), 7.14 (1H, d, $J = 8.8$ Hz), 6.73 (1H, d, $J = 2.4$ Hz), 6.50 (1H, d, $J = 2.4$ Hz), 4.49 (2H, s), 3.88 (3H, s), 3.84 (3H, s), 3.17 (4H, brs), 2.93 (4H, brs), 2.35 (6H, s), 2.23 (3H, s). ^{13}C NMR (100 MHz, DMSO- d_6), δ (ppm): 166.6, 164.1, 160.9, 157.6, 153.3, 153.0, 145.0, 134.3, 130.7(2), 128.4(2), 127.4, 121.7, 120.8, 119.6, 104.8, 101.0, 97.4, 79.2, 71.0, 56.0, 55.6, 54.9(2), 51.1, 48.6, 45.8, 16.3(2). HRMS (ESI)⁺ Calculated for C₃₁H₃₅ClN₅O₅ [M + H]⁺ m/z 614.2148, found 614.2174.

N-(3-Chloro-4-morpholinophenyl)-2-(2,6-dibromo-4-(5,7-dimethoxy-4-oxo-1,4-dihydroquinazolin-2-yl)phenoxy)acetamide (44g).—White powder, mp 268–271 °C, yield 47.6%. ^1H NMR (400 MHz, DMSO- d_6), δ (ppm): 12.17 (1H, s), 10.21 (1H, s), 8.52 (2H, s), 7.88 (1H, d, $J = 2.4$ Hz), 7.56 (1H, dd, $J = 8.8, 2.4$ Hz), 7.16 (1H, d, $J = 8.8$ Hz), 6.81 (1H, s), 6.56 (1H, s), 4.67 (2H, s), 3.89 (3H, s), 3.85 (3H, s), 3.74, (4H, t, $J = 4.4$ Hz), 2.94 (4H, t, $J = 4.0$ Hz). ^{13}C NMR (100 MHz, DMSO- d_6), δ

(ppm): 165.1, 164.4, 160.9, 154.0, 152.4, 149.8, 144.8, 134.3, 132.0(2), 131.3, 127.4, 122.8, 121.7, 120.9, 119.7, 117.7(2), 104.8, 101.5, 98.2, 71.3, 66.4(2), 56.1, 55.7, 51.5(2). HRMS (ESI)⁺ Calculated for C₂₈H₂₅Br₂ClNaN₄O₆ [M + Na]⁺ *m/z* 730.9707, found 730.9714.

N-(3-Chloro-4-morpholinophenyl)-2-(4-(5,7-dimethoxy-4-oxo-1,4-dihydroquinazolin-2-yl)phenoxy)acetamide (44h).—White powder,

mp 247–249 °C, yield 56.0%. ¹H NMR (400 MHz, DMSO-*d*₆), δ (ppm): 10.20 (1H, s), 8.15 (2H, d, *J* = 8.8 Hz), 7.52 (1H, dd, *J* = 8.8, 2.4 Hz), 7.13–7.16 (3H, m), 6.73 (1H, d, *J* = 2.4 Hz), 6.54 (1H, d, *J* = 2.4 Hz), 4.81 (2H, s), 3.89 (3H, s), 3.85 (3H, s), 3.73 (4H, t, *J* = 4.4 Hz), 2.92 (4H, t, *J* = 4.0 Hz). ¹³C NMR (100 MHz, DMSO-*d*₆), δ (ppm): 166.1, 164.4, 161.1, 160.6, 159.5, 153.0, 151.8, 144.6, 134.4, 129.7(2), 127.5, 124.3, 121.4, 120.9, 119.3, 114.7(2), 104.3, 100.3, 97.6, 67.0, 66.4(2), 56.0, 55.7, 51.5(2). HRMS (ESI)⁺ Calculated for C₂₈H₂₇ClNaN₄O₆ [M + Na]⁺ *m/z* 573.1517, found 573.1533.

N-(3-Chloro-4-morpholinophenyl)-2-(4-(5,7-dimethoxy-4-oxo-1,4-dihydroquinazolin-2-yl)-2,6-dimethylphenoxy)acetamide (44i).—Off-white

solid, mp 258–261 °C, yield 51.5%. ¹H NMR (400 MHz, DMSO-*d*₆), δ (ppm): 10.17 (1H, s), 7.90 (3H, s), 7.62 (2H, dd, *J* = 8.8, Hz), 7.15 (1H, d, *J* = 8.8 Hz), 6.75 (1H, d, *J* = 2.4 Hz), 6.54 (1H, d, *J* = 2.4 Hz), 4.49 (2H, s), 3.88 (3H, s), 3.85 (3H, s), 3.73 (4H, t, *J* = 4.4 Hz), 2.93 (4H, t, *J* = 4.0 Hz), 2.35 (6H, s). ¹³C NMR (100 MHz, DMSO-*d*₆), δ (ppm): 165.5, 164.4, 161.0, 159.5, 157.9, 152.9, 151.9, 144.7, 134.4, 130.9(2), 128.6(2), 127.4, 127.2, 121.7, 120.8, 119.6, 104.5, 100.5, 97.7, 71.0, 66.4(2), 56.0, 55.7, 51.5(2), 16.2(2). HRMS (ESI)⁺ Calculated for C₃₀H₃₂ClN₄O₆ [M + H]⁺ *m/z* 579.2010, found 579.2018.

N-(3-Chloro-4-(4-methylpiperazin-1-yl)phenyl)-2-(4-(6-fluoro-4-oxo-1,4-dihydroquinazolin-2-yl)phenoxy)acetamide (44j).—White powder, mp

255–257 °C, yield 58.2%. ¹H NMR (400 MHz, DMSO-*d*₆), δ (ppm): 10.28 (1H, s), 8.18 (2H, d, *J* = 8.8 Hz), 7.87 (1H, d, *J* = 2.4 Hz), 7.76–7.80 (2H, m), 7.70 (1H, td, *J* = 8.8, 2.4 Hz), 7.56 (1H, dd, *J* = 8.8, 2.4 Hz), 7.22 (1H, d, *J* = 8.8 Hz), 7.15 (1H, d, *J* = 8.8 Hz), 3.52 (2H, d, *J* = 11.2 Hz), 3.38 (2H, d, *J* = 11.2 Hz), 3.19–3.22 (2H, m), 3.29 (2H, t, *J* = 13.2 Hz), 2.89 (3H, s). ¹³C NMR (100 MHz, DMSO-*d*₆), δ (ppm): 166.3, 161.8, 161.0, 158.6, 151.4, 145.7, 143.1, 135.1, 130.0(32 Hz), 129.4(2), 127.5, 125.3, 123.1(97.2 Hz), 121.9(33.2 Hz), 121.3(2), 119.3, 114.7(2), 110.6(93.2 Hz), 67.0, 52.8(2), 48.1(2), 42.5. HRMS (ESI)⁺ Calculated for C₂₇H₂₅ClFN₅O₃ [M + Na]⁺ *m/z* 544.1528, found 544.1526.

N-(3-Chloro-4-(4-methylpiperazin-1-yl)phenyl)-2-(4-(6-methoxy-4-oxo-1,4-dihydroquinazolin-2-yl)phenoxy)acetamide (44k).—White powder, mp

243–245 °C, yield 47.7%. ¹H NMR (400 MHz, DMSO-*d*₆), δ (ppm): 10.28 (1H, s), 8.03 (2H, d, *J* = 8.8 Hz), 7.85 (1H, d, *J* = 2.4 Hz), 7.80 (1H, d, *J* = 8.8 Hz), 7.60 (1H, d, *J* = 2.4 Hz), 7.51–7.56 (2H, m), 7.28 (2H, d, *J* = 8.8 Hz), 7.17 (1H, d, *J* = 8.8 Hz), 4.88 (2H, s), 3.90 (3H, s), 3.52 (2H, d, *J* = 12.0 Hz), 3.36 (2H, d, *J* = 12.0 Hz), 3.21 (2H, td, *J* = 12.0, 2.8 Hz), 2.97 (2H, td, *J* = 12.0, 2.8 Hz), 2.87 (3H, s). ¹³C NMR (100 MHz, DMSO-*d*₆), δ (ppm): 166.4, 162.1, 160.0(2), 157.5, 149.7, 143.1, 135.1, 129.1(2), 127.5, 125.7, 124.2, 124.1, 121.5, 121.4, 121.3, 119.3, 114.7(2), 105.9, 67.0, 55.7, 52.9(2), 48.1(2), 42.2. HRMS (ESI)⁺ Calculated for C₂₈H₂₉ClN₅O₄ [M + H]⁺ *m/z* 534.1908, found 534.1899.

N-(3-Chloro-4-(4-methylpiperazin-1-yl)phenyl)-2-(4-(6-chloro-4-oxo-1,4-dihydroquinazolin-2-yl)phenoxy)acetamide (44l).—White powder, mp 281–283 °C, yield 54.5%. ¹H NMR (400 MHz, DMSO-*d*₆), δ (ppm): 12.60 (1H, s), 10.30 (1H, s), 10.05 (1H, s), 8.20 (2H, d, *J* = 8.8 Hz), 8.06 (1H, d, *J* = 2.4 Hz), 7.86 (1H, d, *J* = 2.4 Hz), 7.83 (1H, dd, *J* = 8.8, 2.4 Hz), 7.72 (1H, d, *J* = 8.8 Hz), 7.55 (1H, dd, *J* = 8.8, 2.4 Hz), 7.22 (1H, d, *J* = 8.8 Hz), 7.15 (2H, d, *J* = 8.8 Hz), 4.83 (2H, s), 3.52–3.55 (2H, m), 3.38 (2H, d, *J* = 12.0 Hz), 3.18 (2H, td, *J* = 12.0, 2.8 Hz), 2.99 (2H, td, *J* = 12.0, 2.8 Hz), 2.89 (3H, s). ¹³C NMR (100 MHz, DMSO-*d*₆), δ (ppm): 166.3, 161.4, 160.5, 152.3, 147.6, 143.1, 135.1, 134.6, 130.3, 129.6(2), 129.5, 127.5, 125.2, 124.9, 121.9, 121.3(2), 119.3, 114.7(2), 67.0, 52.9(2), 48.1(2), 42.2. HRMS (ESI)⁺ Calculated for C₂₇H₂₆Cl₂N₅O₃ [M + H]⁺ *m/z* 538.1413, found 538.1408.

N-(3-Chloro-4-(4-methylpiperazin-1-yl)phenyl)-2-(4-(7-chloro-4-oxo-1,4-dihydroquinazolin-2-yl)phenoxy)acetamide (44m).—Off-white solid, mp 280–282 °C, yield 46.2%. ¹H NMR (400 MHz, DMSO-*d*₆), δ (ppm): 12.51 (1H, s), 10.18 (1H, s), 8.19 (2H, d, *J* = 8.8 Hz), 8.12 (1H, d, *J* = 8.8 Hz), 7.80 (1H, d, *J* = 2.4 Hz), 7.45 (1H, d, *J* = 2.4 Hz), 7.51 (2H, dd, *J* = 8.8, 2.4 Hz), 7.13–7.17 (3H, m), 4.81 (2H, s), 3.33 (4H, brs), 2.91–2.93 (4H, m), 2.25 (3H, s). ¹³C NMR (100 MHz, DMSO-*d*₆ + CF₃COOD), δ (ppm): 166.3, 161.6, 160.9, 153.6, 149.4, 143.2, 139.4, 135.2, 129.9(2), 128.1, 127.7, 126.7, 125.9, 124.7, 121.5, 121.4, 119.6, 119.5, 114.9(2), 67.1, 53.0(2), 48.2(2), 42.2. HRMS (ESI)⁺ Calculated for C₂₇H₂₆Cl₂N₅O₃ [M + H]⁺ *m/z* 538.1413, found 538.1415.

N-(3-Chloro-4-(4-methylpiperazin-1-yl)phenyl)-2-(4-(7-methyl-4-oxo-1,4-dihydroquinazolin-2-yl)phenoxy)acetamide (44n).—White powder, mp 279–282 °C, yield 55.5%. ¹H NMR (400 MHz, DMSO-*d*₆), δ (ppm): 12.33 (1H, s), 10.27 (1H, s), 9.91 (1H, s), 8.17 (1H, d, *J* = 8.8 Hz), 8.01 (1H, d, *J* = 8.4 Hz), 7.93 (2H, s), 7.85 (1H, d, *J* = 2.4 Hz), 7.56 (1H, dd, *J* = 8.8, 2.4 Hz), 7.52 (1H, s), 7.31 (1H, dd, *J* = 8.4, 2.4 Hz), 7.22 (1H, d, *J* = 8.8 Hz), 7.14 (1H, d, *J* = 8.8 Hz), 4.82 (2H, s), 3.52 (2H, d, *J* = 11.6 Hz), 3.38 (2H, d, *J* = 11.6 Hz), 3.20 (2H, t, *J* = 12.0 Hz), 2.96 (2H, t, *J* = 12.0 Hz), 2.88 (3H, s), 2.46 (3H, s). ¹³C NMR (100 MHz, DMSO-*d*₆), δ (ppm): 166.3, 162.2, 160.3, 151.9, 148.8, 145.0, 143.1, 135.1, 129.4(2), 127.7, 127.5, 126.8, 125.7, 125.5, 121.3(2), 119.3, 118.3, 114.7(2), 67.0, 52.9(2), 48.1(2), 42.7, 21.4. HRMS (ESI)⁺ Calculated for C₂₈H₂₉ClN₅O₃ [M + H]⁺ *m/z* 518.1959, found 518.1953.

Bioinformatics Analysis.

PrePPI (<https://honiglab.c2b2.columbia.edu/PrePPI/>) was used to predict BRD4 and CK2 related PPI networks. Subsequently, these interacting proteins were annotated and clustered using the Gene Ontology (GO) and the DAVID databases. Finally, the GEPIA tool (<http://gepia.cancer-pku.cn/>) was used to analyze the breast cancer transcriptome data of BRD4 and CK2 obtained from the TCGA database, and a significantly positive correlations identified between BRD4 and CK2 PPI networks were produced by using Cytoscape (version 3.8.2)

Molecular Docking.

Molecular docking follows previous studies.^{14,51} Small molecules were constructed using the Accelrys Discovery Studio (version 3.5; Accelrys, SanDiego, CA, USA) using LibDock

protocol. Small molecules were energy minimized with the CHARMM force field. Then CDocker protocol was performed to rerank the top 10 small molecule compounds. Other parameters were set as default values.

BRD4 and CK2 Enzymatic Assays.

The *in vitro* BRD and CK assays were performed by the drug discovery service of Huawei Pharmaceutical Company. The BRD enzymatic profiling assays were performed with TR-FRET technology.¹⁴ The CK2 and CK1 enzymatic profiling assays were performed by the methods reported in the literature.⁵³

Cellular Thermal Shift Assay (CETSA).

CETSA was performed with intact cells to assay the interaction between **1**, **18**, **44e**, and BRD4/CK2 α . Briefly, MDA-MB-231 cells were incubated with DMSO (0.3% vol/vol), **1** (5 μ M), **18** (5 μ M), or **44e** (5 μ M). After 6 h treatment in the incubator, cells were collected and resuspended in PBS. Following heating at the indicated temperatures (48, 51, 54, 57, 60, and 63 °C) for 3 min, cell suspensions were lysed by three freeze–thaw cycles with liquid nitrogen, thawing at room temperature. The lysates were clarified by centrifugation at 17 000g for 20 min. The soluble proteins in the supernatant were collected and prepared for Western blotting to detect the indicated proteins.

Cell Culture, Antibodies, and Reagents.

MDA-MB-231, MDA-MB-468, and MCF-10A cells were purchased from American Type Culture Collection (ATCC, Manassas, VA, USA). MDA-MB-231 and MCF-10A cells were cultured in DMEM with 10% fetal bovine serum, while MDA-MB-468 cells were cultured in L-15 with 10% fetal bovine serum and incubated with 5% CO₂. Antibodies used in this study were as follows: BRD4 (Cell Signaling Technology, no. 13440S), p-BRD4^{S492} (EMD Millipore, ABE no. 1451), c-Myc (Abcam, ab56), LC3B antibody (Abcam, ab51520), SQSTM1/p62 antibody (Abcam, ab56416), CK2 α (Cell Signaling Technology, no. 2656S), p-AKT^{S129} (Abcam, 133458), GAPDH (Cell Signaling Technology, no. 5174), beclin-1 (Cell Signaling Technology, no. 3495), Bax (Cell Signaling Technology, no. 5023), Bcl-2 (Cell Signaling Technology, no. 2870), caspase-3 (Abcam, ab13847). MTT (M2128), 3-MA (M9281), and Hoechst 33258 were purchased from Solarbio. Bafilomycin A1 (ab120497) was purchased from Abcam.

Generation of JQ1-Resistant Cells.—To generate JQ1-resistant cells, MDA-MB-231 cells were subjected to gradual increases in JQ1 concentrations (72 h pulses every 2 weeks for 6 months).

Cell Viability Assay.—The MDA-MB-231, MDA-MB-468, or MCF-10A cells were dispersed in 96-well plates at a density of 6×10^4 cells/mL. After 24 h incubation, cells were treated with different concentrations of compounds for 24 h. Cell viability was measured by MTT assay. MTT (5 mg/mL) was added, and cells were incubated for an additional 4 h at 37 °C; then the absorbance value was determined with an enzyme-labeling instrument at 490 nm.

Colony Formation Assay.—Cells (500–800 per well) were seeded in 6-well plates and allowed to adhere overnight. Cells were treated with the indicated concentration of compounds or vehicle control for 7–10 days. Cells were fixed with formaldehyde (4%) and stained with crystal violet. The number of colonies was counted. Data represent the mean \pm SD from 3 independent experiments performed in triplicate wells.

Annexin-V/PI Dual Staining.—Cells (1×10^5 per well) were cultured in six-well plates for 24 h. Cells were then cultured in the absence or presence of **44e** (2.5, 5, or 10 μM) for 24 h and then washed twice with cold PBS. The early and late apoptosis cells were identified by flow cytometry (Becton Dickinson, Franklin Lakes, NJ) after applying an Annexin-V/PI Staining Kit (Roche, Germany). The detailed procedures were performed according to the corresponding manufacturer's instructions.

Hoechst Staining.—Cells (2.5×10^4 per well) were plated in 24-well plates, left to adhere overnight, and then incubated with or without **44e** (2.5, 5, or 10 μM) for 24 h. Then, the original growth medium was discarded, cells were washed twice with PBS, followed by addition of Hoechst 33258 for 5 min, and then observed under an Olympus fluorescence microscope.

Autophagy Assay.—A total of 2.5×10^4 cells/well were seeded in a 24-well plate. After transfection with GFP-mRFP-LC3 (HB-AP2100001, HANBIO, China) for 4 h, the original growth medium was replaced with fresh medium, and cells were incubated with or without compounds for 24 h at 37 °C, then analyzed under a fluorescence microscope.

Western Blot Analysis.—Cells were seeded in a 6-well plate (1.5×10^5 cells/well), grown at 37 °C for 24 h, and then treated with compounds and vehicle (DMSO) for 24 h, collected, centrifuged (3000 rpm for 5 min), dissociated, centrifuged again (12000g for 10 min), and quantified (the BCA kit, Beyotime). Western blot analysis was carried out by the following method: In brief, equal amounts of total protein in cell lysate were separated by 10–15% SDS-PAGE and then transferred to PVDF membranes. After being soaked in blocking buffer (5% skimmed milk), the membranes were incubated with corresponding primary antibodies at 4 °C overnight, followed by HRP-conjugated secondary antibody at room temperature for 2 h, and visualized using ECL as the HRP substrate.

Pharmacokinetic Studies.—The pharmacokinetic parameters of **44e** were evaluated. Six Sprague–Dawley (SD) rats (body weight of 200–220 g) were randomly divided into two groups (3 rats in each group) for injection (iv) or oral administration (po). The saline solutions were formulated in 5% DMSO and 10% hydroxypropyl- β -cyclodextrin (HP- β -CD). Two groups of rats were administered a single concentration of **44e** at 1 mg/kg (caudal vein injection) or 10 mg/kg (oral gavage). Blood samples were collected through the jugular vein at the specified time and centrifuged at 7000 rpm for 10 min to obtain the isolated plasma. LC-MS (5500QTRAP system, Applied Biosystems) was used to evaluate the plasma concentration of **44e**.

Xenograft Tumor Models.—All experimental protocols used in this study were carried out in accordance with guidelines of the animal ethics committee (Sichuan University).

Female nude mice (BALB/c, 6–8 weeks, 20–22 g, $n = 48$) were randomized into two groups (24 mice per group) and injected with MDA-MB-231 cells (5×10^6 cells/mouse) or MDA-MB-468 cells (5×10^6 cells/mouse). When the tumors of all mice reached 100 mm^3 in volume ($V = L \times W^2/2$), the mice were randomly grouped by weight and coded according to the tumor types ($n = 6$ in each group) and treated via intragastric administration of 0.2 mL of saline, **1 + 18** (50 mg/kg, combined at a mole ratio of 1:1), or **44e** (25 or 50 mg/kg) once a day for 19 days. Meanwhile, the tumor volume and body weight were measured every 3 days during treatment. At the end of treatment, all mice were sacrificed. The tumor tissues and main tissues were harvested and weighed. Then, the tumor tissues were frozen in liquid nitrogen or fixed in formalin immediately for immunohistochemistry analysis and HE staining.

HE Staining.—The fixed tissues were dehydrated and paraffin embedded. Then tissues were sliced into 4 mm thick slices, stained for 10–15 min with hematoxylin, washed for 2 min (tap water), differentiated for 30 s (different gradients hydrochloric acid and ethanol), washed for 5 min (warm water), and finally placed into the eosin solution for 2 min before regular dehydration and sealing with resinene. All the specimens were evaluated according to the pathological examination SOP procedure.

Immunohistochemistry Analysis (IHC).—Tumor sections were immersed in EDTA antigen retrieval buffer (pH 8.0) or citrate buffer (pH 6.0), and microwave was used for antigen retrieval. Then the slides were incubated with anti-Ki-67 antibody (1:500), anti-BRD4 antibody (1:500), anti-c-Myc antibody (1:500), anti-CK2 α antibody (1:500), anti-p-AKT^{S129} antibody (1:400), or anti-LC3B antibody (1:400) for 30–40 min at 37 °C. Normal rabbit or mouse IgG was used as a negative control. The slides were then treated with HRP polymer conjugated secondary antibody for 30 min and developed with diaminobenzidine solution. Meyer's hematoxylin was used as a counterstain.

Statistical Analysis.

All cell experiments were performed independently at least three times. The data are expressed as the mean \pm SD and analyzed with GraphPad Prism 7.0. Statistical comparisons were made by one-way ANOVA and Student's test. $p < 0.05$ was considered statistically significant.

Supplementary Material

Refer to Web version on PubMed Central for supplementary material.

ACKNOWLEDGMENTS

This work was supported by the National Natural Science Foundation of China (Grant Numbers 81922064, 81874290, 81903502, and 81803365), the Applied Basic Research Programs of Science and Technology Department of Sichuan Province (Grant Numbers 2020YJ0105, 2020YJ0094), the Fundamental Research Funds for the Central Universities (Grant Number 2021SCU12102), China Postdoctoral Science Foundation (Grant Number 2020M673268), and Health Commission of Sichuan Province (Grant Number 20PJ002). C.-M.C.'s research is sponsored by the U.S. National Institutes of Health (Grant 1RO1CA251698-01) and the Cancer Prevention and Research Institute of Texas (CPRIT; Grants RP180349 and RP190077).

ABBREVIATIONS

AKT	protein kinase B
BC	breast cancer
BafA1	bafilomycin A1
BLBC	basal-like breast cancer
BRD4	bromodomain-containing protein 4
CK2	casein kinase 2
DBU	1,8-diazabicyclo[5.4.0]undec-7-ene
DMAc	dimethylacetamide
EDCI	1-ethyl-3-(3-dimethylaminopropyl)carbodiimide
EGFR	epidermal growth factor receptor
ER	estrogen receptor
ERK	extracellular signal-regulated kinase
GFP	green fluorescent protein
HE	hematoxylin–eosin
HER2	human epidermal growth factor receptor 2
HOAc	acetic acid
HOBt	hydroxybenzotriazole
HRESIMS	high resolution electrospray ionization mass spectroscopy
IHC	immunohistochemistry analysis
IC₅₀	half-maximal inhibitory concentration
MAPK	mitogen-activated protein kinase
MTT	3-(4,5-dimethylthiazol-2-yl)-2,5-diphenyltetrazolium bromide
3-MA	3-methyladenine
NMM	<i>N</i> -methylmorpholine
PE	polyethylene
PARP	poly(ADP-ribose) polymerase
PI3K	phosphoinositide 3-kinase
PR	progesterone receptor

PTSA	<i>p</i> -toluenesulfonic acid
Q-TOF	quadrupole time of flight
SAR	structure–activity relationship
TCGA	The Cancer Genome Atlas
TEA	triethylamine
TFA	trifluoroacetic acid
TNBC	triple-negative breast cancer
TMS	tetramethylsilane
TR-FRET	time resolved fluorescence resonance energy transfer
VEGFR2	vascular endothelial growth factor 2

REFERENCES

- (1). Siegel RL; Miller KD; Jemal A Cancer statistics, 2020. *CA-Cancer. Ca-Cancer J. Clin* 2020, 70, 7–30. [PubMed: 31912902]
- (2). Xu T; Zhang JF; Yang CC; Pluta R; Wang G; Ye TH; Ouyang L Identification and optimization of 3-bromo-*N*-(4-hydroxybenzylidene)-4-methylbenzohydrazide derivatives as mTOR inhibitors that induce autophagic cell death and apoptosis in triplenegative breast cancer. *Eur. J. Med. Chem* 2021, 219, 113424. [PubMed: 33862514]
- (3). Franzoi MA; Romano E; Piccart M Immunotherapy for early breast cancer: too soon, too superficial, or just right? *Ann. Oncol* 2021, 32, 323–336. [PubMed: 33307202]
- (4). Vagia E; Mahalingam D; Cristofanilli M The landscape of targeted therapies in TNBC. *Cancers* 2020, 12, 916. [PubMed: 32276534]
- (5). Tang P; Zhang JF; Liu J; Chiang CM; Ouyang L Targeting bromodomain and extraterminal proteins for drug discovery: from current progress to technological development. *J. Med. Chem* 2021, 64, 2419–2435. [PubMed: 33616410]
- (6). Zhang JF; Ouyang L Proteolysis-targeting chimeras in breast cancer therapy. *Future Med. Chem* 2020, 12, 2175–2177. [PubMed: 33225735]
- (7). Da Motta LL; Ledaki I; Purshouse K; Haider S; De Bastiani MA; Baban D; Morotti M; Steers G; Wigfield S; Bridges E; Li JL; Knapp S; Ebner D; Klamt F; Harris AL; McIntyre A The BET inhibitor JQ1 selectively impairs tumour response to hypoxia and downregulates CA9 and angiogenesis in triple negative breast cancer. *Oncogene* 2017, 36, 122–132. [PubMed: 27292261]
- (8). Verma N; Müller AK; Kothari C; Panayotopoulou E; Kedan A; Selitrennik M; Mills GB; Nguyen LK; Shin S; Karn T; Holtrich U; Lev S Targeting of PYK2 synergizes with EGFR antagonists in basal-like TNBC and circumvents HER3-associated resistance via the NEDD4-NDRG1 axis. *Cancer Res.* 2017, 77, 86–99. [PubMed: 27793840]
- (9). Loi S; Dushyanthen S; Beavis PA; Salgado R; Denkert C; Savas P; Combs S; Rimm DL; Giltneane JM; Estrada MV; Sánchez V; Sanders ME; Cook RS; Pilkinton MA; Mallal SA; Wang K; Miller VA; Stephens PJ; Yelensky R; Doimi FD; Gómez H; Ryzhov SV; Darcy PK; Arteaga CL; Balko JM RAS/MAPK activation is associated with reduced tumor-infiltrating lymphocytes in triple-negative breast cancer: therapeutic cooperation between MEK and PD-1/PD-L1 immune checkpoint inhibitors. *Clin. Cancer Res* 2016, 22, 1499–1509. [PubMed: 26515496]
- (10). Delaloge S; DeForceville L Targeting PI3K/AKT pathway in triple-negative breast cancer. *Lancet Oncol.* 2017, 18, 1293–1294. [PubMed: 28800863]
- (11). Curtin NJ; Szabo C Poly(ADP-ribose) polymerase inhibition: past, present and future. *Nat. Rev. Drug Discovery* 2020, 19, 711–736. [PubMed: 32884152]

- (12). Jhan JR; Andrechek ER Triple-negative breast cancer and the potential for targeted therapy. *Pharmacogenomics* 2017, 18, 1595–1609. [PubMed: 29095114]
- (13). Lord CJ; Ashworth A PARP inhibitors: synthetic lethality in the clinic. *Science* 2017, 355, 1152–1158. [PubMed: 28302823]
- (14). Chang XS; Sun DJ; Shi DF; Wang G; Chen Y; Zhang K; Tan HD; Liu J; Liu B; Ouyang L Design, synthesis, and biological evaluation of quinazolin-4(3*H*)-one derivatives co-targeting poly-(ADP-ribose) polymerase-1 and bromodomain containing protein 4 for breast cancer therapy. *Acta Pharm. Sin. B* 2021, 11, 156–180. [PubMed: 33532187]
- (15). Gornstein EL; Sandefur S; Chung JH; Gay LM; Holmes O; Erlich RL; Soman S; Martin LK; Rose AV; Stephens PJ; Ross JS; Miller VA; Ali SM; Blau S BRCA2 reversion mutation associated with acquired resistance to olaparib in estrogen receptor-positive breast cancer detected by genomic profiling of tissue and liquid biopsy. *Clin. Breast Cancer* 2018, 18, 184–188. [PubMed: 29325860]
- (16). Feng L; Wang G; Chen Y; He G; Liu B; Liu J; Chiang CM; Ouyang L Dual-target inhibitors of bromodomain and extraterminal proteins in cancer: A review from medicinal chemistry perspectives. *Med. Res. Rev* 2021, DOI: 10.1002/med.21859.
- (17). Filippakopoulos P; Knapp S Targeting bromodomains: epigenetic readers of lysine acetylation. *Nat. Rev. Drug Discovery* 2014, 13, 337–356. [PubMed: 24751816]
- (18). Wu SY; Chiang CM The double bromodomain-containing chromatin adaptor BRD4 and transcriptional regulation. *J. Biol. Chem* 2007, 282, 13141–13145. [PubMed: 17329240]
- (19). Wu SY; Nin DS; Lee AY; Simanski S; Kodadek T; Chiang CM BRD4 phosphorylation regulates HPV E2-mediated viral transcription, origin replication, and cellular MMP-9 expression. *Cell Rep.* 2016, 16, 1733–1748. [PubMed: 27477287]
- (20). Ramadoss M; Mahadevan V Targeting the cancer epigenome: synergistic therapy with bromodomain inhibitors. *Drug Discovery Today* 2018, 23, 76–89. [PubMed: 28943305]
- (21). Wu SY; Lee CF; Lai HT; Yu CT; Lee JE; Zuo H; Tsai SY; Tsai MJ; Ge K; Wan Y; Chiang CM Opposing functions of BRD4 isoforms in breast cancer. *Mol. Cell* 2020, 78, 1114–1132. [PubMed: 32446320]
- (22). Chiang CM Phospho-BRD4: transcription plasticity and drug targeting. *Drug Discovery Today: Technol.* 2016, 19, 17–22.
- (23). Marcotte R; Sayad A; Brown KR; Sanchez-Garcia F; Reimand J; Haider M; Virtanen C; Bradner JE; Bader GD; Mills GB; Pe'er D; Moffat J; Neel BG Functional genomic landscape of human breast cancer drivers, vulnerabilities, and resistance. *Cell* 2016, 164, 293–309. [PubMed: 26771497]
- (24). Andrieu G; Tran AH; Strissel KJ; Denis GV BRD4 regulates breast cancer dissemination through Jagged1/Notch1 signaling. *Cancer Res.* 2016, 76, 6555. [PubMed: 27651315]
- (25). Zawistowski JS; Bevill SM; Goulet DR; Stuhlmiller TJ; Beltran AS; Olivares-Quintero JF; Singh D; Sciaky N; Parker JS; Rashid NU; Chen X; Duncan JS; Whittle MC; Angus SP; Velarde SH; Golitz BT; He X; Santos C; Darr DB; Gallagher K; Graves LM; Perou CM; Carey LA; Earp HS; Johnson GL Enhancer remodeling during adaptive bypass to MEK inhibition is attenuated by pharmacologic targeting of the p-TEFb complex. *Cancer Discovery* 2017, 7, 302–321. [PubMed: 28108460]
- (26). Devaiah BN; Mu J; Akman B; Uppal S; Weissman JD; Cheng D; Baranello L; Nie Z; Levens D; Singer DS MYC protein stability is negatively regulated by BRD4. *Proc. Natl. Acad. Sci. U. S. A* 2020, 117, 13457–13467. [PubMed: 32482868]
- (27). Liu ZQ; Wang PY; Chen HY; Wold EA; Tian B; Brasier AR; Zhou J Drug discovery targeting bromodomain-containing protein 4. *J. Med. Chem* 2017, 60, 4533–4558. [PubMed: 28195723]
- (28). Pan ZP; Li X; Wang YJ; Jiang QL; Jiang L; Zhang M; Zhang N; Wu FB; Liu B; He G Discovery of thieno[2,3-*d*]pyrimidine-based hydroxamic acid derivatives as bromodomain-containing protein 4/histone deacetylase dual inhibitors induce autophagic cell death in colorectal carcinoma cells. *J. Med. Chem* 2020 63, 3678–3700. [PubMed: 32153186]
- (29). Kulikowski E; Rakai BD; Wong N Inhibitors of bromodomain and extra-terminal proteins for treating multiple human diseases. *Med. Res. Rev* 2021, 41, 223–245. [PubMed: 32926459]

- (30). Fong CY; Gilan O; Lam EY; Rubin AF; Ftouni S; Tyler D; Stanley K; Sinha D; Yeh P; Morison J; Giotopoulos G; Lugo D; Jeffrey P; Lee SC; Carpenter C; Gregory R; Ramsay RG; Lane SW; Abdel-Wahab O; Kouzarides T; Johnstone RW; Dawson SJ; Huntly BJ; Prinjha RK; Papenfuss AT; Dawson MA BET inhibitor resistance emerges from leukaemia stem cells. *Nature* 2015, 525, 538–542. [PubMed: 26367796]
- (31). Rathert P; Roth M; Neumann T; Muerdter F; Roe JS; Muhar M; Deswal S; Cerny-Reiterer S; Peter B; Jude J; Hoffmann T; Boryn LM; Axelsson E; Schweifer N; Tontsch-Grunt U; Dow LE; Gianni D; Pearson M; Valent P; Stark A; Kraut N; Vakoc CR; Zuber J Transcriptional plasticity promotes primary and acquired resistance to BET inhibition. *Nature* 2015, 525, 543–547. [PubMed: 26367798]
- (32). Calder J; Nagelberg A; Luu J; Lu D; Lockwood WW Resistance to BET inhibitors in lung adenocarcinoma is mediated by casein kinase phosphorylation of BRD4. *Oncogenesis*. 2021, 10, 27. [PubMed: 33712563]
- (33). Licciardello MP; Workman P A new chemical probe challenges the broad cancer essentiality of CK2. *Trends Pharmacol. Sci* 2021, 42, 313–315. [PubMed: 33771354]
- (34). Wang YJ; Wang XY; Xu G; Gou SH Novel CK2-specific Pt(II) compound reverses cisplatin-induced resistance by inhibiting cancer cell stemness and suppressing DNA damage repair in non-small cell lung cancer treatments. *J. Med. Chem* 2021, 64, 4163–4178. [PubMed: 33784109]
- (35). Wang YJ; Lv ZD; Chen FH; Wang X; Gou SH Discovery of 5-(3-Chlorophenylamino)benzo[c][2,6]naphthyridine derivatives as highly selective CK2 inhibitors with potent cancer cell stemness inhibition. *J. Med. Chem* 2021, 64, 5082–5098. [PubMed: 33834781]
- (36). Hwang DW; So KS; Kim SC; Park KM; Lee YJ; Kim SW; Choi CM; Rho JK; Choi YJ; Lee JC Autophagy induced by CX-4945, a casein kinase 2 inhibitor, enhances apoptosis in pancreatic cancer cell lines. *Pancreas* 2017, 46, 575–581. [PubMed: 28196025]
- (37). Wu SY; Lee AY; Lai HT; Zhang H; Chiang CM Phospho switch triggers BRD4 chromatin binding and activator recruitment for gene-specific targeting. *Mol. Cell* 2013, 49, 843–857. [PubMed: 23317504]
- (38). Shu S; Lin CY; He HH; Witwicki RM; Tabassum DP; Roberts JM; Janiszewska M; Huh SJ; Liang Y; Ryan J; Doherty E; Mohammed H; Guo H; Stover DG; Ekram MB; Brown J; D'Santos C; Krop IE; Dillon D; McKeown M; Ott C; Qi J; Ni M; Rao PK; Duarte M; et al. Response and resistance to BET bromodomain inhibitors in triple negative breast cancer. *Nature*. 2016, 529, 413–417. [PubMed: 26735014]
- (39). Becherel OJ; Jakob B; Cherry AL; Gueven N; Fusser M; Kijas AW; Peng C; Katyal S; McKinnon PJ; Chen J; Epe B; Smerdon SJ; Taucher-Scholz G; Lavin MF CK2 phosphorylation-dependent interaction between aprataxin and MDC1 in the DNA damage response. *Nucleic Acids Res.* 2010, 38, 1489–1503. [PubMed: 20008512]
- (40). Zhou B; Ritt DA; Morrison DK; Der CJ; Cox AD Protein kinase CK2 α maintains extracellular signal-regulated kinase (ERK) activity in a CK2 α kinase-independent manner to promote resistance to inhibitors of RAF and MEK but not ERK in BRAF mutant melanoma. *J. Biol. Chem* 2016, 291, 17804–17815. [PubMed: 27226552]
- (41). Loizou JI; El-Khamisy SF; Zlatanou A; Moore DJ; Chan DW; Qin J; Sarno S; Meggio F; Pinna LA; Caldecott KW The protein kinase CK2 facilitates repair of chromosomal DNA single-strand breaks. *Cell* 2004, 117, 17–28. [PubMed: 15066279]
- (42). Zhang QC; Petrey D; Deng L; Qiang L; Shi Y; Thu CA; Bisikirska B; Lefebvre C; Accili D; Hunter T; Maniatis T; Califano A; Honig B Structure-based prediction of protein-protein interactions on a genome-wide scale. *Nature* 2012, 490, 556–560. [PubMed: 23023127]
- (43). Zhang QC; Petrey D; Garzón JI; Deng L; Honig B PrePPI: a structure-informed database of protein-protein interactions. *Nucleic Acids Res.* 2012, 41, D828–D833. [PubMed: 23193263]
- (44). Huang DW; Sherman BT; Lempicki RA Bioinformatics enrichment tools: paths toward the comprehensive functional analysis of large gene lists. *Nucleic Acids Res.* 2009, 37, 1–13. [PubMed: 19033363]
- (45). Huang DW; Sherman BT; Lempicki RA Systematic and integrative analysis of large gene lists using DAVID bioinformatics resources. *Nat. Protoc* 2009, 4, 44–57. [PubMed: 19131956]

- (46). Tang ZF; Li CW; Kang BX; Gao G; Li C; Zhang ZM GEPIA: a web server for cancer and normal gene expression profiling and interactive analyses. *Nucleic Acids Res.* 2017, 45, W98–W102. [PubMed: 28407145]
- (47). Zhang L; Zhang L; Guo Y; Xiao M; Feng L; Yang C; Wang G; Ouyang L MCDB: A comprehensive curated mitotic catastrophe database for retrieval, protein sequence alignment, and target prediction. *Acta Pharm. Sin. B* 2021, 11, 3092. [PubMed: 34729303]
- (48). Wang G; Zhao YQ; Liu Y; Sun DJ; Zhen YQ; Liu J; Fu L; Zhang L; Ouyang L Discovery of a novel dual-target inhibitor of ERK1 and ERK5 that induces regulated cell death to overcome compensatory mechanism in specific tumor types. *J. Med. Chem* 2020, 63, 3976–3995. [PubMed: 32078308]
- (49). Noblejas-López MDM; Nieto-Jimenez C; Burgos M; GómezJuárez M; Montero JC; Esparís-Ogando A; Pandiella A; Galán-Moya EM; Ocaña A Activity of BET-proteolysis targeting chimeric (PROTAC) compounds in triple negative breast cancer. *J. Exp. Clin. Cancer. Res* 2019, 38, 383. [PubMed: 31470872]
- (50). Ouyang L; Zhang L; Liu J; Fu L; Yao D; Zhao Y; Zhang S; Wang G; He G; Liu B Discovery of a small-molecule bromodomain-containing protein 4 (BRD4) inhibitor that induces AMP-activated protein kinase-modulated autophagy-associated cell death in breast cancer. *J. Med. Chem* 2017, 60, 9990–10012. [PubMed: 29172540]
- (51). Ouyang L; Zhang L; Zhang S; Yao D; Zhao Y; Wang G; Fu L; Lei P; Liu B Small-molecule activator of UNC-51-Like Kinase 1 (ULK1) that induces cytoprotective autophagy for parkinson's disease treatment. *J. Med. Chem* 2018, 61, 2776–2792. [PubMed: 29561612]
- (52). Zhang L; Fu LL; Zhang SY; Zhang J; Zhao YQ; Zheng YX; He G; Yang SY; Ouyang L; Liu B Discovery of a small molecule targeting ULK1-modulated cell death of triple negative breast cancer in vitro and in vivo. *Chem. Sci* 2017, 8, 2687–2701. [PubMed: 28553505]
- (53). Kashem MA; Nelson RM; Yingling JD; Pullen SS; Prokopowicz AS; Jones JW; Wolak JP; Rogers GR; Morelock MM; Snow RJ; Homon CA; Jakes S Three mechanistically distinct kinase assays compared: Measurement of intrinsic ATPase activity identified the most comprehensive set of ITK inhibitors. *J. Biomol Screening* 2007, 12, 70–83.

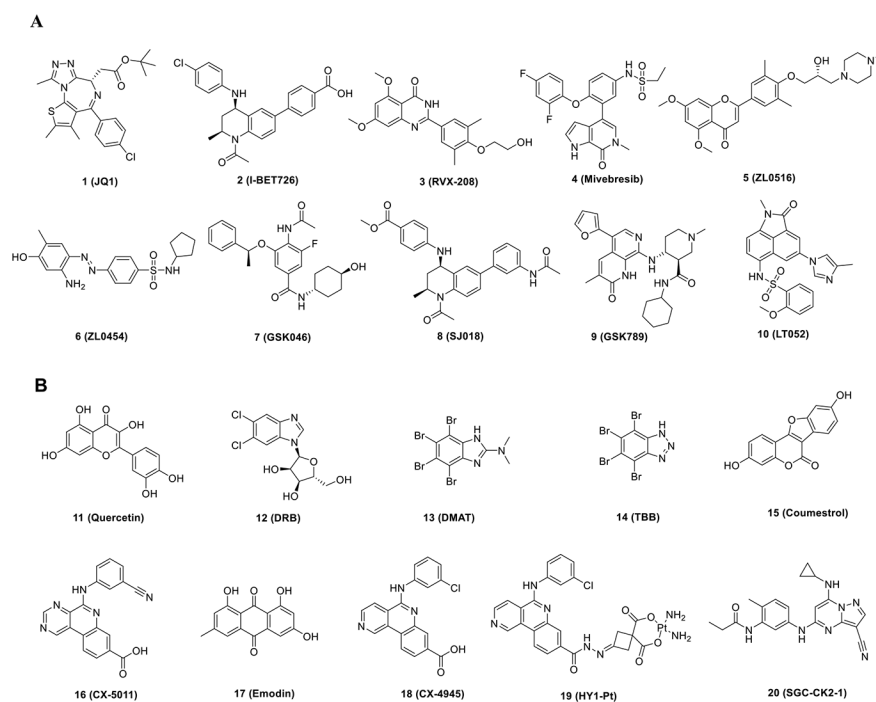


Figure 1. Structures representing known BRD4 and CK2 inhibitors. (A) Representative published BRD4 inhibitors with diverse scaffolds. (B) Representative published CK2 inhibitors with diverse scaffolds.

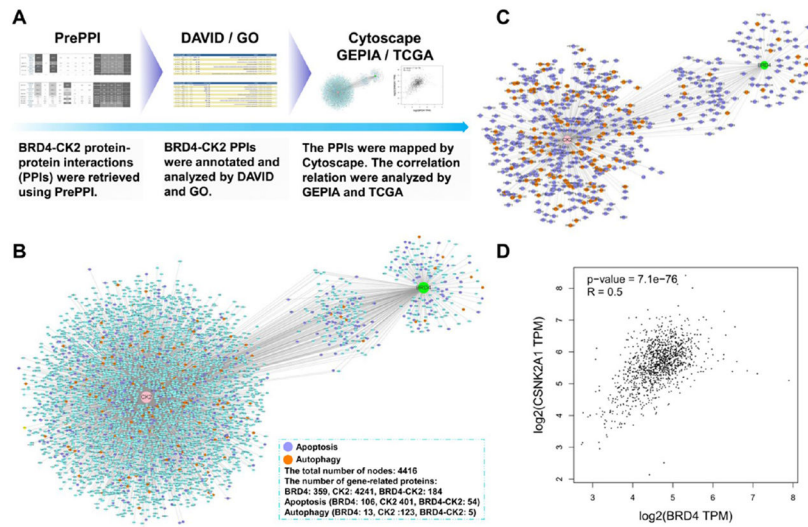


Figure 2. Bioinformatics analysis. (A) Workflow of bioinformatics analysis of BRD4–CK2 association. (B) Clustering of BRD4 and CK2 interacting protein networks related to cell autophagy and apoptosis. (C) Predicted BRD4 and CK2 related proteins involved in the regulation of cell apoptosis and autophagy-associated cell death. (D) Correlation between BRD4 and CK2 in BC.

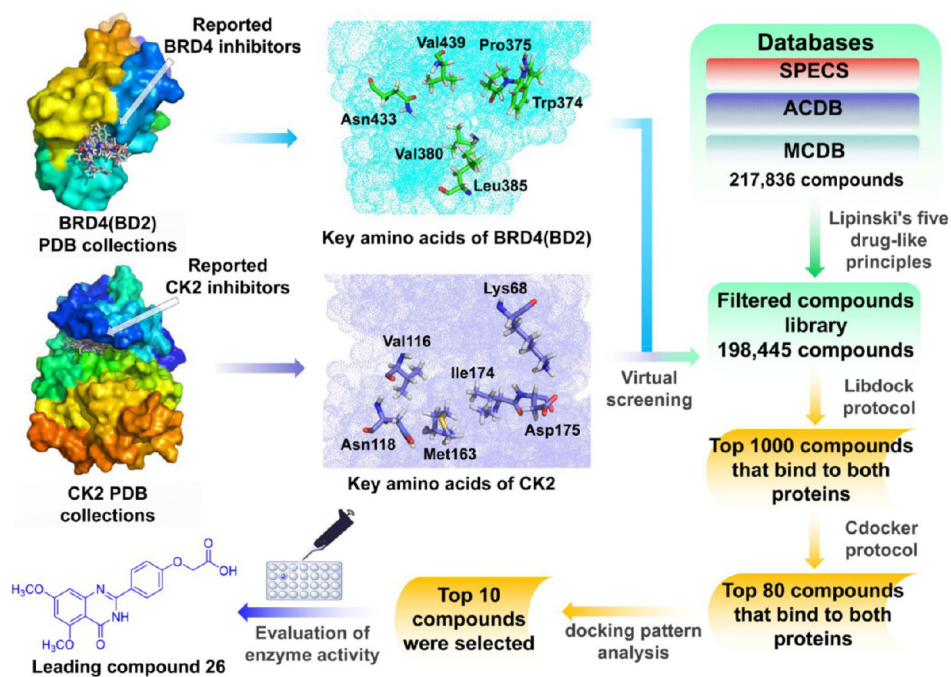


Figure 3. Workflow of designing BRD4–CK2 inhibitors based on extracted amino acid residues and virtual screening.

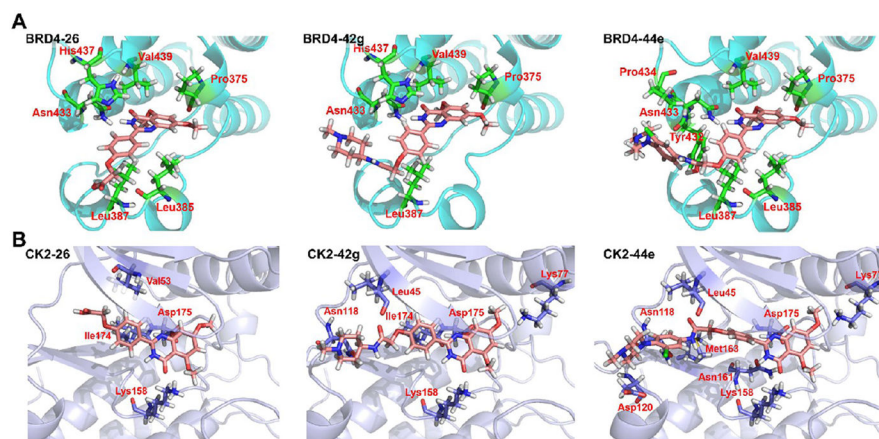


Figure 4. Binding mode analysis of **26**, **42g**, and **44e**. (A, B) Docking poses show the interaction of **26**, **42g**, and **44e** with BRD4 (BD2) (PDB ID 5UOO) and CK2 (PDB ID 6RFE), respectively. Oxygen atoms are colored in red and nitrogen atoms in blue.

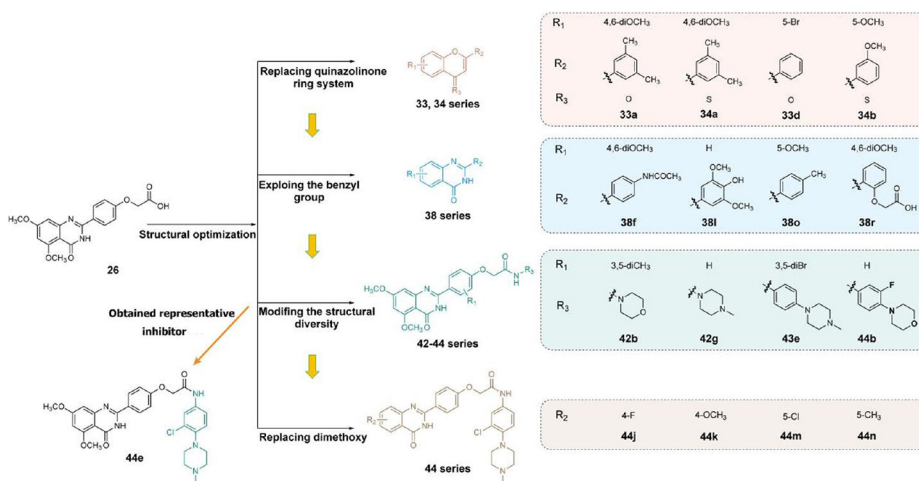


Figure 5. Structural optimization and discovery of BRD4-CK2 dual-target inhibitors. Representative compounds are shown.

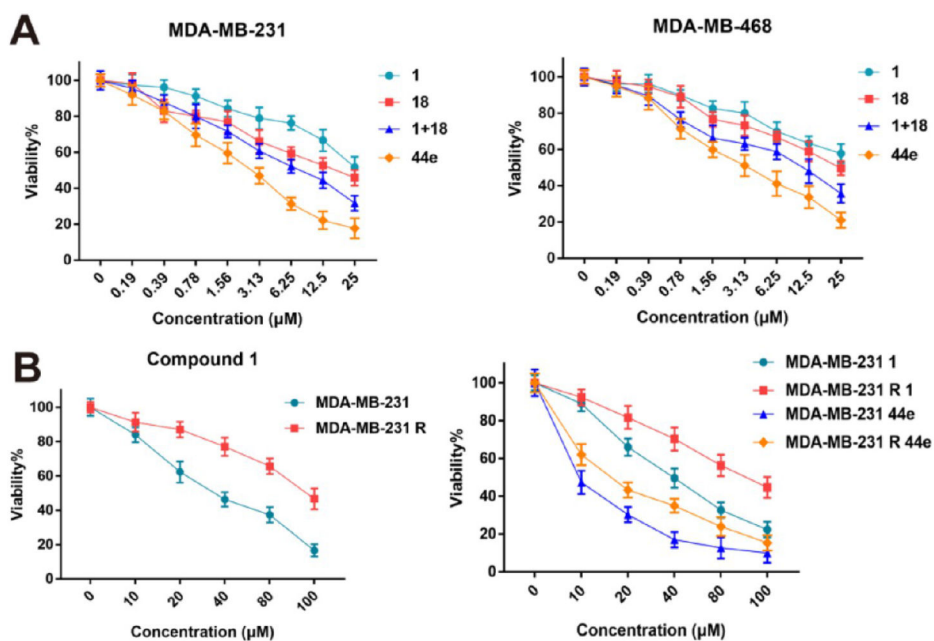


Figure 6. Antiproliferative activity of candidate compound **44e**. (A) Antiproliferative activity of **1**, **18**, **1 + 18**, and **44e** toward MDA-MB-231 and MDA-MB-468 cells. (B) Antiproliferative activity of **44e** toward compound **1**-resistant MDA-MB-231R cells.

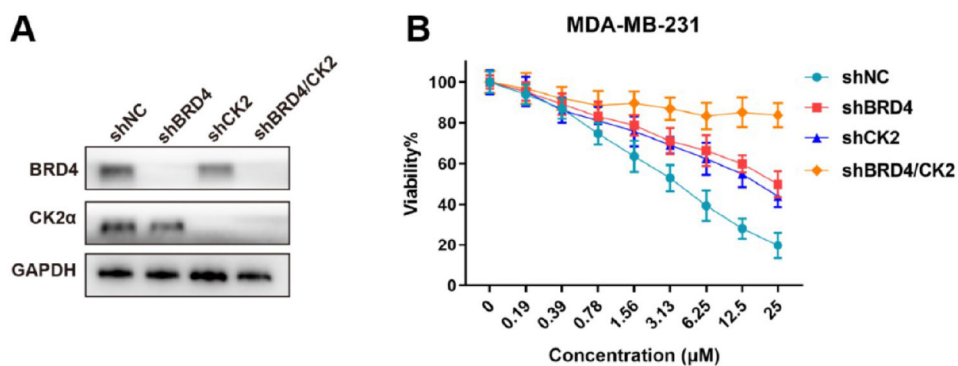


Figure 7. Antiproliferative activity of candidate compound **44e** relies on BRD4 and CK2. (A) BRD4, CK2, or BRD4/CK2 knockdown efficiency in MDA-MB-231 cells as determined by Western blots. GAPDH was used as a control. (B) MDA-MB-231 cell viability after 24 h at different concentrations of **44e**.

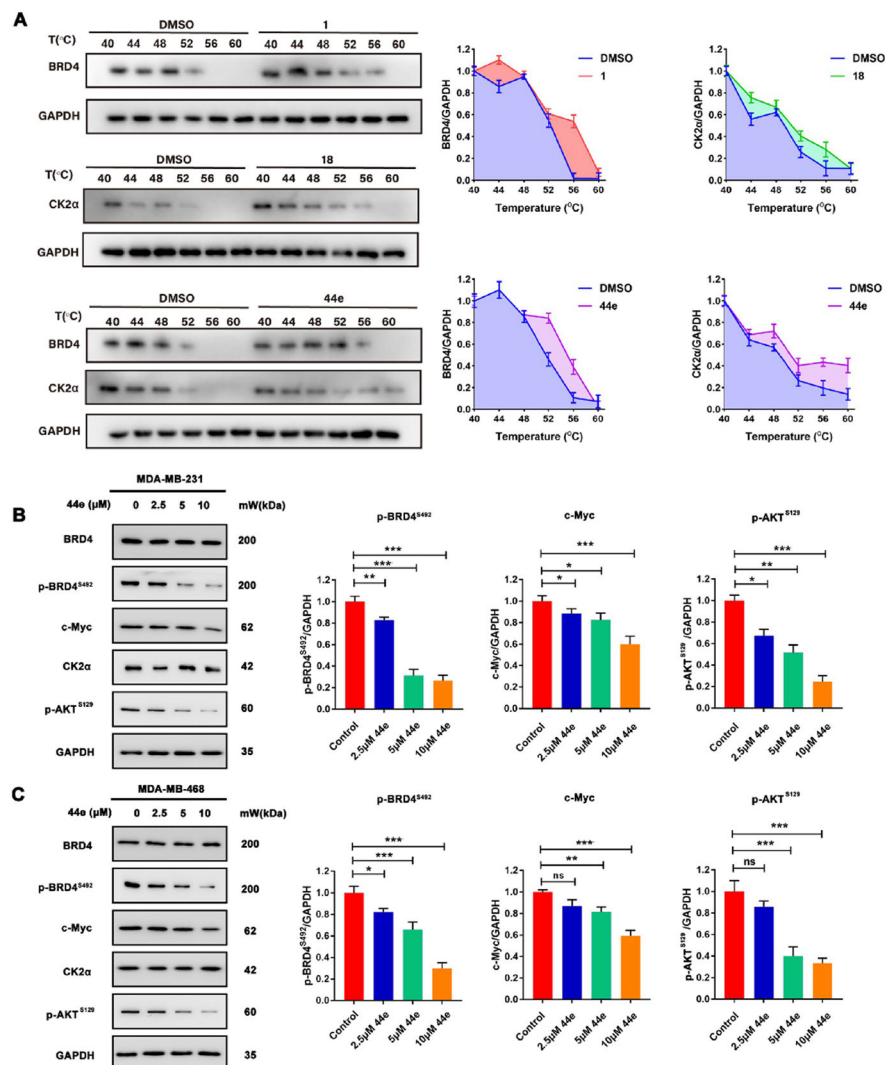


Figure 8. Western blotting assay. (A) CETSA assay detected the thermal stability of BRD4 and CK2 in MDA-MB-231 cells treated with **1**, **18**, and **44e**. (B, C) Expression of BRD4, p-BRD4^{S492}, c-Myc, CK2 α , and p-AKT^{S129} in MDA-MB-231 and MDA-MB-468 cells treated with 0, 2.5, 5, and 10 μ M of **44e** for 24 h. Error bar shows SD; * $p < 0.05$, ** $p < 0.01$, *** $p < 0.001$, **** $p < 0.0001$ compared with the control groups.

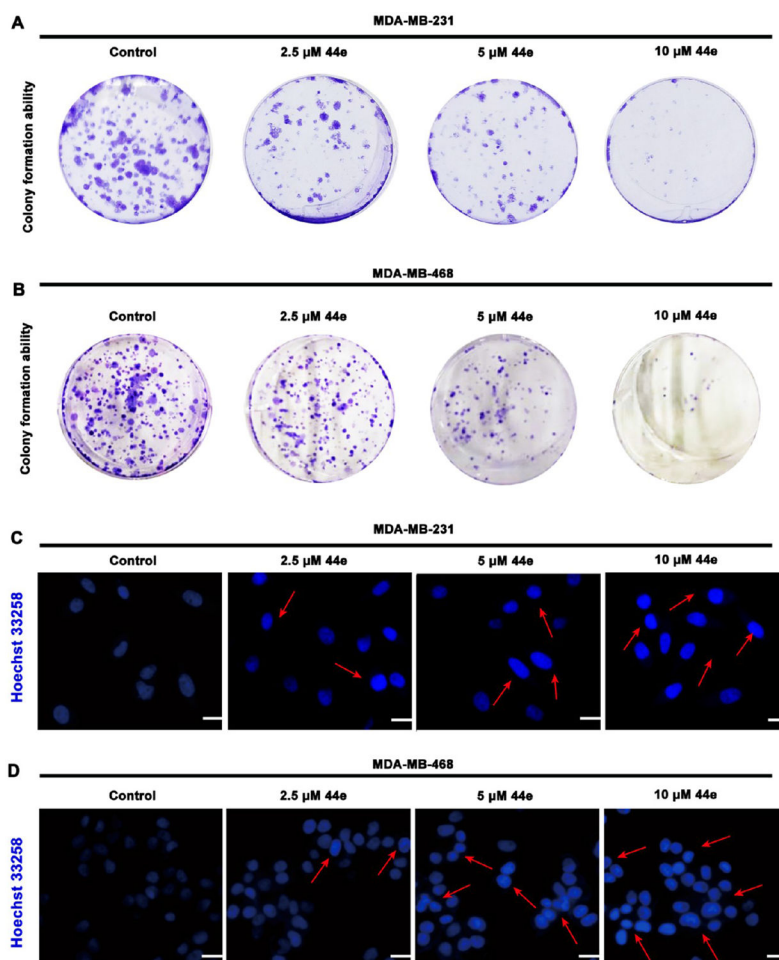


Figure 9. Compound **44e** inhibits colony formation and promotes apoptosis in TNBC cells. (A, B) Colony formation assay. MDA-MB-231 and MDA-MB-468 cells were treated with 0, 2.5, 5, and 10 μM of **44e** for 7 days. (C, D) Hoechst 33258 staining assay. MDA-MB-231 and MDA-MB-468 cells treated with 0, 2.5, 5, and 10 μM of **44e** for 24 h. Scale bar, 10 μm .

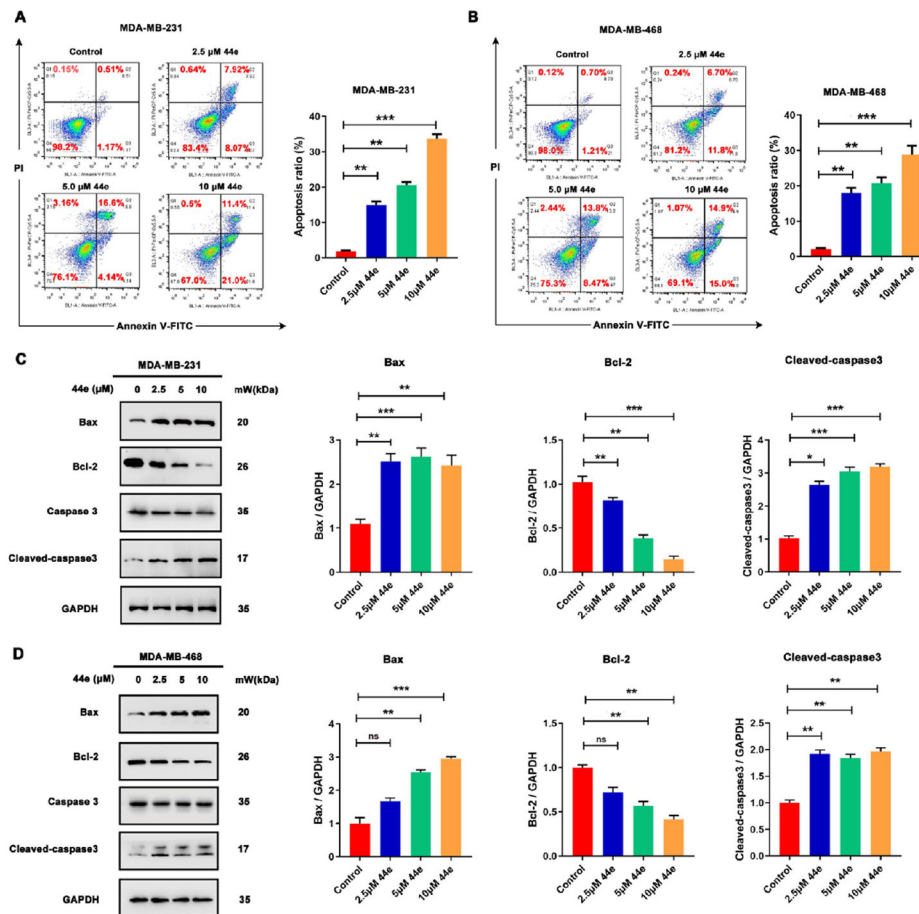


Figure 10.

Apoptotic effect of **44e** on TNBC cells. (A, B) MDA-MB-231 and MDA-MB-468 cells were treated with indicated concentrations of **44e** for 24 h. Apoptosis ratios were determined by flow cytometry analysis of Annexin-V/PI double staining. A representative image and quantification of apoptosis are presented. (C, D) Cells were treated with **44e** at different concentrations for 24 h. The levels of apoptosis-related proteins, including Bcl-2, Bax, caspase-3, and cleaved caspase-3, were analyzed by Western blotting. GAPDH was used as load control. Error bar shows SD; * $p < 0.05$, ** $p < 0.01$, *** $p < 0.001$, **** $p < 0.0001$ compared with the control groups.

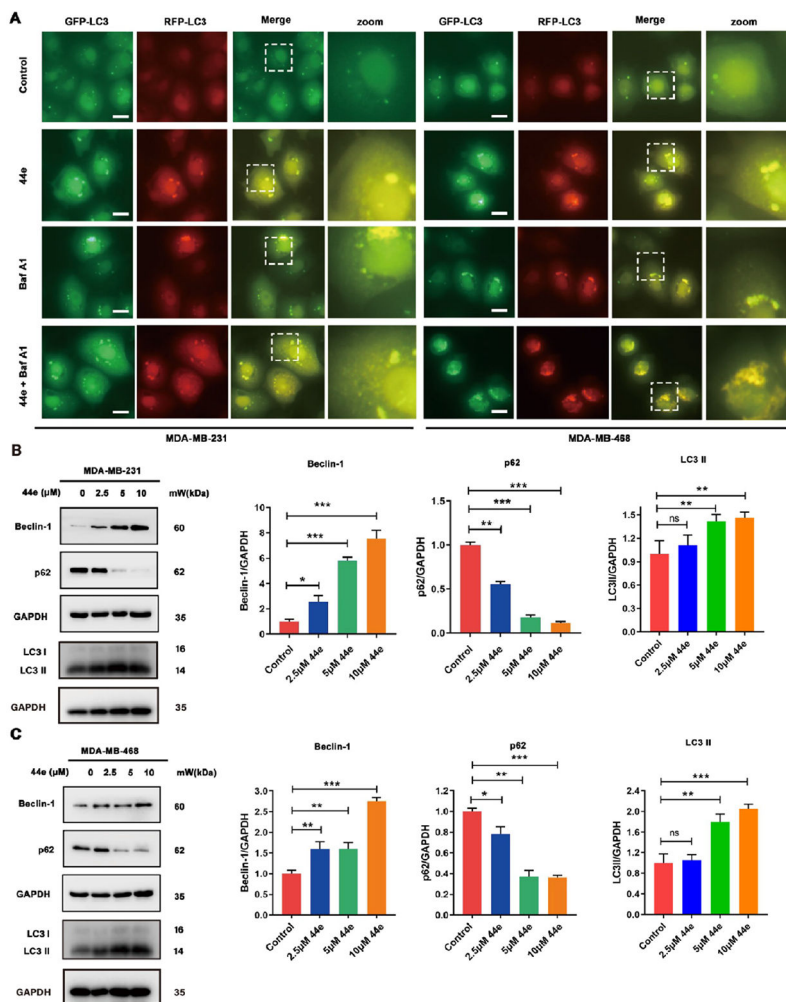


Figure 11.

Compound **44e** induces regulated autophagy in TNBC cells. (A) MDA-MB-231 and MDA-MB-468 cells were transfected with GFP-mRFP-LC3 adenovirus, following co-incubation with **44e** (5 μ M) in the presence or absence of BafA1 (10 nM). Scale bar, 10 μ m. (B, C) Expression levels of Beclin-1, LC3, and p62 in MDA-MB-231 and MDA-MB-468 cells treated with 5 μ M **44e**, analyzed by Western blotting. GAPDH was used as load control. Error bar shows SD; * $p < 0.05$, ** $p < 0.01$, *** $p < 0.001$, **** $p < 0.0001$ compared with the control groups.

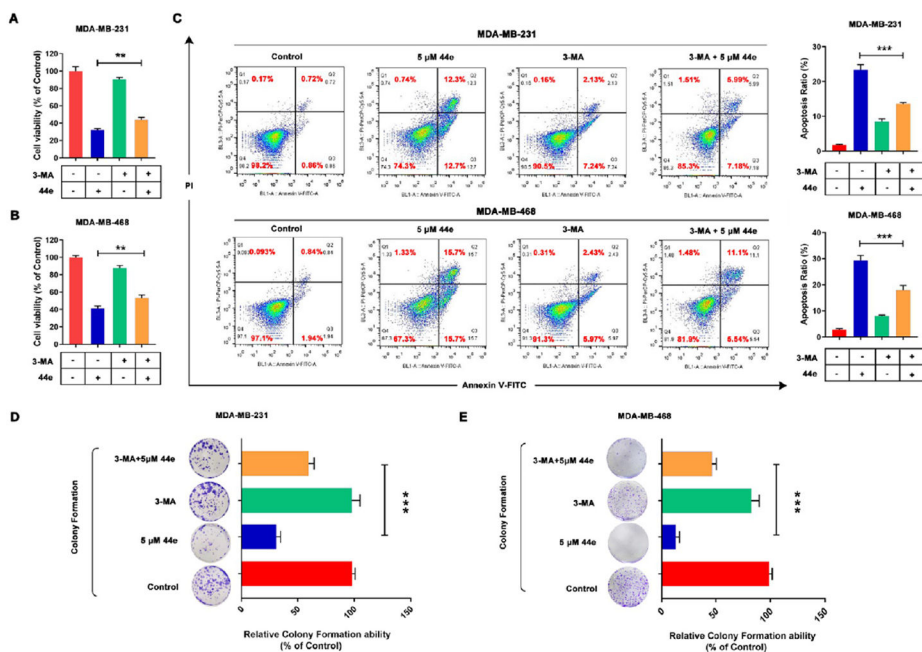
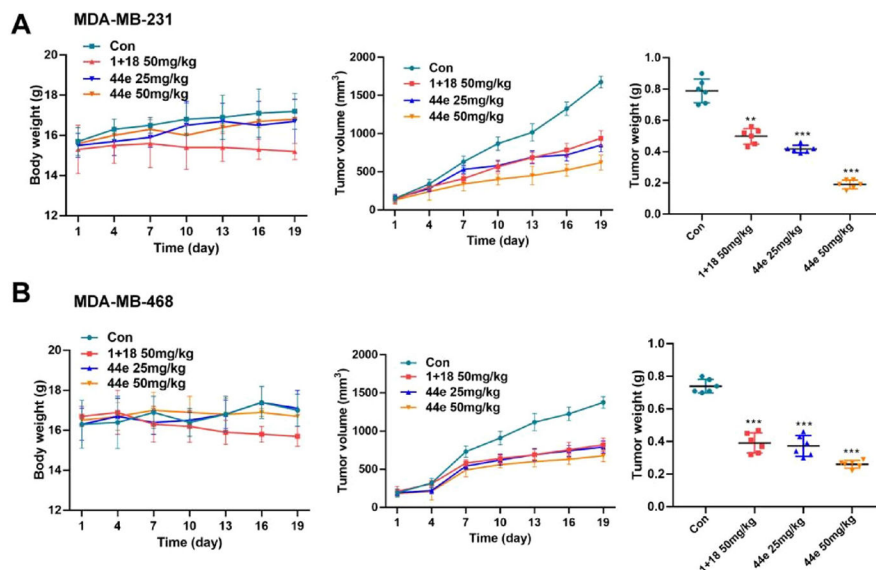


Figure 12.

Mechanism of autophagy in **44e**-induced cell death in TNBC cells. (A, B) MDA-MB-231 and MDA-MB-468 cell viability was measured by MTT assay. Cells were treated with **44e** at 5 μ M or combined with 3-MA at 1 mM treated for 24 h. 3-MA was added 1 h before treatment with **44e**. (C) MDA-MB-231 and MDA-MB-468 cell apoptosis ratios were analyzed by flow cytometry with Annexin-V/PI double staining. Cells were treated with **44e** at 5 μ M or combined with 3-MA at 1 mM for 24 h. 3-MA was added 1 h before treatment with **44e**. (D, E) Colony formation assay in MDA-MB-231 and MDA-MB-468 cells. Cells treated with **44e** at 5 μ M or combined with 3-MA at 1 mM. Error bar shows SD; * $p < 0.05$, ** $p < 0.01$, *** $p < 0.001$ compared with the control groups.

**Figure 13.**

Antitumor activity of **44e** in the MDA-MB-231 and MDA-MB-468 xenograft models.

(A) Body weights, tumor volumes, and tumor weights following treatment by oral administration with 25 or 50 mg/kg **44e** or 50 mg/kg **1 + 18** in the MDA-MB-231 tumor xenograft model. (B) Body weights, tumor volumes, and tumor weights following the treatment by oral administration with 25 or 50 mg/kg **44e** or 50 mg/kg **1 + 18** in the MDA-MB-468 tumor xenograft model. Error bar shows SD; * $p < 0.05$, ** $p < 0.01$, *** $p < 0.001$ compared with the control groups.

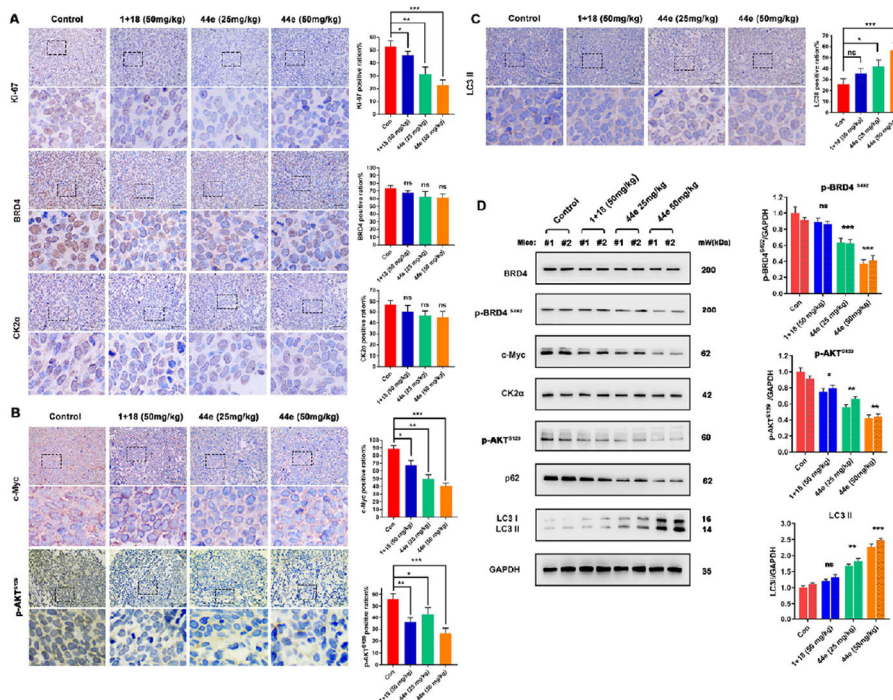
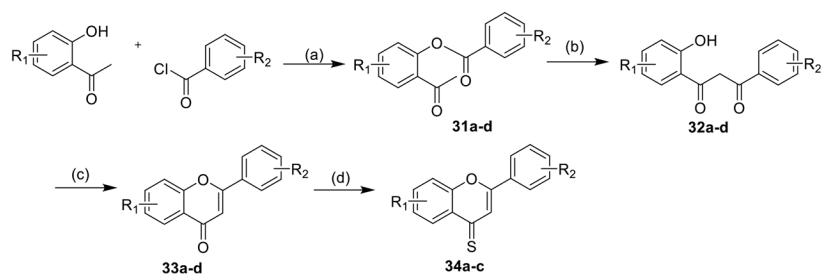
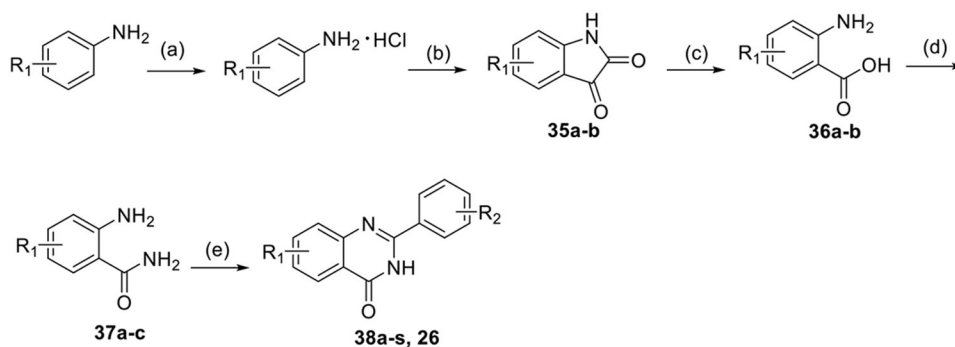


Figure 14.

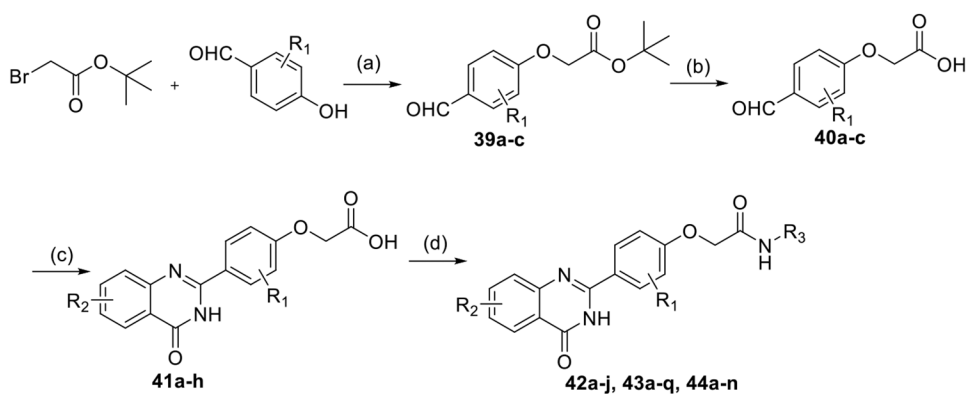
Potential therapeutic effects of **44e** *in vivo*. (A–C) Representative images of IHC analysis of Ki-67, BRD4, c-Myc, CK2 α , p-AKT^{S129}, and LC3II markers in different groups from MDA-MB-231 xenograft tumor model. Scale bar, 40 μ m. (D) Two individual tumor tissues (1 and 2) excised from the MDA-MB-231 xenograft tumor model were analyzed. The expression levels of BRD4, c-Myc, CK2 α , p-AKT^{S129}, p62, and LC3II were detected by Western blot analysis. Error bar shows SD; * p < 0.05, ** p < 0.01, *** p < 0.001, **** p < 0.0001 compared with the control groups.

**Scheme 1^a**

^aReagents and conditions: (a) pyridine, DBU, 80 °C, 1.5 h; (b) pyridine, KOH, 50–80 °C, 2 h; (c) HOAc, 1% H₂SO₄, 90–110 °C, 2 h; (d) dry toluene, Lawesson's reagent, 110 °C, 4 h.

**Scheme 2^a**

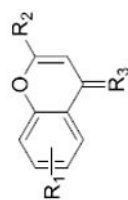
^aReagents and conditions: (a) HCl/Et₂O, rt, overnight; (b) (COCl)₂, 160 °C, 2.5 h; (c) NaOH, H₂O₂, 80 °C, 0.5 h; (d) ammonium hydroxide, HOBt, EDCI, NMM, THF, overnight, rt; (e) benzaldehyde derivatives, DMAC, PTSA, NaHSO₃, 120 °C, 4–8 h.

**Scheme 3^a**

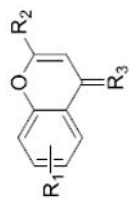
^aReagents and conditions: (a) K₂CO₃, DMF, 80 °C, 3 h; (b) DCM, TFA, rt, 2 h; (c) DMAC, PTSA, NaHSO₃, 120 °C, 4–8 h; (d) DMF, Et₃N, HOBT, EDCI, rt, 24 h.

BRD4 and CK2 Inhibition Rates and *In Vitro* Anti-Proliferative Activities of Compounds 33a–d and 34a–c

Table 1.



NO.	R ₁	R ₂	R ₃	Kinase inhibitory activity (1)				Anti-proliferative active (IC ₅₀ , μM) ^[d]	
				BRD4	CK2	MDA-MB-231	MDA-MB-468	μM) ^[d]	μM) ^[d]
33a	4,6-diOCH ₃		O	13.55 ± 0.21	9.13 ± 1.96	47.75 ± 2.83	39.65 ± 2.15		
33b	5-OCH ₃		O	6.05 ± 1.29	12.56 ± 0.23	45.71 ± 3.04	> 50		
33c	5-OCH ₃		O	4.26 ± 0.71	10.37 ± 0.85	> 50	> 50		
33d	5-Br		O	5.92 ± 0.37	11.76 ± 0.48	33.48 ± 1.70	48.23 ± 3.61		



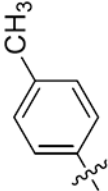
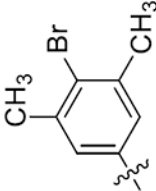
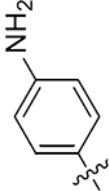
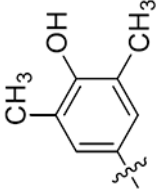
NO.	R ₁	R ₂	R ₃	Kinase inhibitory activity (I ₅₀ , %) ^(d)				Anti-proliferative active (IC ₅₀ , μM) ^(b)		
				BRD4	CK2	MDA-MB-231	MDA-MB-468			
34a	4,6-diOCH ₃		S	14.80 ± 0.53	7.32 ± 0.89	> 50	> 50	> 50		
34b	5-OCH ₃		S	4.37 ± 0.60	14.19 ± 0.52	> 50	> 50	> 50		
34c	5-OCH ₃		S	6.91 ± 0.34	13.95 ± 0.14	> 50	> 50	> 50		

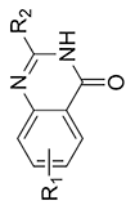
^a Reported compounds were tested in triplicate. Data are presented as mean ± SD.

^b IC₅₀ values were determined from cell viability assay for 24 h.

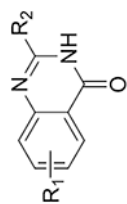
BRD4 and CK2 Inhibition Rates and *In Vitro* Antiproliferative Activities of Compounds 38a–s and 26

Table 2.

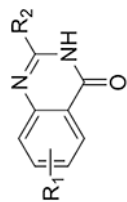
NO.	R ₁	R ₂	Kinase inhibitory activity (I μM, %) ^(a)				Anti-proliferative active (IC ₅₀ ^b μM) ^(b)	
			BRD4	CK2	MDA-MB-231	MDA-MB-468		
38a	4,6-diOCH ₃		16.26 ± 0.48	13.17 ± 2.23	45.61 ± 3.16	38.42 ± 0.47		
38b	4,6-diOCH ₃		18.18 ± 1.32	8.46 ± 0.41	25.21 ± 0.32	29.62 ± 1.29		
38c	4,6-diOCH ₃		10.65 ± 1.18	15.41 ± 0.20	36.52 ± 2.03	> 50		
38d	4,6-diOCH ₃		21.25 ± 1.65	16.13 ± 0.61	17.53 ± 3.23	19.26 ± 1.82		



NO.	R ₁	R ₂	Kinase inhibitory activity (I μM, %) ^(d)				Anti-proliferative active (IC ₅₀ μM) ^(e)		
			BRD4	CK2	MDA-MB-231	MDA-MB-468			
38e	4,6-diOCH ₃		19.61 ± 2.71	10.22 ± 2.54	23.21 ± 2.61	22.32 ± 2.15			
38f	4,6-diOCH ₃		17.46 ± 0.38	14.14 ± 2.15	27.31 ± 0.19	24.71 ± 1.39			
38g	4,6-diOCH ₃		13.11 ± 1.24	9.46 ± 0.98	43.86 ± 0.62	39.41 ± 1.76			
38h	4,6-diOCH ₃		5.62 ± 2.28	17.57 ± 1.29	>50	44.62 ± 2.11			



NO.	R_1	R_2	Kinase inhibitory activity (I μM), % ^(d)					Anti-proliferative active (IC_{50} μM) ^(e)		
			BRD4	CK2	MDA-MB-231	MDA-MB-468	MDA-MB-231	MDA-MB-468		
38i	4,6-diOCH ₃		11.74 ± 2.42	16.83 ± 0.58	38.30 ± 1.54	29.34 ± 1.27	>50	>50	>50	
38j	H		3.28 ± 1.45	7.72 ± 1.61	>50	>50	>50	>50		
38k	H		1.31 ± 2.22	14.59 ± 1.54	>50	>50	>50	>50		
38l	H		5.62 ± 0.41	11.83 ± 1.78	>50	>50	>50	>50		
38m	5-OCH ₃		2.82 ± 0.02	14.40 ± 2.49	>50	41.21 ± 3.25	>50	>50		



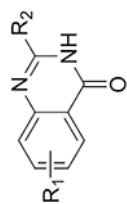
NO.	R ₁	R ₂	Kinase inhibitory activity (I μM, %) ^(d)				Anti-proliferative active (IC ₅₀ μM) ^(e)	
			BRD4	CK2	MDA-MB-231	MDA-MB-468		
38n	5-OCH ₃		5.35 ± 0.42	14.33 ± 1.91	>50		43.72 ± 2.08	
38o	5-OCH ₃		2.52 ± 1.03	13.63 ± 1.52	>50		30.41 ± 1.63	
38p	4,6-diOCH ₃		17.46 ± 2.30	16.81 ± 0.31	21.08 ± 0.16		8.33 ± 0.47	
38q	4,6-diOCH ₃		19.23 ± 0.31	21.63 ± 1.44	25.62 ± 2.36		22.73 ± 0.29	
38r	4,6-diOCH ₃		18.22 ± 1.53	20.43 ± 0.57	36.72 ± 1.08		18.56 ± 1.01	
38s	4,6-diOCH ₃		16.09 ± 2.64	17.17 ± 1.69	22.02 ± 2.05		13.82 ± 0.29	

Author Manuscript

Author Manuscript

Author Manuscript

Author Manuscript



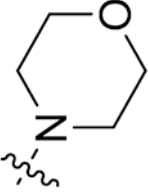
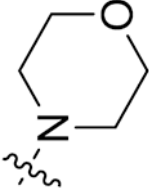
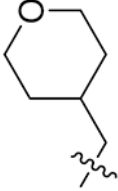
NO.	R ₁	R ₂	Kinase inhibitory activity (I μM, %) ^(a)				Anti-proliferative active (IC ₅₀ μM) ^(b)	
			BRD4	CK2	MDA-MB-231	MDA-MB-468		
26	4,6-diOCH ₃		35.72 ± 1.53	26.44 ± 0.57	19.72 ± 1.08	18.56 ± 1.37		

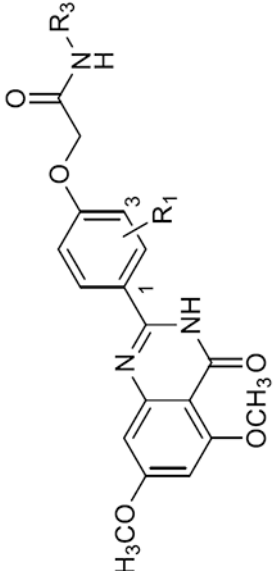
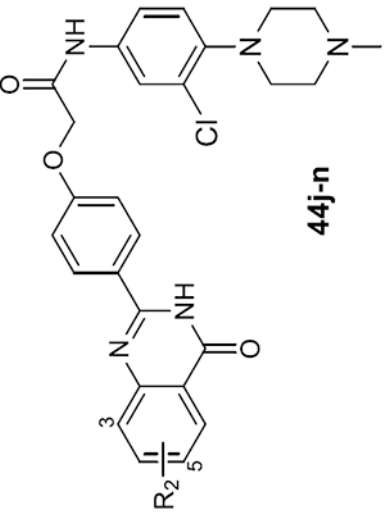
^a Reported compounds were tested in triplicate. Data are presented as mean ± SD.

^b IC₅₀ values were determined from cell viability assay for 24 h.

Table 3.

BRD4 and CK2 Inhibition Rates and *In Vitro* Antiproliferative Activity of Compounds 3, 14, 42a-j, 43a-q, and 44a-n

NO.	R ₁	R ₂	R ₃	Kinase inhibitory activity (I μM, %) ^(d)			Anti-proliferative active (IC ₅₀ μM) ^(b)		
				BRIM	CK2	MDA-MB-231	MDA-MB-468		
42a	H	-		45.29 ± 1.42	42.20 ± 1.25	14.71 ± 1.55	12.54 ± 0.87		
42b	3,5-diCH ₃	-		42.58 ± 0.82	40.31 ± 1.76	20.57 ± 0.62	18.50 ± 1.23		
42c	H	-		43.19 ± 3.47	43.43 ± 2.59	21.21 ± 2.80	26.61 ± 0.85		

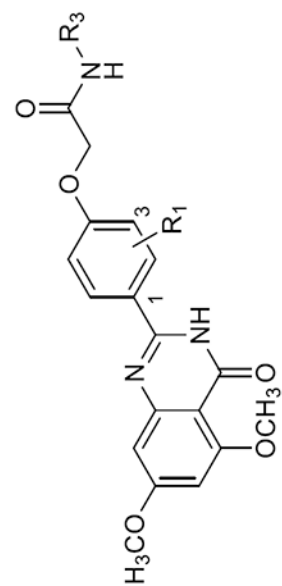
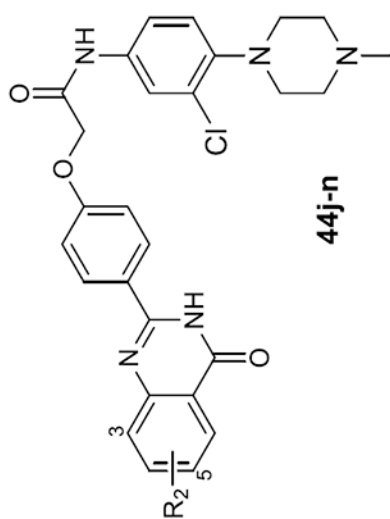
	42a-j, 43a-q, 44a-i
	44j-n

Author Manuscript

Author Manuscript

Author Manuscript

Author Manuscript



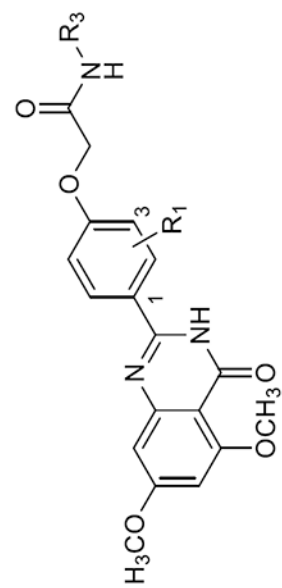
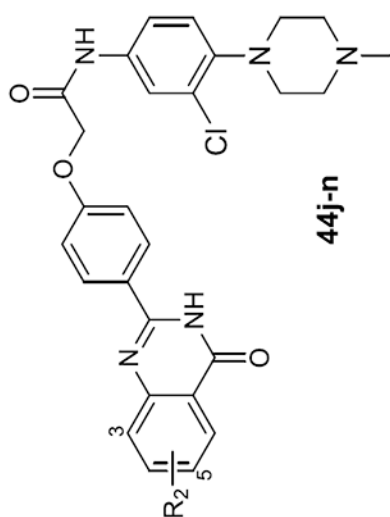
NO.	R ₁	R ₂	R ₃	Kinase inhibitory activity (1)				Anti-proliferative active (IC ₅₀ , μM) ^(b)	
				BRIM	CK2	MDA-MB-231	MDA-MB-468	μM	μM
42d	3,5-diCH ₃	-		37.47 ± 1.42	33.70 ± 3.64	23.61 ± 0.58	25.56 ± 1.57		
42e	3,5-diBr	-		51.11 ± 3.47	47.43 ± 2.19	16.93 ± 0.87	14.81 ± 1.66		
42f	3,5-diCH ₃	-		52.38 ± 1.15	49.23 ± 2.59	17.21 ± 2.80	15.55 ± 2.21		
42g	H	-		55.71 ± 2.02	53.64 ± 1.79	12.82 ± 1.72	13.65 ± 0.23		

Author Manuscript

Author Manuscript

Author Manuscript

Author Manuscript



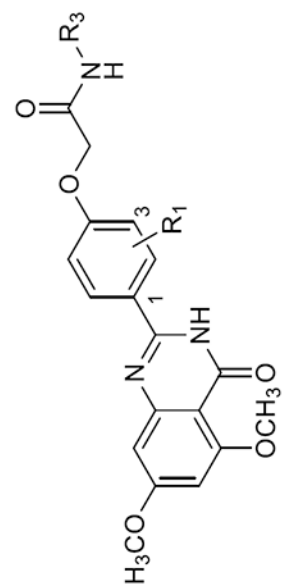
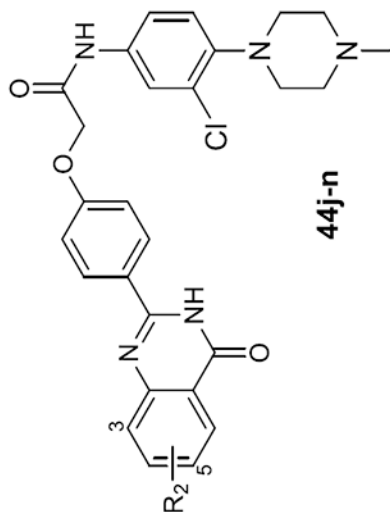
NO.	R ₁	R ₂	R ₃	Kinase inhibitory activity (1)			Anti-proliferative active (IC ₅₀ , μM) ^(b)	
				μM, % ^(a)	CK2	MDA-MB-231	MDA-MB-468	
42h	H			54.19 ± 1.28	47.43 ± 1.09	23.37 ± 1.35	15.03 ± 0.26	
42i	3,5-diCH ₃			53.50 ± 3.47	42.14 ± 0.33	24.41 ± 2.81	16.55 ± 1.80	
42j	3,5-diCH ₃	-		56.14 ± 3.09	25.61 ± 6.57	>50	30.31 ± 1.56	

Author Manuscript

Author Manuscript

Author Manuscript

Author Manuscript



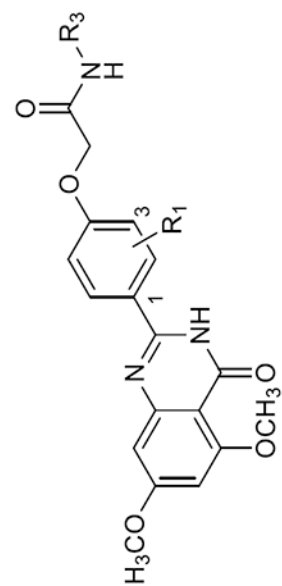
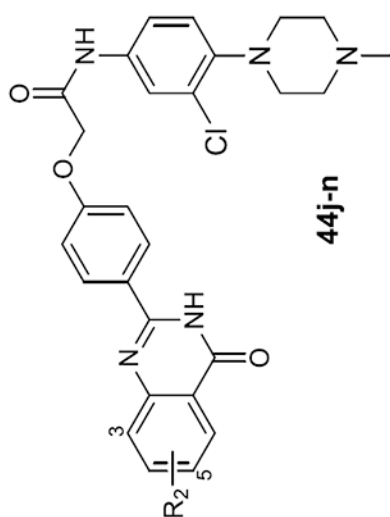
NO.	R ₁	R ₂	R ₃	Kinase inhibitory activity (1)				Anti-proliferative active (IC ₅₀ , μM) ^(b)	
				BRIM	CK2	MDA-MB-231	MDA-MB-468	μM) ^(a)	μM) ^(b)
43a	H	-		62.10 ± 0.52	55.68 ± 2.07	13.12 ± 1.67	16.62 ± 2.21		
43b	3,5-diCH ₃	-		57.39 ± 2.06	51.38 ± 1.69	22.37 ± 2.30	17.24 ± 1.63		
43c	3,5-diCH ₃	-		78.36 ± 4.07	69.31 ± 2.19	10.81 ± 1.85	12.59 ± 1.24		
43d	3,5-diCH ₃	-		72.44 ± 2.87	57.08 ± 1.27	14.57 ± 1.64	15.74 ± 2.66		

Author Manuscript

Author Manuscript

Author Manuscript

Author Manuscript



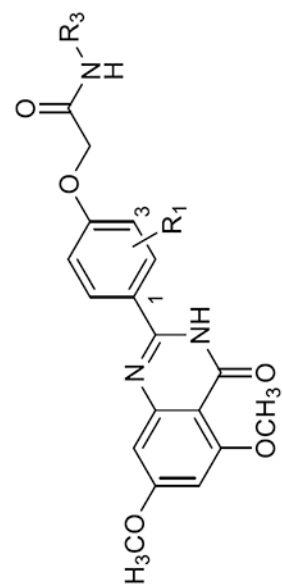
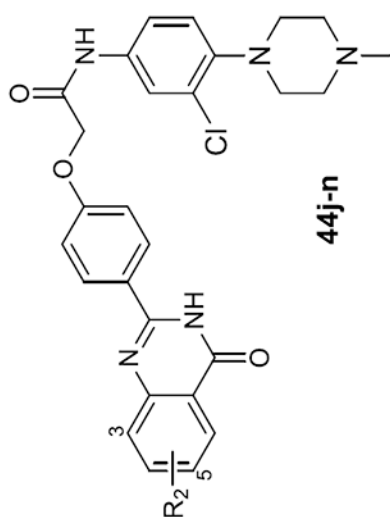
NO.	R ₁	R ₂	R ₃	Kinase inhibitory activity (1 μM, %) ^(a)				Anti-proliferative active (IC ₅₀ μM) ^(b)		
				BRIM	CK2	MDA-MB-231	MDA-MB-468			
43e	3,5-diBr	-		62.58 ± 0.52	58.47 ± 1.23	13.64 ± 2.17	15.83 ± 1.11			
43f	H	-		82.30 ± 2.73	80.02 ± 4.22	6.46 ± 0.62	8.80 ± 1.15			
43g	H	-		74.33 ± 1.28	56.02 ± 1.90	13.22 ± 0.54	8.07 ± 1.68			
43h	H	-		69.01 ± 2.30	51.44 ± 0.65	17.32 ± 0.79	11.50 ± 0.54			

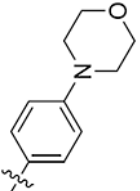
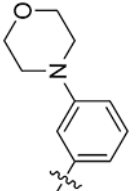
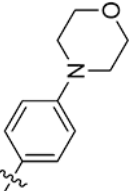
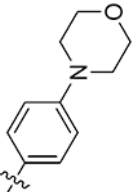
Author Manuscript

Author Manuscript

Author Manuscript

Author Manuscript



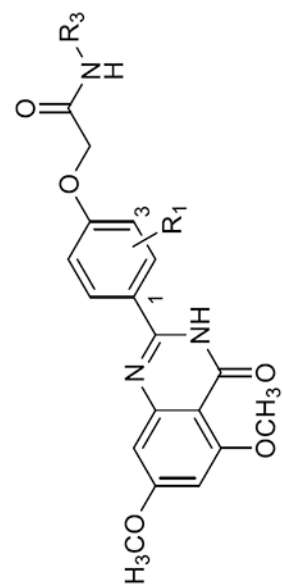
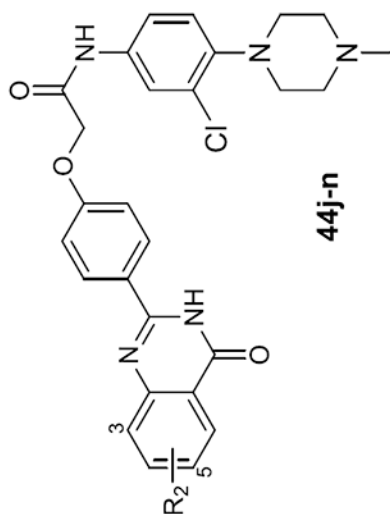
NO.	R ₁	R ₂	R ₃	Kinase inhibitory activity (1)				Anti-proliferative active (IC ₅₀ , μM) ^(b)	
				BRIM	CK2	MDA-MB-231	MDA-MB-468	μM) ^(a)	μM) ^(b)
43i	3,5-diCH ₃	-		81.44 ± 1.15	63.61 ± 0.34	8.23 ± 1.39	9.49 ± 1.18		
43j	3,5-diCH ₃	-		73.71 ± 0.83	55.73 ± 1.86	11.26 ± 0.93	13.44 ± 0.77		
43k	3,5-diBr	-		67.20 ± 1.52	58.29 ± 3.62	13.21 ± 2.21	15.11 ± 1.75		
43l	H	-		80.65 ± 3.98	75.39 ± 2.52	7.67 ± 1.03	9.54 ± 0.74		

Author Manuscript

Author Manuscript

Author Manuscript

Author Manuscript



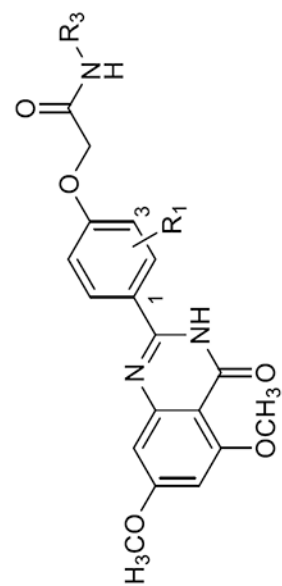
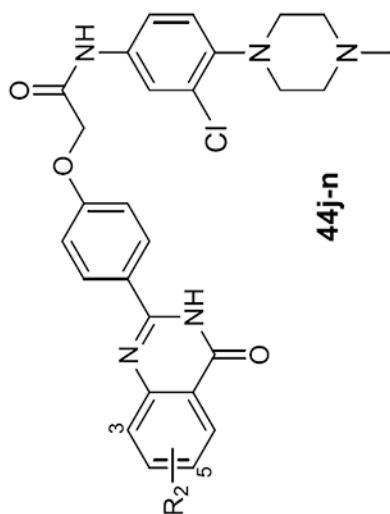
NO.	R ₁	R ₂	R ₃	Kinase inhibitory activity (1)			Anti-proliferative active (IC ₅₀ , μM) ^(b)	
				BRIM	CK2	MDA-MB-231	MDA-MB-468	
43m	H	-		61.74 ± 2.03	60.02 ± 1.38	15.53 ± 0.91	17.80 ± 1.22	
43n	3,5-diCH ₃	-		69.24 ± 3.67	70.51 ± 0.54	13.43 ± 2.53	9.43 ± 1.09	
43o	3,5-diBr	-		56.39 ± 0.46	62.47 ± 1.23	16.35 ± 2.02	15.63 ± 1.26	

Author Manuscript

Author Manuscript

Author Manuscript

Author Manuscript



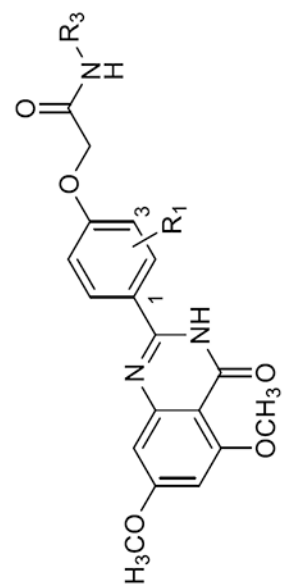
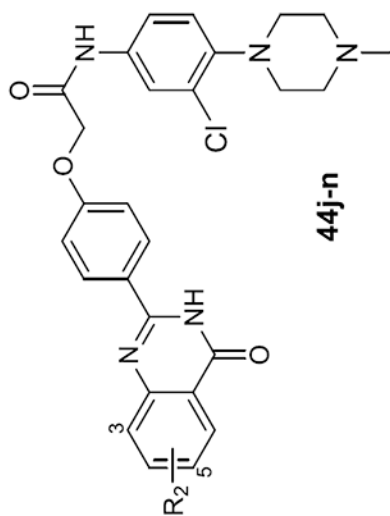
NO.	R ₁	R ₂	R ₃	Kinase inhibitory activity (I			Anti-proliferative active (IC ₅₀ ,		
				μM, %) ^(a)	CK2	MDA-MB-231	μM) ^(b)	MDA-MB-468	
43p	H	-		71.06 ± 2.96	75.20 ± 1.38	10.27 ± 2.03	11.63 ± 0.46		
43q	H	-		68.51 ± 1.72	67.52 ± 0.71	19.56 ± 1.63	7.82 ± 4.02		
44a	3,5-diCH ₃	-		83.29 ± 3.45	76.21 ± 2.53	10.30 ± 1.23	9.16 ± 0.93		

Author Manuscript

Author Manuscript

Author Manuscript

Author Manuscript



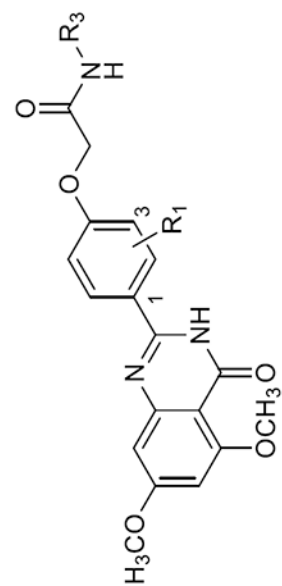
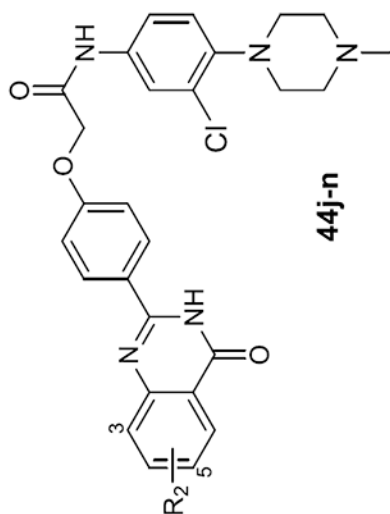
NO.	R ₁	R ₂	R ₃	Kinase inhibitory activity (1)				Anti-proliferative active (IC ₅₀ , μM) ^(b)	
				BRIM	CK2	MDA-MB-231	MDA-MB-468	μM) ^(a)	μM) ^(b)
44b	H	-		85.43 ± 2.65	79.61 ± 3.65	7.09 ± 0.25	8.58 ± 1.51		
44c	H	-		85.37 ± 1.58	82.46 ± 0.13	6.30 ± 2.37	7.55 ± 1.73		
44d	3,5-diCH ₃	-		87.61 ± 2.73	80.23 ± 0.42	5.72 ± 1.45	8.33 ± 1.17		
44e	H	-		92.28 ± 0.66	90.65 ± 1.39	2.66 ± 0.81	3.52 ± 0.58		

Author Manuscript

Author Manuscript

Author Manuscript

Author Manuscript



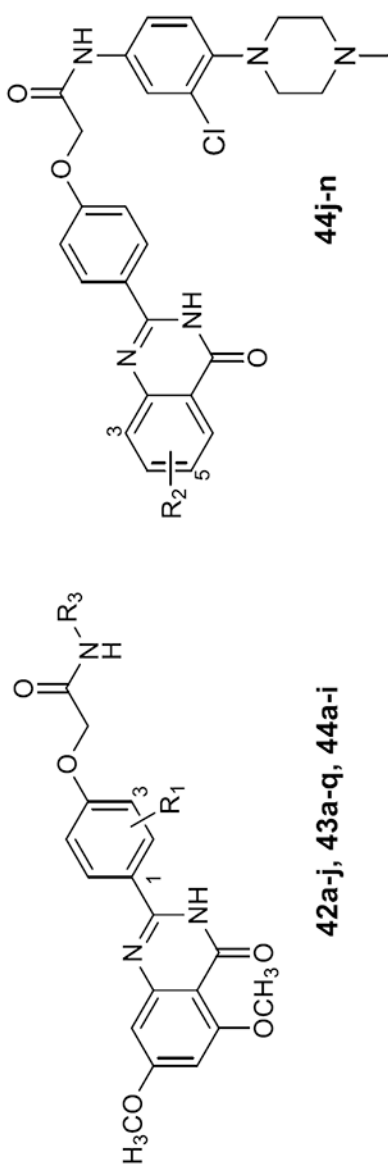
NO.	R ₁	R ₂	R ₃	Kinase inhibitory activity (1)				Anti-proliferative active (IC ₅₀ , μM) ^(b)	
				BRIM	CK2	MDA-MB-231	MDA-MB-468	μM	μM
44f	3,5-diCH ₃	-		89.27 ± 1.47	85.40 ± 0.38	3.49 ± 1.23	4.58 ± 0.52		
44g	3,5-diBr	-		79.30 ± 2.50	86.29 ± 1.47	4.02 ± 1.92	5.53 ± 0.28		
44h	H	-		83.52 ± 1.54	75.19 ± 0.73	4.52 ± 0.56	8.29 ± 1.92		
44i	3,5-diCH ₃	-		85.47 ± 0.28	70.13 ± 2.94	10.23 ± 0.95	6.31 ± 1.94		

Author Manuscript

Author Manuscript

Author Manuscript

Author Manuscript

**44j-n****42a-j, 43a-q, 44a-i**

NO.	R ₁	R ₂	R ₃	Kinase inhibitory activity (1)			Anti-proliferative active (IC ₅₀ , μM) ^b		
				BRIM	CK2	MDA-MB-231	MDA-MB-468	MDA-MB-468	
44j	-	4-F	-	45.26 ± 0.57	68.27 ± 1.39	6.94 ± 0.68	7.51 ± 1.13	7.51 ± 1.13	
44k	-	4-OCH ₃	-	55.60 ± 1.62	72.03 ± 2.82	14.59 ± 0.77	16.36 ± 0.85	16.36 ± 0.85	
44l	-	4-Cl	-	51.49 ± 3.02	75.61 ± 1.12	14.40 ± 0.58	15.27 ± 0.72	15.27 ± 0.72	
44m	-	5-Cl	-	47.29 ± 1.16	65.93 ± 1.80	5.21 ± 0.82	6.23 ± 0.55	6.23 ± 0.55	
44n	-	5-CH ₃	-	48.20 ± 0.47	74.70 ± 2.11	17.36 ± 0.56	16.22 ± 1.83	16.22 ± 1.83	
1	-	-	-	97.03 ± 1.32	6.60 ± 0.41	29.51 ± 1.70	30.19 ± 0.69	30.19 ± 0.69	
18	-	-	-	7.14 ± 1.51	98.53 ± 1.87	14.25 ± 0.62	20.92 ± 1.04	20.92 ± 1.04	
1+	-	-	-	-	-	-	-	-	
18^c	-	-	-	-	-	7.37 ± 0.39 (CI = 0.78) ^d	9.10 ± 0.14 (CI = 0.61) ^d	9.10 ± 0.14 (CI = 0.61) ^d	

^aReported compounds were tested in triplicate. Data are presented as mean ± SD.^bIC₅₀ values were determined from cell viability assay for 24 h.^cCombined at a mole ratio of 1:1.^dUsing the Chou-Talalay method.

Table 4.CK1, CK2, and BRD Inhibitory Profiles of Compounds 44e, 1, and 18 (nM)^a

target	44e	1	18
BRD2 BD1	>10000	185 ± 24	<i>b</i>
BRD2 BD2	8700 ± 420	32 ± 4	<i>b</i>
BRD3 BD1	9200 ± 670	76 ± 8	<i>b</i>
BRD3 BD2	>10000	61 ± 7	<i>b</i>
BRD4 BD1	193 ± 60	92 ± 13	<i>b</i>
BRD4 BD2	98 ± 35	44 ± 5	<i>b</i>
BRD4 (BD1 + BD2)	180 ± 20	84 ± 10	<i>b</i>
BRDT BD1	>10000	207 ± 23	<i>b</i>
BRDT BD2	>10000	185 ± 21	<i>b</i>
CK2	230 ± 43	<i>b</i>	4 ± 1
CK1	>10000	<i>b</i>	>10000

^aReported compounds were tested in triplicate. Data are presented as mean ± SD.^bNot determined.

Table 5.Pharmacokinetic Profile of 44e^a

parameter	iv (1 mg/kg)	po (10 mg/kg)
$T_{1/2}$ (h)	4.21 ± 0.57	5.14 ± 0.71
C_{max} (ng/mL)	237 ± 11	206 ± 6
AUC _{0-t} (ng·h/mL)	579 ± 49	2079 ± 130
AUC _{0-∞} (ng·h/mL)	588 ± 36	2090 ± 146
V_z (L/kg)	21.1 ± 2.6	
CL ((mL/min)/kg)	57.4 ± 1.3	
F (%)		32.5

^aAll data were obtained by triple testing (mean ± SD) in SD rats.